

X-ray Millisecond Pulsars in the Galactic Globular Clusters

by

Jiaqi Zhao

A thesis submitted in partial fulfillment of the requirements for the degree of

Master of Science

Department of Physics

University of Alberta

© Jiaqi Zhao, 2021

Abstract

In this thesis we study X-ray millisecond pulsars (MSPs) in the Galactic globular clusters (GCs) to better understand the X-ray emission from them. We analyze 55 ks and 290 ks of *Chandra* X-ray observations of the clusters M13 and Omega Cen, respectively. We find confident X-ray counterparts to five of the six MSPs recently discovered in M13, while we place an upper limit of the X-ray luminosity for the sixth. We also find optical counterparts to two M13 pulsars, which are likely white dwarfs, using the *Hubble Space Telescope*. In addition, we detect X-ray counterparts to two newly found MSPs in the GC Omega Cen. We then compile previous X-ray studies of MSPs to present a comprehensive census of X-ray MSPs in 29 GCs, including 64 MSPs with detected X-ray luminosities and 111 MSPs with X-ray upper limits. We find most detected X-ray MSPs have luminosities between $\sim 10^{30}$ erg s $^{-1}$ to 3×10^{31} erg s $^{-1}$ (0.3–8 keV). We estimate the total number of MSPs in 36 GCs based on the correlation between the number of MSPs and stellar encounter rate in GCs, and suggest that around 600 to 1500 MSPs exist in those GCs. Finally, we estimate the number of X-ray-detectable MSPs in the Galactic bulge, and suggest there are between 1–90 MSPs with $L_X > 10^{33}$ erg s $^{-1}$ and ~ 20 –900 MSPs with $L_X > 10^{32}$ erg s $^{-1}$ in the bulge.

Preface

This thesis is an original work by Jiaqi Zhao under the supervision of Professor Craig O. Heinke at the University of Alberta. All data used in this thesis are publicly available.

I have published the content of Chapter 2 in Zhao et al. (2021) in Monthly Notices of the Royal Astronomical Society (MNRAS). I reduced the *Chandra* observations and analyzed the data. Co-author Yue Zhao was responsible for reducing and analyzing the optical observations and data by the *Hubble Space Telescope*. Co-author Craig O. Heinke helped me understand and interpret the statistical significance of the results and its theoretical implications. The whole work was done with the guidance of Professor Heinke.

The work described in Chapter 3 makes up a paper to be submitted to MNRAS. I was responsible for reducing, collecting and analyzing the *Chandra* observations and data. Co-author Craig O. Heinke assisted me in understanding the X-ray properties of millisecond pulsars and interpreting the implications and predictions from our results. This work was guided by Professor Heinke.

*To Jocelyn Bell Burnell,
who first discovered radio pulsars and changed astronomy forever.*

Acknowledgements

First and foremost, I would like to thank my supervisor Professor Craig O. Heinke for his continuous guidance and help. I always feel so grateful and lucky for being his student. I would also like to thank the entire University of Alberta astrophysics group who have provided support through my master's program. I am also thankful to my family and friends for their support, especially to Murph and our cat, Dreamer, for their company during the hard pandemic time. Finally, I would like to thank the Rocky Mountains who always comfort and inspire me.

Contents

1	Introduction	1
1.1	Millisecond pulsars	1
1.1.1	The formation of MSPs	2
1.1.2	MSP binary types	2
1.2	X-ray emission from MSPs	4
1.2.1	Chandra X-ray Observatory	4
1.2.2	Thermal X-ray emission	5
1.2.3	Non-thermal X-ray emission	5
1.3	X-ray sources in GCs	6
1.4	The Galactic Center Excess	8
1.5	The arc of the thesis	10
2	MSPs in the Globular Cluster M13	11
2.1	Introduction	11
2.2	Observation and data reduction	13
2.2.1	Chandra observations	13
2.2.2	Optical observations	16
2.3	Data analysis and results	17
2.3.1	X-ray spectral fits	17
2.3.2	Optical/UV photometry	21
2.3.3	Optical/UV counterparts	21
2.4	Discussion	26
2.5	Conclusions	30

3	X-ray Census of GC MSPs	31
3.1	Introduction	31
3.2	Data Collection and Reduction	33
3.2.1	GC MSPs with X-ray analysis	37
3.2.2	GC X-ray analysis in this work	38
3.3	Analysis and Results	42
3.3.1	X-ray spectral fits of 2 MSPs in ω Cen	42
3.3.2	X-ray sources in M53, NGC 6342, and NGC 6517	45
3.3.3	X-ray luminosity function of GC MSPs	48
3.3.4	Number of MSPs versus stellar encounter rate	54
3.4	Discussion	57
3.5	Conclusions	62
4	Conclusions and Prospects	64
	References	67
	Appendix A Upper limits of X-ray luminosities	98

List of Tables

2.1	<i>Chandra</i> Observations of M13	14
2.2	HST observations used in this work.	17
2.3	Spectral fits for the M13 MSPs.	20
3.1	Parameters for the GCs in this work.	34
3.2	<i>Chandra</i> Observations of M53, NGC 6342, and NGC 6517	39
3.3	<i>Chandra</i> Observations of ω Cen	40
3.4	Spectral fits for J1326–4728 A and B.	45
3.5	Basic X-ray properties of catalogue sources in M53, NGC 6342, and NGC 6517.	47
3.6	Determined X-ray luminosities of GC MSPs	51
3.7	Estimates of MSP population in GCs	56
3.8	Estimates of the number of X-ray MSPs in the bulge	62
A.1	111 GC MSPs with upper limits of X-ray luminosities.	98

List of Figures

2.1	Merged 0.5–7 keV <i>Chandra</i> X-ray image of M13	15
2.2	X-ray spectra and best fits for five MSPs in M13.	22
2.3	$UV_{275} - U_{336}$ and $U_{336} - B_{438}$ CMDs of M13.	23
2.4	$V_{606} - I_{814}$ CMD of M13.	24
2.5	V_{606} finding charts for MSP D and MSP F.	27
3.1	<i>Chandra</i> X-ray images in the band 0.3–8 keV of M53, NGC 6342, and NGC 6517.	40
3.2	Merged <i>Chandra</i> X-ray image of ω Cen in the band of 0.3–8 keV.	41
3.3	X-ray spectra and best fits of two MSPs in ω Cen.	44
3.4	The differential X-ray luminosity distributions of GC MSPs cat- alogued in this work.	49
3.5	The number of MSPs in a globular cluster versus the stellar encounter rate.	58

Chapter 1

Introduction

Since the first pulsar was discovered in 1967 by Jocelyn Bell (see Hewish et al., 1968), a new and fascinating area of astronomy and astrophysics has been opened. So far, more than 3,000 pulsars have been detected in the Galaxy,¹ providing a large and rich sample to study the physics of these peculiar objects, which are also useful tools to explore other fields of astronomy.

A pulsar is believed to be a highly magnetized and fast rotating neutron star (NS) that emits electromagnetic radiation from above its polar caps. As the pulsar rotates, its radiation beam sweeps across the observer at its rotation period, generating pulses.

1.1 Millisecond pulsars

Radio millisecond pulsars (MSPs) are a distinct group in the pulsar population with short rotation periods of $P \lesssim 30$ ms, and low spin-down rates of $\dot{P} \sim 10^{-21} - 10^{-19}$. Hence, MSPs have large characteristic ages $\tau \gtrsim 1$ Gyr and relatively low magnetic field strengths of $\sim 10^8 - 10^{10}$ G. The first discovered MSP is known as PSR B1937+21 ($P \sim 1.56$ ms; Backer et al., 1982), while the fastest spinning pulsar found to date is an MSP in the globular cluster Terzan 5 (known as PSR J1748–2446ad; $P \sim 1.40$ ms; Hessels et al., 2006). Given their extremely stable rotation and regular pulsations, MSPs have many applications in a wide variety of astronomical and astrophysical problems, such

¹see the ATNF Pulsar Catalogue (Manchester et al., 2005) <https://www.atnf.csiro.au/research/pulsar/psrcat/>

as the detection of low-frequency gravitational waves (see e.g., Hobbs et al., 2010).

1.1.1 The formation of MSPs

Most ‘normal’ pulsars (i.e., slow-rotating and young pulsars) are generated in core-collapse (Type II) supernovae (Lyne and Graham-Smith, 2012b). After a pulsar formed, it continuously consumes rotational energy through electromagnetic radiation principally, and hence its spin period increases to a few seconds, until its radiation becomes undetectable.

However, a “dead” pulsar may be “recycled” if it lies in a close binary system with a low-mass companion star, where the neutron star may accrete mass and angular momentum from its companion, resulting in a spin-up to a rotational period of a few milliseconds (Alpar et al., 1982; Bhattacharya and van den Heuvel, 1991; Papitto et al., 2013). During the accretion stage, the overflowing mass intensely interacts with the NS gravitational potential, creating luminous thermal X-ray emission (Lyne and Graham-Smith, 2012a), and the pulsar becomes accretion-powered. These X-ray binaries, namely low-mass X-ray binaries (LMXBs), are now known to be progenitors of radio MSPs. Once the accretion phase is finished, the pulsar is recycled and becomes a rotation-powered MSP (or radio MSP). It is interesting to note that an MSP can switch between accretion-powered and rotation-powered states; such an object is referred to as a transitional MSP (see e.g., Papitto et al., 2013; Bassa et al., 2014; Linares et al., 2014).

1.1.2 MSP binary types

Since MSPs are the descendants of NS-LMXBs, it is expected that many MSPs still exist in binary systems. In fact, MSP binary systems are commonly observed and found to be diverse and intriguing. With the extensive observations in recent years, MSP binaries are further grouped into several sub-categories according to the degeneracy of their companion stars.

MSPs coupled with low-mass non-degenerate stars are the so-called ‘spider’ MSPs, which have attracted huge interest recently. The companion masses of

spider pulsars have a bi-modal distribution (Roberts, 2011; Strader et al., 2019) and hence spider pulsars are categorized into two distinct sub-groups: redbacks (RBs) with companion masses of $\sim 0.2 M_{\odot}$; and black widows (BWs) with companion masses of $\sim 0.02 M_{\odot}$. A large number of BWs and all of the RBs detected in GCs show eclipses of their radio emission², which are likely caused by the obstacle of material stripped from the companion by the violent pulsar wind (see e.g., Podsiadlowski, 1991; van Paradijs et al., 1988). The first spider pulsar was found by Fruchter et al. (1988), and 39 spider pulsars have been found in GCs so far. Recent novel studies of spider pulsar systems have attracted more attention to these types of MSPs (e.g. Main et al., 2018).

MSPs also are commonly found in binary systems with compact objects, and mostly with helium-core white dwarfs (WDs; e.g., Camilo and Rasio, 2005). Some WD companions can even be detected in optical observations, using e.g., the *Hubble Space Telescope* (e.g., Edmonds et al., 2001; Ferraro et al., 2001; Bassa et al., 2003; Sigurdsson et al., 2003; Pallanca et al., 2014). MSPs coupled with neutron stars have been discovered in about 20 systems (see e.g., Ferdman et al., 2014; Cameron et al., 2018; Stovall et al., 2018), and most impressively, a MSP has been found in a binary system with a pulsar, which is the only discovered binary pulsar system to date (PSR J0737–3039, Burgay et al., 2003). These MSP-NS binary systems are a unique laboratory for testing general relativity and have been successfully used to indirectly detect gravitational radiation (see e.g., Taylor et al., 1979; Lyne et al., 2004; Kramer et al., 2006). Although MSP-black hole (BH) binary systems have not been detected yet, theoretical studies predict the existence of such systems (e.g., Belczynski et al., 2013). Moreover, recent detection of two NS-BH mergers by the *Laser Interferometer Gravitational-wave Observatory* (LIGO; Abbott et al., 2021) provides observational support for the idea of MSP-BH binaries.

²see <http://www.naic.edu/~pfreire/GCpsr.html>

1.2 X-ray emission from MSPs

Radio MSPs were first identified as X-ray sources by Becker and Trümper (1993), who detected pulsed X-ray emission from an MSP binary system, PSR J0437–4715, using observations by the *ROSAT* telescope. However, X-ray observations and studies of MSPs were limited until the launch of *Chandra* and *XMM-Newton*. Particularly, the unique angular resolution of *Chandra* has significantly enhanced the detection and analysis of X-ray MSPs both in GCs and in the Galactic field. For instance, X-ray counterparts to radio MSPs have been detected in 47 Tuc (Bogdanov et al., 2006), M28 (Bogdanov et al., 2011b), NGC 6752 (Forestell et al., 2014), Terzan 5 (Bogdanov et al., 2021), etc. These studies have established that MSPs are generally faint X-ray sources, with typical luminosities of $L_X \lesssim 10^{31}$ erg s⁻¹, with some MSPs getting as bright as to $\sim 10^{33}$ erg s⁻¹. In addition, X-rays from MSPs can be further grouped into sub-classes based on the X-ray properties: thermal X-ray emitters; non-thermal pulsed emitters; and non-thermal non-pulsed emitters.

1.2.1 Chandra X-ray Observatory

The Chandra X-ray Observatory (CXO or *Chandra*)³ is NASA’s flagship mission for X-ray astronomy, such as detecting X-ray emission from stars and clusters. *Chandra* features an order of magnitude improvement in spatial resolution over other X-ray observatories (on-axis resolution of 0.5 arcsec), great sensitivity from 0.1 to 10 keV, and the capability for high spectral resolution observations. There are two focal plane instruments carried by *Chandra*. One is the High Resolution Camera (HRC), which is used for high resolution imaging and fast timing measurements; the other one is the Advanced CCD Imaging Spectrometer (ACIS) which provides the capability to simultaneously acquire high-resolution images and spectra.

Data from *Chandra* can be analysed by using CIAO (Chandra Interactive Analysis of Observations), the software package developed by the Chandra X-ray Center. In particular, Sherpa, the modeling and fitting package of CIAO,

³see https://cxc.cfa.harvard.edu/cdo/about_chandra/

enables users to establish complex models from simple definitions and fit those models to data, using various statistics and optimization methods. X-ray spectral modeling requires “forward modeling”, where a proposed model of the source is folded through the instrument response, and the folded model is compared to the observed spectrum. Archival CXO data are publicly available at the Chandra Data Archive⁴. Retrieved CXO data are generally needed to be reprocessed in CIAO to recalibrate the event data for further use, such as filtering the energy band and extracting spectra.

1.2.2 Thermal X-ray emission

Thermal X-ray emission from the surface of the neutron star is commonly observed from MSPs, especially from isolated MSPs and MSPs coupled with WDs (e.g., Bogdanov et al., 2006; Zhao et al., 2021), which show soft and blackbody-like spectra. The X-ray luminosities of thermally-emitting MSPs are relatively low, ranging from $\sim 1 \times 10^{30}$ erg s⁻¹ to $\sim 9 \times 10^{30}$ erg s⁻¹ in the band 0.3–8 keV (see Chapter 3, below). Thermal emission from an MSP likely originates from the hotspots near the magnetic poles on the surface of the NS, which are heated by the returning relativistic particles from the pulsar magnetosphere (see e.g., Harding and Muslimov, 2002). Intriguingly, the X-rays from the NS surface may carry information about the NS itself, such as mass and radius, and hence are important for constraining the NS mass-radius relation and equation of state (Bogdanov et al., 2019a,b). Recent observations by the Neutron Star Interior Composition Explorer (*NICER*) also have revealed more details about the location and structure of hotspots on an MSP (see e.g., Miller et al., 2019; Riley et al., 2019).

1.2.3 Non-thermal X-ray emission

Non-thermal pulsed emission

So far, dominant non-thermal pulsed X-ray emission has been detected from only three MSPs: PSR J0218+4232; B1821–24 (in the cluster M28; aka

⁴<https://cxc.cfa.harvard.edu/cda/>

M28A); and B1937+21 (see Zavlin, 2007; Bogdanov, 2018), which are the youngest and most energetic among the MSP population. This type of X-ray emission usually can be observed as X-ray pulsations in narrow pulses with power-law spectra, believed to be produced by relativistic particles accelerated in the pulsar magnetosphere. Non-thermal pulsed magnetospheric X-rays are also believed to be present at a low level in the X-ray spectra of many other MSPs (e.g., Zavlin et al., 2002; Zavlin, 2006; Bogdanov and Grindlay, 2009), and have been confirmed in the prototype MSP PSR J0437-4715 (Guillot et al., 2016).

Non-thermal non-pulsed emission

X-ray observations of spider pulsars commonly exhibit substantial non-thermal X-ray emission with no pulsations (e.g. Stappers et al., 2003; Bogdanov et al., 2005). The emission is most likely generated from the collision between relativistic pulsar wind and material from the companion star (e.g. Arons and Tavani, 1993; Stappers et al., 2003; Gentile et al., 2014), producing an intra-binary shock that emits non-thermal non-pulsed X-rays.

1.3 X-ray sources in GCs

Globular clusters are large and dense collections of stars, which are tightly bound by gravity. GCs play important roles in many ways within the Galaxy, such as the formation and evolution of galactic structure, the dynamics of stellar systems, and the nature of X-ray sources (see Harris and Racine, 1979, for a review of Galactic GCs). To date, more than 150 GCs have been found in the Galaxy and many more likely remain undiscovered.

Since GCs are gravitationally bound together, their shapes are generally spherical and their cores are of higher concentrations than outer regions. Hence, the morphology of a GC can be characterized by the core radius and the half-light radius (or effective radius): the former is defined to be the radius at which the surface brightness drops to a half of the central value, while the latter is the radius within which half of the GC’s luminosity is contained.

Moreover, the surface brightness profiles of a few GCs, such as NGC 6266 and Terzan 1, are found with power-law cusps, and these GCs most likely have suffered core collapse. This dynamical process is believed to be the migration of a portion of the stars from the core region to outer regions, resulting in a loss of energy from the remaining core stars, and thus the contraction of the core region (Ashman and Zepf, 1998).

Bright X-ray sources with $L_X \gtrsim 10^{36}$ erg s⁻¹ were first discovered in GCs by the observations of *Uhuru* (Giacconi et al., 1972, 1974). It was soon noticed that the number of luminous X-ray sources per unit mass in GCs is orders of magnitude higher than the number per unit mass in the Galactic field (e.g. Katz, 1975). The overabundance of X-ray sources in GCs is believed to be a consequence of the highly efficient formation of X-ray binaries (XRBs) in clusters (see e.g. Verbunt and Hut, 1987), where the XRBs are likely formed through tidal capture of massive star remnants (Clark, 1975; Fabian et al., 1975), direct collisions between neutron stars and giants (Sutantyo, 1975), or exchange interactions between neutron stars and low-mass stars in binaries (Hills, 1976). In the Galactic field, however, XRBs are mostly formed via binary evolution.

Apart from those luminous X-ray sources found in GCs (see Verbunt and Lewin, 2006, for a review), GCs also contain a large number of low-luminosity ($L_X < 10^{35}$ erg s⁻¹) X-ray sources, including LMXBs, MSPs, cataclysmic variables (CVs), and magnetically active binaries. For our research of interest in this work, we only focus on X-ray MSPs in GCs.

Observations have shown that MSPs are significantly overabundant in globular clusters, compared to the Galactic field. This is anticipated given the high stellar densities in GC cores, which create numerous LMXBs (as well as other types of X-ray binaries) and hence produce a large number of MSPs. To date, 230 pulsars have been found in 36 GCs, with 210 MSPs ($P \lesssim 25$ ms)⁵. Particularly, 39 pulsars have been discovered in the cluster Terzan 5, with 38 MSPs (including the fastest spinning MSP found to date), and 27 pulsars have been found in 47 Tuc, all of which are rotating at periods of a few milliseconds.

⁵see <http://www.naic.edu/~pfreire/GCpsr.html>

Therefore, GCs provide remarkable places to observe MSPs in large populations.

Thanks to the exceptional angular resolution of the *Chandra* X-ray telescope and deep exposures on GCs by it, many X-ray counterparts to GC MSPs have been detected, and a number of them have been well studied in X-rays, e.g., through X-ray spectral fitting (e.g. Bogdanov et al., 2006, 2011b). Moreover, many MSPs found in GCs are of great interest. For example, M28A is one of the most X-ray-bright radio MSPs found in the Galaxy, with $L_X = 1.4 \times 10^{33}$ erg s⁻¹ in the band 0.3–8 keV (see e.g. Bogdanov et al., 2011b). In addition, while only three tMSPs have been discovered to date, one has been confirmed in M28, known as PSR J1824–2452I or M28I (Papitto et al., 2013; Linares et al., 2014). Also at least two tMSP candidates have been reported in two GCs (Bahramian et al., 2018; Paduano et al., 2021). Therefore, GCs are ideal places for observing and studying a variety of X-ray MSPs, which helps us extensively understand the X-ray properties of MSPs.

1.4 The Galactic Center Excess

Since the launch of the *Fermi* Gamma-ray Space Telescope and its onboard Large Area Telescope (LAT), *Fermi* has been observing the entire sky, including the direction towards the Galactic Center, in the energy range of about 8 keV to 300 GeV, and found many intriguing phenomena. One of the most fascinating and puzzling findings by *Fermi* is the so-called Galactic Center gamma-ray excess (GCE), which is an excess of gamma-ray radiation towards the Galactic Center, peaking at ~ 2 GeV (see Murgia, 2020, for a review). The GCE was first claimed by Goodenough and Hooper (2009), and confirmed in the following studies by different groups (e.g., Hooper and Goodenough, 2011; Abazajian and Kaplinghat, 2012; Gordon and Macías, 2013; Calore et al., 2015; Daylan et al., 2016; Ajello et al., 2016). The origin of GCE is still unclear and controversial. However, based on its spectrum and spatial morphology, two explanations stand out: gamma rays produced by dark matter self-annihilation; and/or emission from a large number of unresolved MSPs.

It is predicted that dark matter made up by weakly interacting massive particles (WIMPs) can self-annihilate to produce gamma rays (see e.g. Bertone et al., 2005), and such gamma-ray emission is expected to be brightest towards the Galactic Center due to the high concentration of dark matter there (e.g. Springel et al., 2008). Therefore, the discovery of GCE is naturally considered as possible evidence of the existence and self-annihilation of dark matter in the Galactic Center (e.g. Goodenough and Hooper, 2009; Hooper and Goodenough, 2011), especially since the spatial distribution and spectral characteristics of the GCE are consistent with those of the predicted dark matter annihilation (e.g. Daylan et al., 2016; Di Mauro, 2021).

Another, more astrophysical interpretation suggests that the GCE originates from the gamma-ray emission produced by a large number of unresolved MSPs residing in the Galactic Center, given that their gamma-ray spectra and morphology are also compatible with those of the GCE (e.g., Abazajian and Kaplinghat, 2012; Brandt and Kocsis, 2015; Gonthier et al., 2018; Macias et al., 2018). In particular, Brandt and Kocsis (2015) suggested that such an MSP population in the Galactic Center might be generated from GCs disrupted by evaporation and gravitational tides. Based on the gamma-ray observations of MSPs resolved by *Fermi*, different groups generated MSP population syntheses and calculated the number of MSPs required to produce the GCE, which vary from $\sim 2,000$ to $\sim 40,000$ (e.g., Yuan and Zhang, 2014; Cholis et al., 2015b; Ploeg et al., 2017; Gonthier et al., 2018).

Other explanations of the GCE also have been proposed, including cosmic ray outbursts and/or interactions with molecular clouds in the Galactic Center region (e.g., Carlson and Profumo, 2014; Cholis et al., 2015a; Chernyshov et al., 2021). However, the origin of GCE is still a subject of debate, and hopefully, additional observations in other bands, such as X-rays, will reveal the nature of GCE.

1.5 The arc of the thesis

In this chapter, I briefly introduced MSP population in the Galaxy and X-ray emission from them. To better understand the X-ray properties of MSPs in GCs and subsequent implications, I will discuss a few X-ray MSPs in clusters in the following chapters. In Chapter 2, we look into the X-ray observations of M13 and analyze the X-ray properties of the six MSPs therein. In Chapter 3, we first present the X-ray analysis of two MSPs in Omega Cen, and then we compile X-ray MSPs in GCs and present a comprehensive X-ray census of GC MSPs. We also calculate predictions for the X-ray-detectable MSPs in the Galactic bulge in Chapter 3. We draw conclusions and discuss prospects in Chapter 4.

Chapter 2

MSPs in the Globular Cluster M13

2.1 Introduction

Radio millisecond pulsars (MSPs), also known as rotation-powered MSPs, are fast-spinning pulsars (spin periods $P \lesssim 30$ ms) with low spin-down rates ($\dot{P} \sim 10^{-21} - 10^{-19}$), implying large characteristic ages $\tau \equiv P/(2\dot{P}) \gtrsim 1$ Gyr, and relatively low magnetic field strengths $B_p \propto (P\dot{P})^{1/2} \sim 10^8 - 10^{10}$ G. Low-mass X-ray binaries (LMXBs) are conventionally considered the progenitors of MSPs, where a neutron star (NS) is spun up by accreting material from its companion star until it has a rotational period of a few milliseconds (Alpar et al., 1982; Bhattacharya and van den Heuvel, 1991). The high stellar densities of globular clusters (GCs) create numerous LMXBs, which then produce MSPs, and hence GCs provide ideal places to observe them in large numbers (Camilo and Rasio, 2005). To date, the total number of pulsars found in 30 GCs is 157, and more than 90% of them are MSPs¹.

MSPs are mostly found in binary systems, which is consistent with the evolution of MSPs via LMXBs. The so-called “spider” MSP binaries represent a distinct group of MSP binary systems with low-mass nondegenerate companion stars. Specifically, spider binaries are classified into two groups based on the companion masses: black widows with companion masses $M_c \sim 0.02 M_\odot$, and redbacks with companion masses $M_c \sim 0.2 M_\odot$ (Roberts, 2011). Alter-

¹For an up-to-date catalog of pulsars in GCs, see <http://www.naic.edu/~pfreire/GCpsr.html>

natively, MSPs may be coupled with compact objects, such as helium-core white dwarfs (WDs), which are the most common companions to MSPs in GCs (e.g. Camilo and Rasio, 2005). MSPs coupled with another neutron star or even a detected radio pulsar have been discovered in a few systems, like PSR J0737 – 3039 (Burgay et al., 2003).

Radio MSPs are also faint X-ray emitters, with typical luminosities of $L_X \sim 10^{30} - 10^{31} \text{ erg s}^{-1}$. For a few relatively young and energetic MSPs, like PSR B1821–24, the X-ray luminosities can reach up to $\sim 10^{33} \text{ erg s}^{-1}$ (e.g. Bogdanov et al., 2011b). The X-rays produced by MSPs can be characterized based on their spectral properties, namely thermal (blackbody-like spectra) or non-thermal (power-law spectra) emission (Becker and Trümper, 1999; Bogdanov, 2018). Thermal X-ray emission is believed to be generated from the hot surface of the NS, specifically from the hot spots near the magnetic polar caps, heated by the return flow of relativistic particles from the pulsar magnetosphere (e.g. Harding and Muslimov, 2002). Non-thermal X-ray emission can be further categorized into two sub-groups, i.e. pulsed and non-pulsed non-thermal emission. Pulsed non-thermal X-rays are observed with narrow X-ray pulsations, implying highly beamed X-ray radiation, which is most likely produced in the pulsar magnetosphere (Verbunt et al., 1996; Saito et al., 1997; Takahashi et al., 2001). Therefore, only very energetic MSPs with relatively strong spin-down luminosities could emit such X-ray radiation (e.g. Possenti et al., 2002). Non-pulsed non-thermal X-ray emission is commonly detected from spider pulsar systems, where the relativistic pulsar wind may collide with the material from its companion star, creating an intra-binary shock and emitting non-pulsed, non-thermal X-rays (e.g. Arons and Tavani, 1993; Stappers et al., 2003; Bogdanov et al., 2005; Gentile et al., 2014; Roberts et al., 2015).

The globular cluster M13 (NGC 6205) is located in the constellation of Hercules, with a low foreground reddening of $E(B - V) = 0.02$ (Harris, 1996, 2010 edition). The distance is slightly uncertain, with a range of reported values (mostly isochrone fitting to the colour-magnitude diagram, but also using RR Lyrae variables and the tip of the red giant branch) from $7.1 \pm 0.1 \text{ kpc}$ (Deras et al., 2019; Harris, 1996, (2010 revision)) to $7.9 \pm 0.5 \text{ kpc}$ (Barker

and Paust, 2018; Sandquist et al., 2010). We use the distance of 7.4 ± 0.2 kpc from the recent comprehensive study of Gontcharov et al. (2020) in this work. Should the true distance lie at 7.1 or 7.9 kpc, then values of luminosities in this paper would change by up to 10%.

To date, six MSPs have been found in M13 by several radio surveys (Kulkarni et al., 1991; Anderson, 1993; Hessels et al., 2007; Wang et al., 2020). PSRs J1641 + 3627A (hereafter MSP A) and J1641 + 3627C (hereafter MSP C) are isolated, while the other four MSPs are in binary systems. Specifically, PSR J1641 + 3627E (MSP E) is found in an eclipsing black widow system, with a minimum companion mass of $\sim 0.019 M_{\odot}$ (Wang et al., 2020). The nature of the companions for PSRs J1641 + 3627B (MSP B), J1641 + 3627D (MSP D), and J1641 + 3627F (MSP F) is not clear so far. New, precise radio timing solutions for the six MSPs in M13 were reported recently by Wang et al. (2020) using Five-hundred-meter Aperture Spherical radio Telescope (FAST) observations.

In this paper, we present X-ray spectral analyses of the six MSPs in M13 using archival *Chandra* observations. We also investigate the optical counterparts to those MSPs in binary systems, based on observations from the *Hubble Space Telescope* (*HST*). This work is organized as follows. In section 2.2, we describe the observations and data reduction procedures. In section 2.3, we present the X-ray spectral fitting results for the six MSPs, and the search for counterparts to the MSPs in optical/UV bands. We discuss the X-ray spectral properties and the nature of the companion stars in section 2.4. Finally, we draw conclusions in section 2.5.

2.2 Observation and data reduction

2.2.1 Chandra observations

The X-ray data used in this work consists of two *Chandra X-ray Observatory* observations of M13 in 2006, with a total exposure time of 54.69 kiloseconds (see Table 2.1). For both observations, the core of M13 was positioned on the back-illuminated ACIS-S3 chip and configured in FAINT mode.

Table 2.1: *Chandra* Observations of M13

Telescope/ Instrument	Date of Observation	Observation ID	Exposure Time (ks)
<i>Chandra</i> /ACIS-S	2006 Mar 09	7290	27.9
<i>Chandra</i> /ACIS-S	2006 Mar 11	5436	26.8

The data reduction and analysis were performed using CIAO² (version 4.12, CALDB 4.9.1, Fruscione et al. 2006). We first reprocessed the data with the `chandra_repro` script to generate new level 2 event files of the observations, applying the newest calibration updates and bad pixel files. We filtered the data to the energy range 0.5–7 keV, where the X-ray emission from MSPs may dominate over the instrumental background. No background flares were seen in the *Chandra* data.

We created a co-added image of M13 by merging the event files from the two observations using `reproject_obs` script. In Figure 2.1, the positions of the six MSPs are marked by blue circles with 1'' radii, centered on the precise radio pulsar timing positions (Wang et al., 2020). Other brighter X-ray sources are also visible in this image, including a quiescent low-mass X-ray binary (Shaw et al., 2018) and cataclysmic variables (e.g. Servillat et al., 2011). We formally detected the X-ray counterparts to most of the MSPs by applying the CIAO tool `wavdetect`, a Mexican-Hat Wavelet source detection tool (Freeman et al., 2002). We specified the wavelet scales (a list of radii in pixels) of 1.0, 1.4, and 2.0, and a significance threshold for source detection of 10^{-4} (false sources per pixel). Consequently, five X-ray counterparts were detected, all but MSP A, with positions consistent with the radio positions.

To analyse the X-ray spectra of the MSPs, we extracted the emission from the circular regions with a radius of 1'' centered on the radio positions in energy band 0.5–7 keV (Figure 2.1) for each MSP, using the `specextract` script. The extraction process was performed separately for each observation, and then we used the `combine_spectra` script to co-add the spectra correspondingly for each pulsar to obtain the combined spectra for spectral analysis. The

²Chandra Interactive Analysis of Observations, available at <https://cxc.harvard.edu/ciao/>

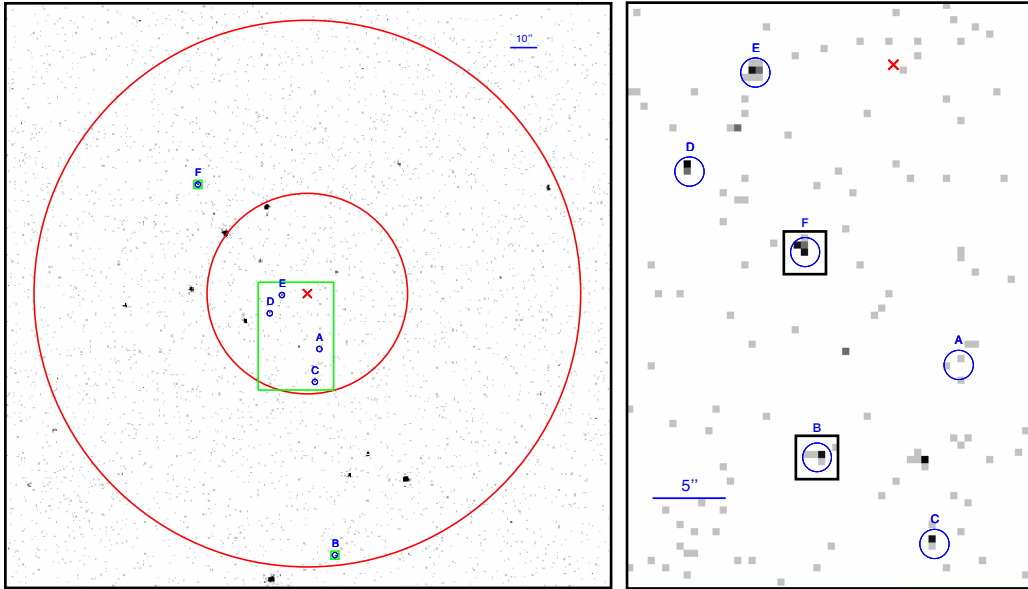


Figure 2.1: Left: merged 0.5–7 keV Chandra X-ray image of M13, with the positions of the 6 known MSPs labeled (blue circles with 1'' radii and letters). The center of M13 is marked with a red cross. The smaller red circle shows the 0'.62 core radius of M13, while the larger one shows the 1'.69 half-light radius of M13 (Harris, 1996, 2010 edition). The green boxes surrounding the MSPs are detailed in the right figure. Right: the 28'' \times 40'' core region of M13 which includes MSPs A, C, D, and E (the largest green box in the left figure). MSPs B and F are inset at source-free places with the same scale. The X-ray emission from all MSPs but A are clearly visible. North is up, and east is to the left. Brighter X-ray sources visible in the left image include cataclysmic variables and a quiescent X-ray binary (see Servillat et al., 2011; Shaw et al., 2018).

background was taken from source-free annular regions around the MSPs.

2.2.2 Optical observations

We use imaging data taken by the Wide Field Camera 3 (WFC3; GO-12605) and Advanced Camera for Surveys (ACS; GO-10775) on board the *HST*. GO-12605 (PI: Piotto) contains exposures in two UV filters, F275W (UV₂₇₅) and F336W (U₃₃₆), along with an exposure in F438W (B₄₃₈); while GO-10775 (PI: Sarajedini) is comprised of exposures in V₆₀₆ (F606W) and I₈₁₄ (F814W). For all filters, we retrieved the FLC data products from the Mikulsky Archive for Space Telescope (MAST)³; these are images that have been pipe-lined, flat-fielded, and have charge transfer efficiency trails removed. Detailed information on these observations is summarised in Table 2.2.

To search for faint potential counterparts to the MSPs, we use the DRIZZLEPAC software (version 3.1.6)⁴ to generate combined *HST* images. FLC files in each filter are first re-aligned by the `TweakReg` tool to a reference image (chosen to be the longest FLC exposure) and then combined using the `AstroDrizzle` tool. `AstroDrizzle` corrects for geometric distortion, flags cosmic rays and small-scale detector defects, and combines images with user-defined re-sampling. We use $pixfrac = 1.0$ and oversample the combined images by a factor of two, so the final images have half the original pixel scales (0.02"/pixel for WFC3, 0.025"/pixel for ACS).

Starting from December 2019, MAST released updated absolute astrometry information for ACS and WFC3 data. Most FLC data products are now aligned to the Gaia DR2 catalogue, reducing the astrometric uncertainties to ~ 10 mas⁵. The observed M13 fields contain stars included in Gaia DR2, so we use the default WCS information to set our absolute astrometry.

³<https://archive.stsci.edu/hst/search.php>

⁴<https://www.stsci.edu/scientific-community/software/drizzlepac>

⁵<https://archive.stsci.edu/contents/newsletters/may-2020/new-absolute-astrometry-for-some-hst-data-products>

GO	Exposure (s)	Observation Start	Instrument	Filter
10775	567	2006-04-02 10:41	ACS/WFC	F606W (V_{606})
10775	567	2006-04-02 12:15	ACS/WFC	F814W (I_{814})
12605	1281	2012-05-14 01:52	WFC3/UVIS	F275W (UV_{275})
12605	1281	2012-05-17 03:54	WFC3/UVIS	F275W (UV_{275})
12605	700	2012-05-14 02:24	WFC3/UVIS	F336W (U_{336})
12605	700	2012-05-17 04:48	WFC3/UVIS	F336W (U_{336})
12605	92	2012-05-14 01:49	WFC3/UVIS	F438W (B_{438})
12605	92	2012-05-17 03:26	WFC3/UVIS	F438W (B_{438})

Table 2.2: HST observations used in this work.

2.3 Data analysis and results

2.3.1 X-ray spectral fits

We performed all spectral fits using CIAO’s modeling and fitting application, Sherpa⁶. X-ray emission from MSP A was only detected in the latter observation (Obs ID: 5436) with just two photons. We cannot determine whether the two photons originated from MSP A, or are just background emission. However, we fitted the spectrum of MSP A, and set the obtained fits as the upper limits, finding $L_X < 1.3 \times 10^{30} \text{ erg s}^{-1}$. The other five MSPs in M13 (MSPs B, C, D, E, and F) show faint and relatively soft X-ray emission (Figure 2.2), with X-ray luminosities $\sim 3 \times 10^{30} - 10^{31} \text{ erg s}^{-1}$. We adopted the WSTAT statistic⁷, a Poisson log-likelihood function including a Poisson background, within Sherpa to fit X-ray spectra with few photons. In addition, we grouped the data to include at least one photon in each bin due to the limited number of photons (Humphrey et al., 2009). For all six detected MSPs, we fitted the spectra by fixing the hydrogen column density (N_H) to the cluster. We estimated N_H from the known reddening (Harris, 1996, 2010 edition) and an appropriate conversion factor (Bahramian et al., 2015) and obtained a value of $1.7 \times 10^{20} \text{ cm}^{-2}$, given that interstellar extinction $E(B - V)$ generally gives the best predictions of N_H (He et al., 2013).

We considered spectral models of the X-ray emission from MSPs (Bogdanov

⁶Available at <https://cxc.cfa.harvard.edu/sherpa/>

⁷See <https://heasarc.gsfc.nasa.gov/xanadu/xspec/manual/XSappendixStatistics.html> for more details.

et al., 2006) involving a blackbody (BB), a power-law (PL), and combinations of these. For the BB model, we used the `xsbbodyrad` model in Sherpa, and the free parameters were the effective temperature and the normalized radius. The PL model was fitted using `xspgprlw`, with the photon index and flux as free parameters. Figure 2.2 shows the X-ray spectra and best fits of the six MSPs, and the best-fit models and parameters are given in Table 2.3. We used the Q-value, which is a measure of what fraction of simulated spectra would have a larger value of the reduced statistic than the observed one, if the assumed model and the best-fit parameters are true, to indicate the goodness of the fits. The Q-values in Table 2.3 are above 0.05, indicating that these are reasonable fits and hence the Q-values themselves did not rule out any models.

The spectra of all six MSPs in M13 are well described by either a pure BB model or a pure PL model. (We tested BB+PL and BB+BB models, but these did not give better fits, so we only discuss simple one-component fits henceforth.) Although we cannot rule out either model from Q-values alone, other fitting parameters, like effective temperature and photon index, provide reasons to exclude models. For instance, if we fit the spectra of MSPs C, D, and F using a PL model, the obtained photon indices are nearly 4, which are empirically not observed from MSPs, given the typical photon indices of MSPs $\Gamma \sim 1.5$ (e.g. Zhang and Cheng, 2003; Bogdanov et al., 2006, 2011b). Similarly, if we fit MSPs B and E using a single BB model, the fitted effective temperatures are too high while the fitted effective radii are too small for MSPs, compared to other MSPs in GCs (e.g. Bogdanov et al., 2006; Forestell et al., 2014), and hence we can rule out the BB model for these two MSPs. Alternatively, the spectra of MSPs B and E are well described by a pure power-law model, with spectral photon indices $\Gamma = 1.8 \pm 0.7$ and 2.2 ± 0.6 , respectively. Given that MSP E is a “black widow” pulsar, the bulk of its observed non-thermal X-rays are likely to be produced by interaction of the relativistic particle wind from the pulsar with matter lost from the companion. MSPs C, D, and F have X-ray spectra well fitted with a pure blackbody spectrum, implying no or little X-ray emission from a pulsar magnetosphere and/or intra-binary shock. Blackbody-like X-ray spectra are common from

MSPs (e.g. Bogdanov et al., 2006), and likely originate from small hot spots at the magnetic poles heated by relativistic particles in the pulsar magnetosphere (e.g. Harding and Muslimov, 2002).

Particularly, since we only have two photons from MSP A, we need to fix one more parameter to obtain at least one degree of freedom. In order to determine the upper limit of the luminosity of MSP A, we fixed the effective temperature T_{eff} and photon index Γ for the BB and PL models in the fitting processes, respectively. The value of the fixed T_{eff} was obtained by averaging the fitted T_{eff} of MSPs C, D, and F, giving a value of $T_{\text{eff}} = 1.6 \times 10^6$ K, while the fixed Γ was given by the mean value of photon indices of MSPs B and E, providing $\Gamma = 2.0$ (see Table 2.3). Both models gave an upper limit of X-ray luminosity of 1.3×10^{30} erg s $^{-1}$ (0.3–8 keV).

MSP	Spectral Model ^a	$R_{\text{eff}}^{\text{b}}$ (km)	T_{eff} (10^6 K)	Photon Index	Reduced Stat ^c /Q-value	F_X (0.3–8 keV) (10^{-15} erg cm ⁻² s ⁻¹)
A	BB	$0.3^{+0.1}_{-0.1}$	[1.6] ^d	–	0.09/0.77	$0.2^{+0.2}_{-0.1}$
	PL	–	–	[2.0] ^d	0.31/0.58	$0.2^{+0.1}_{-0.1}$
B	BB	$0.02^{+\infty}_{-0.02}$ ^e	$7.4^{+\infty}_{-7.4}$ ^e	–	1.55/0.17	$1.1^{+\infty}_{-1.1}$ ^e
	PL	–	–	1.8 ± 0.7	1.11/0.35	$1.4^{+0.7}_{-0.7}$
C	BB	$0.4^{+0.3}_{-0.4}$ ^f	$1.5^{+0.4}_{-0.4}$	–	0.23/0.88	$0.6^{+0.2}_{-0.1}$
	PL	–	–	3.9 ± 1.2	0.29/0.83	$0.9^{+0.6}_{-0.6}$
D	BB	$0.4^{+0.3}_{-0.4}$ ^f	$1.6^{+0.4}_{-0.4}$	–	1.42/0.21	$0.9^{+0.2}_{-0.1}$
	PL	–	–	3.7 ± 0.9	2.05/0.07	$1.3^{+0.7}_{-0.7}$
E	BB	$0.07^{+0.04}_{-0.07}$ ^f	$3.8^{+1.0}_{-1.0}$	–	0.84/0.58	$1.2^{+1.9}_{-0.9}$
	PL	–	–	2.2 ± 0.6	0.75/0.67	$1.9^{+0.7}_{-0.7}$
F	BB	$0.4^{+0.2}_{-0.4}$ ^f	$1.7^{+0.3}_{-0.3}$	–	0.94/0.48	$1.2^{+0.2}_{-0.1}$
	PL	–	–	3.7 ± 0.7	1.04/0.40	$2.0^{+0.8}_{-0.8}$

Table 2.3: Spectral fits for the M13 MSPs. a) PL = power-law, BB = blackbody. The hydrogen column density was fixed to $N_{\text{H}} = 1.7 \times 10^{20}$ cm⁻². All uncertainties are 1σ . b) R_{eff} calculated assuming a distance of 7.1 kpc. c) Reduced statistic, calculated by the fit statistic divided by the degrees of freedom. d) Obtained by averaging the best spectral fits of other MSPs. See section 2.3.1 for more details. e) Bounds unavailable. f) Model reached lower bound.

2.3.2 Optical/UV photometry

We use the DOLPHOT software (version 2.0) to generate photometry catalogues for the WFC3 and ACS images. DOLPHOT is a photometry package based on HSTPHOT (Dolphin, 2000) which provides pipelines to perform aperture and PSF photometry on individual FLC images. We first choose the U_{336} and I_{814} drizzle-combined images⁸ as the reference frames for WFC3 and ACS, on which DOLPHOT runs a detection algorithm to find stars. The reference images also provide master coordinates (x, y) to which stars on individual FLC frames are transformed. In the next step, we mask the flagged bad pixels in all FLC images using the `wfc3mask` and `acsmask` tools. These tools also multiply the FLC images and the pixel areas, converting the pixel units to electrons. The final photometry routine runs on separate CCD chips, which are extracted from the FLC images by the `splitgroups` tool. These chip-specific images are also needed for the `calcsky` tool to create corresponding sky images. With all these preparations, we finally run the `dolphot` routine for WFC3 and ACS, adapting a photometry aperture (`img_RApert`, in pixels) of 8, and a PSF radius (`img_RPSF`, in pixels) of 15, while defining a sky annulus (`img_RSky`, in pixels) with inner and outer radii of 9 and 14, respectively, for PSF photometry. The final magnitudes are calibrated to the VEGMAG system using updated photometry zeropoints for ACS⁹ (Sirianni et al., 2005) and WFC3¹⁰.

We keep stars with $S/N > 5$ and rule out non-star objects, leaving cleaned catalogues to make colour-magnitude diagrams (CMDs; Figure 2.3, 2.4). These catalogues are used to compare the potential counterpart’s photometry with the bulk of stars of the cluster.

2.3.3 Optical/UV counterparts

Since the radio timing solution provides much more accurate localisation (\sim mas; Wang et al. 2020) than the *Chandra* imaging (error radius $\sim 0.5''$), we ex-

⁸Note that the drizzle-combined images used here are in their native pixel scales.

⁹<https://acszeropoints.stsci.edu/>

¹⁰<https://www.stsci.edu/hst/instrumentation/wfc3/data-analysis/photometric-calibration/uvis-photometric-calibration>

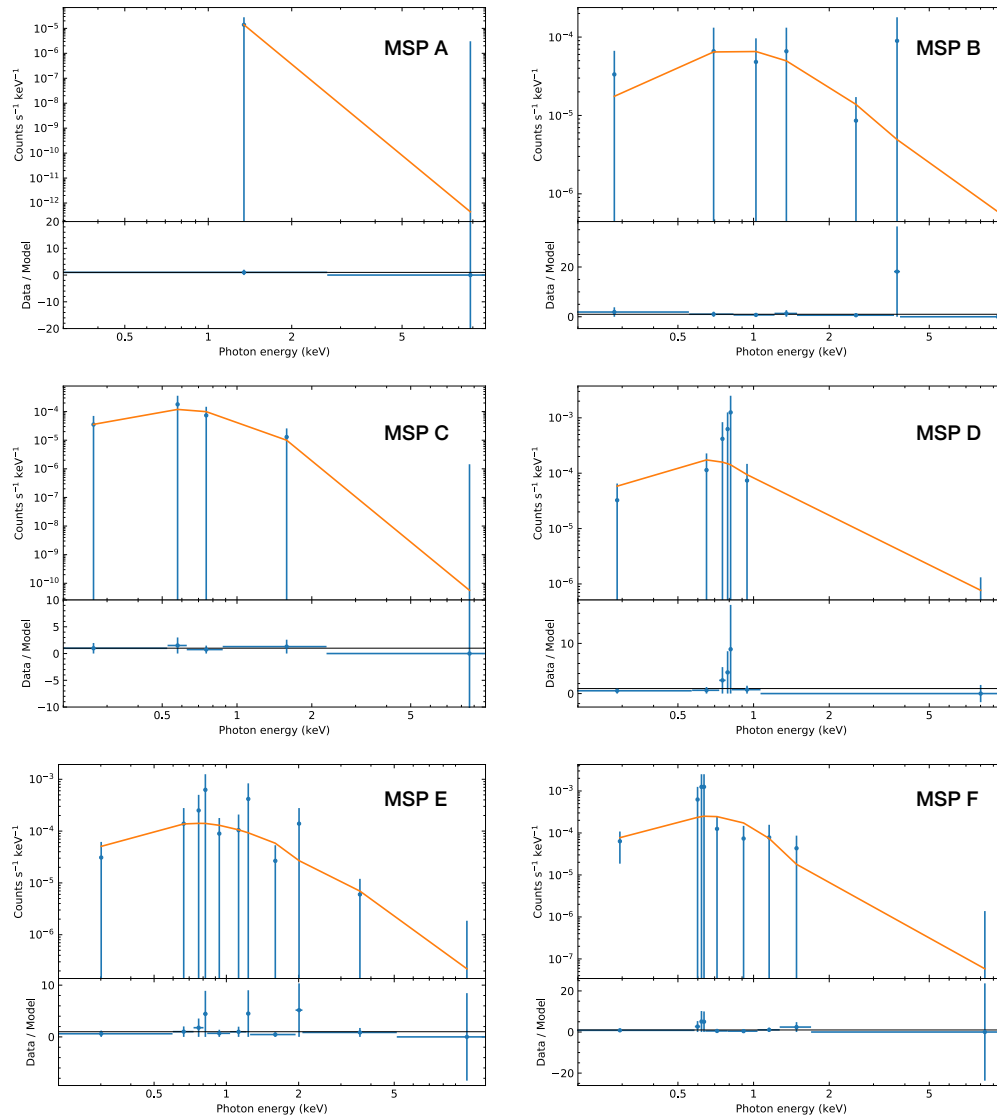


Figure 2.2: X-ray spectra and best fits for five MSPs in M13. The data are binned with 1 count/bin, and fitted using the WSTAT statistic.

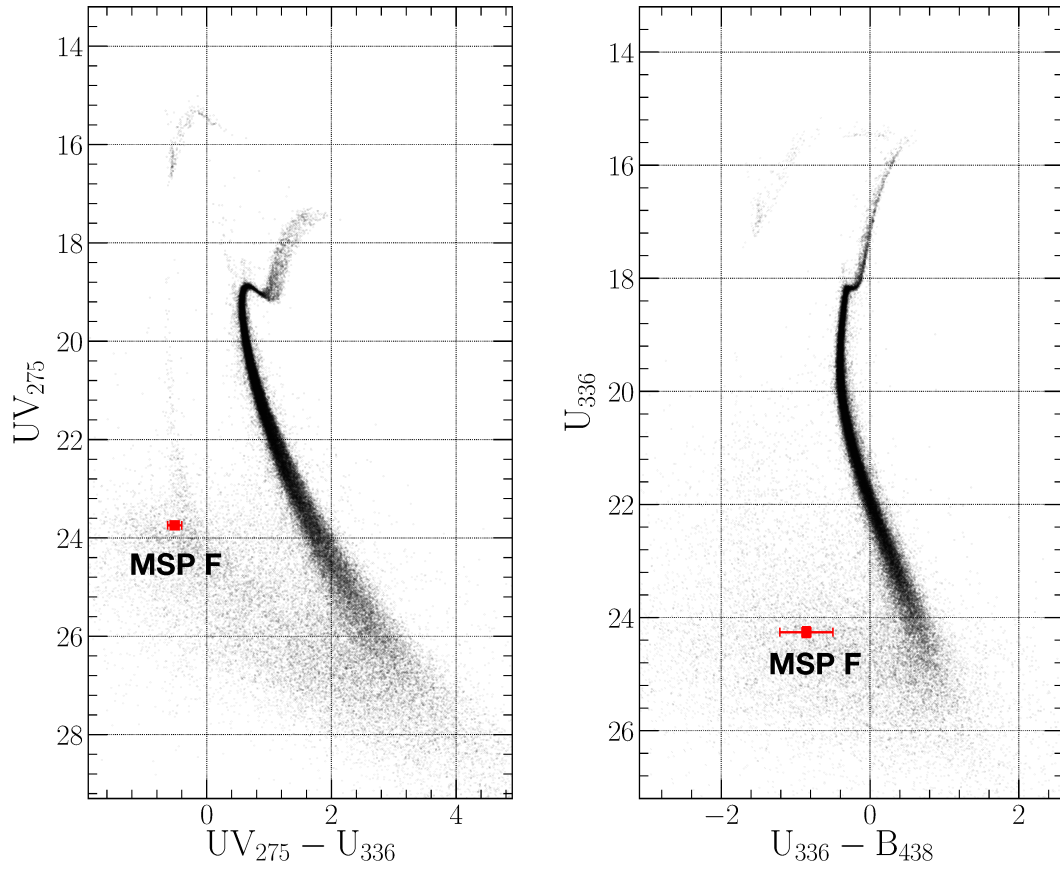


Figure 2.3: $UV_{275} - U_{336}$ and $U_{336} - B_{438}$ CMDs of M13. The red square marks the location of the counterpart to MSP F, which is bluer than the main sequence, consistent with the white dwarf cooling sequence.

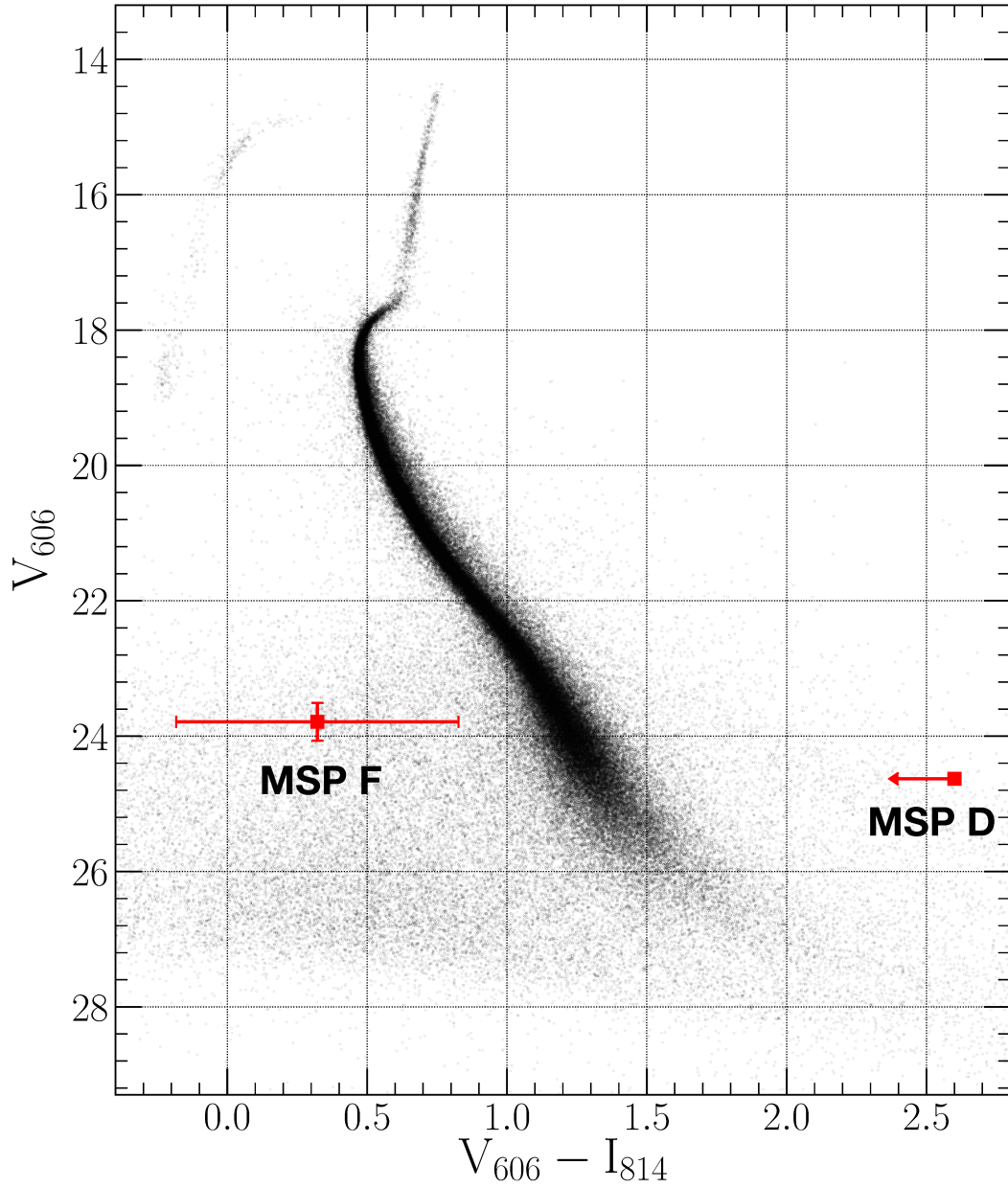


Figure 2.4: $V_{606} - I_{814}$ CMD of M13. Red squares mark the counterparts to MSP D and MSP F. The former was not detected in I_{814} , so only a 3σ upper limit is put on its $V_{606} - I_{814}$ colour.

pect potential counterparts in the vicinity of the corresponding radio position. We therefore search around the radio timing positions for optical counterparts in the drizzle-combined images; this leads to the discovery of optical/UV counterparts to two of the 6 MSPs: MSP D and F, both of which are very close ($\approx 0.02''$) to the radio positions. We report their photometric properties in the following paragraphs.

MSP D

The counterpart to MSP D is a faint star 15 mas north from the radio timing position (Figure 2.5). Although the counterpart is visible by visual inspection in the V_{606} -band image (Figure 2.5), it was not measured by DOLPHOT. We hereby make a rough estimate of its magnitude by performing aperture photometry, using an aperture of $0.1''$ to enclose most of the PSF of the star. Since the counterpart is in the vicinity of a very bright star, we also estimate background counts with the same aperture size in a nearby source-free region. The background-subtracted counts are then calibrated to DOLPHOT magnitude by $V_{606} = -2.5 \log_{10}(\text{net counts}) + 33.31$, giving $V_{606} \approx 24.63$. We set a lower limit on the I_{814} band magnitude at 3 times the local background counts, which gives $I_{814} \gtrsim 22.03$. The upper limit on the $V_{606} - I_{814}$ colour is on the red side of the main sequence.

MSP F

We found a faint star ≈ 22 mas east from the radio timing position (Figure 2.5). The counterpart to MSP F appears to be bluer than the main sequence on all three CMDs (Figure 2.3, 2.4), and overlaps the white dwarf cooling sequence on the $UV_{275} - U_{336}$ CMD. This is expected in MSPs descended from binary evolution with a giant companion (e.g., Stairs, 2004), wherein the NS exhausts the companion's envelope via continued mass accretion, resulting in a WD companion (e.g., Sigurdsson et al., 2003; Splaver et al., 2005; Cadelano et al., 2019). After submission of this manuscript, we became aware of Cadelano et al. (2020), which independently identified the optical counterpart to the MSP M13 F, and used photometry in additional *HST* filters to characterize

the companion as a $0.23 M_{\odot}$ He-core white dwarf. Our optical counterpart analysis is consistent with theirs, though not as constraining.

Chance coincidence

We estimate the number of chance coincidences (N_c) by dividing the cluster field into concentric annuli centered on the cluster, and calculating the probability of a coincidence within our search area. The radio position offers a much smaller search area than the X-ray position, so we use the radio error circle to assess the chance coincidence rate. The uncertainty in the radio position comes from the uncertainty in the radio timing position from Wang et al. (2020), which we estimate to be 3 mas at most (noting that the uncertainty in declination is missing from M13 F in Wang et al. 2020’s Table 2), and from the uncertainty in *HST*’s absolute astrometry (10 mas, see §2.2), giving a total uncertainty in the radio position in the *HST* frame of ~ 10 mas.

Based on the $UV_{275} - U_{336}$ CMD, we count numbers of objects that align with the main sequence and the white dwarf sequence within each annulus. We did not apply proper-motion cleaning to the CMD, since we are comparing the estimated counts to actual observed numbers of sources in each search area. The counts are then divided by the annulus areas to give the N_c per unit area, which is then multiplied by the search area of MSP D and MSP F (10 mas of radius) to give the N_c per search area. We estimate ≈ 0.001 main sequence stars within the search region of MSP D, and $\approx 4 \times 10^{-6}$ WDs in the search region of MSP F. Both counterparts to these MSPs are therefore very unlikely to be chance coincidences.

2.4 Discussion

The majority of X-ray emission from most isolated MSPs is thermal radiation with blackbody-like spectra (e.g. Bogdanov et al., 2006; Forestell et al., 2014), which is believed to result from polar cap heating from inverse Compton scattering (e.g. Harding and Muslimov, 2002). The observed spectrum of MSP C is a typical example of those of isolated MSPs. However, some rela-

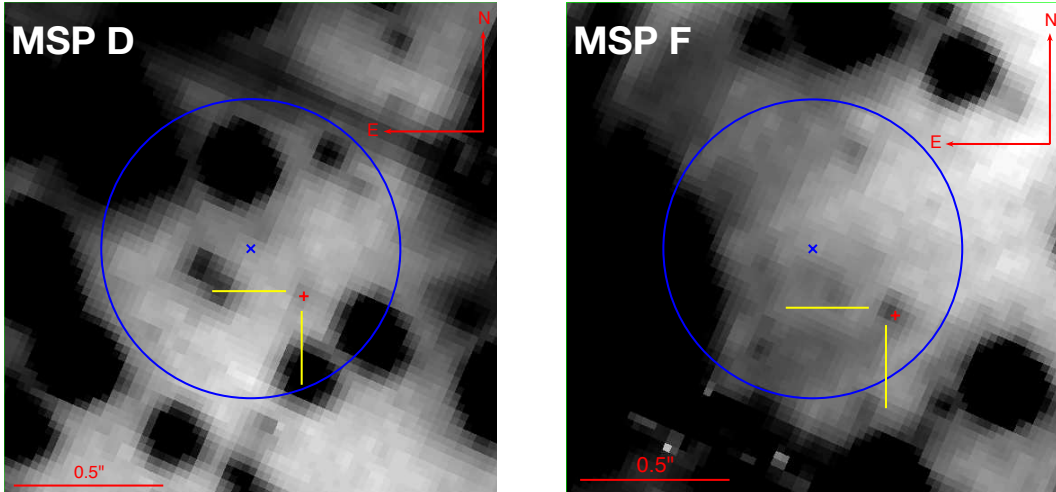


Figure 2.5: V_{606} finding charts for MSP D (left) and MSP F (right), showing a $1''.65 \times 1''.65$ square region centred on the X-ray position. North is up, and east is to the left. The blue cross in each chart indicates the centre of the X-ray position error circle, while the blue circle shows the 95% error region given the X-ray counts (Hong et al., 2005). The red cross marks the radio timing position from Wang et al. (2020), and the optical counterparts are indicated with yellow crosshairs.

tively young MSPs with high spin-down power, like B1821–24 in the globular cluster M28 (Saito et al., 1997; Bogdanov et al., 2011b), produce pulsed non-thermal radiation generated by relativistic particles accelerated in the pulsar magnetosphere.

Intriguingly, given the upper limit of X-ray luminosity of $1.3 \times 10^{30} \text{ erg s}^{-1}$ (0.3–8 keV), MSP A is unusually faint, compared to other GC MSPs. We compare it to MSPs detected in Chandra X-ray observations that reached a sensitivity limit of $L_X < 10^{30} \text{ erg s}^{-1}$. Only one MSP among 23 studied in X-rays in 47 Tuc (Bogdanov et al., 2006; Ridolfi et al., 2016; Bhattacharya et al., 2017), namely PSR J0024–7205aa (Bhattacharya et al., 2017), and one MSP among the five MSPs in NGC 6752, namely PSR J1910–5959E (Forestell et al., 2014), have X-ray luminosities slightly less than that upper limit of MSP A. Bogdanov et al. (2011b) study 12 MSPs in M28, and report detections of 8 MSPs with L_X between 1.0×10^{30} for M28 D, and $10^{33} \text{ erg s}^{-1}$ for M28 A, with three upper limits due to confusing, brighter sources.¹¹ Four other

¹¹Bogdanov et al. (2011b) report an upper limit $< 1.0 \times 10^{30} \text{ erg s}^{-1}$ for M28 I, but the

nearby globular clusters have deep X-ray and radio observations, with known MSPs: M22, NGC 6397, M71, and M4. Those four clusters each contain one, brighter, MSP (Grindlay et al., 2001; Bassa et al., 2004; Elsner et al., 2008; Amato et al., 2019). Thus, among 47 detectable MSPs in these eight well-studied clusters, MSP A is one of the faintest four in X-rays (along with 47 Tuc aa, NGC 6752 E, and M28 D), and possibly the faintest. We cannot rule out either X-ray spectral model, by either Q-values or the fitted parameters, for MSP A. We prefer, however, the BB model, as MSP A is an isolated MSP. MSP A may have a relatively small spindown power, producing its relatively small X-ray luminosity. We cannot calculate its characteristic age or spindown power, due to its acceleration within the gravitational potential of M13, which produces an observed negative spin period derivative. Alternatively, MSP A may appear to have a low X-ray luminosity due to an unfavorable inclination of its spin axis with respect to Earth, with one or both hot spots on the far side from Earth (Riley et al. 2019 and Miller et al. 2019 showed that PSR J0030+0451 has both hot spots in a single hemisphere).

MSPs B, D, E, and F are in binary systems, with orbital periods ranging from 0.1 to 1.4 days (Wang et al., 2020). The X-ray spectra of MSPs B and E are well described by a pure power-law model, indicating that the X-rays from them are predominantly non-thermal. Non-pulsed non-thermal emission is anticipated for MSP E, since it has been identified as an eclipsing black widow pulsar. In eclipsing spider pulsar systems, X-rays are thought to originate from intra-binary shocks, driven by the interaction of the relativistic pulsar wind with matter from its companion star (e.g. MSPs J0023–7203J and J0024–7204W in 47 Tuc, Bogdanov et al., 2006). Particularly, intra-binary shock emission with orbital modulation has been observed in many spider pulsar binaries (e.g. Bogdanov et al., 2011a; Gentile et al., 2014; Al Noori et al., 2018).

The nature of the companion star of MSP B, which is in a 1.39-day orbit and has a minimum mass of $0.16 M_{\odot}$ (assuming a pulsar mass of $1.4 M_{\odot}$,

position of M28 I used there proved to be incorrect, and the true L_X of M28 I in its pulsar mode is $1 - 2 \times 10^{32}$ erg s⁻¹ Papitto et al. (2013); Linares et al. (2014).

Wang et al., 2020), is not clear yet. The best-fit spectral model (a power-law of photon index 1.8 ± 0.7) requires either a magnetospheric origin (and thus a relatively high spindown energy loss rate to produce this), or an intrabinary shock origin, in which case (given the companion mass) MSP B would be a redback system. We consider the 21 MSPs in the globular cluster 47 Tuc with X-ray spectra that can be individually fit (Bogdanov et al., 2006; Ridolfi et al., 2016; Bhattacharya et al., 2017). The 17 systems that are not black widows and redbacks are all best fit by thermal blackbody spectra, while two of the three black widows (47 Tuc J,O,R), and the redback (47 Tuc W) all showed dominant power-law components to their spectra. Thus, it seems likely that MSP B is a redback system. No eclipses were detected in the radio observations of MSP B (Wang et al., 2020), which could be due to a relatively low inclination, as observed in the black widows 47 Tuc I and P (Freire et al., 2003). As intra-binary shocks are expected to emit X-rays in all directions (though not isotropically), the non-thermal X-rays may be detected at any inclination.

The optical counterparts to MSPs D and F were found with *HST* observations (Figure 2.5). According to the position of the counterpart to MSP F on the CMDs of M13 (Figure 2.3), as well as the minimum companion mass of $\sim 0.18 M_{\odot}$, a white dwarf is the most likely companion star of MSP F. We also found a plausible optical counterpart to MSP D, which is only detected in the V band. We cannot identify the nature of MSP D’s companion star definitively, due to its very faint magnitude leading to a large uncertainty of its location on the CMD (see Figure 2.4). The observed magnitudes are consistent with the rather broad expectations of MSP white dwarf companions (van Kerkwijk et al., 2005).

The X-ray spectrum of MSP D is well described by a pure blackbody model, implying that emission from the neutron star surface dominates, and that there is no intra-binary shock. Since all known redback binary systems show hard non-thermal X-ray emission (Bogdanov, 2018), this indicates that MSP D is probably not in a redback binary. With a minimum companion mass of $\sim 0.18 M_{\odot}$, we suggest that the companion star of MSP D is also a

helium-core white dwarf.

2.5 Conclusions

In this report, we have presented X-ray and optical studies of the six MSPs in the globular cluster M13 by using archival *Chandra* and *HST* observations. Five of the six MSPs are firmly detected (MSPs B, C, D, E, and F) by *Chandra*, with X-ray luminosities $L_X \sim 3 \times 10^{30} - 10^{31} \text{ erg s}^{-1}$ (0.3–8 keV), while MSP A is plausibly detected with an upper limit in X-ray luminosity of $1.3 \times 10^{30} \text{ erg s}^{-1}$. The uncommonly X-ray-faint properties of MSP A may imply that one or both its hot spots are on the far side from Earth.

The X-ray spectra of the six MSPs are well-described by either a single blackbody or a single power-law model. As expected, the spectra of two isolated MSPs, MSPs A and C, are well fitted by a pure blackbody model, indicating thermal X-ray emission from the surface of these two objects. The identified black widow binary system, MSP E (Hessels et al., 2007; Wang et al., 2020), emits principally non-thermal X-rays which are likely generated from intra-binary shock. Similarly, the X-ray emission from MSP B, a binary system with a companion of mass $\sim 0.2 M_\odot$ (Wang et al., 2020), is non-thermal as well. Based on its non-thermal spectral properties and companion mass, we suggest MSP B is a redback binary system.

We searched for the optical counterparts to the four MSP binary systems in M13 using *HST* archival data in the vicinity of the respective radio timing positions, and discovered optical counterparts to MSPs D and F. The position of the counterpart to MSP F on color-magnitude diagrams shows that the companion star is most likely a white dwarf. The counterpart to MSP D is faint and only observed in V band, resulting in a large uncertainty of its position on color-magnitude diagrams. However, given MSP D’s blackbody-like X-ray spectrum and companion mass of $\sim 0.2 M_\odot$ (Wang et al., 2020), we argue that the counterpart to MSP D is also likely to be a helium-core white dwarf. To our knowledge, this is the first use of the X-ray properties of a radio millisecond pulsar to predict the nature of its companion star.

Chapter 3

X-ray Census of GC MSPs

3.1 Introduction

Galactic globular clusters (GCs) are ideal birthplaces for low-mass X-ray binaries (LMXBs), since the high stellar densities in GC cores provide significant chances for stellar interactions, such as tidal capture and exchange interactions (see e.g., Fabian et al., 1975; Hills, 1976). LMXBs are the progenitors of millisecond pulsars (MSPs), where the neutron star (NS) is spun up by accreting mass and angular momentum from its companion to a period of a few milliseconds (Alpar et al., 1982; Bhattacharya and van den Heuvel, 1991; Papitto et al., 2013). Therefore, it is not surprising that GCs show an overabundance of MSPs compared to the Galactic field, and many MSPs exist in binary systems.

Rotation-powered MSPs are rapidly and stably spinning pulsars, with spin periods $P \lesssim 25$ ms and spin-down rates $\dot{P} \sim 10^{-20}$, with lifetimes of Gyrs. Apart from isolated MSPs, MSPs in binaries can be further categorized according to the degeneracy of the companion star. Those MSPs coupled with non-degenerate companion stars are usually referred to as ‘spider’ MSPs, and based on the companion masses, they are further grouped as redbacks ($M_c \sim 0.2 M_\odot$, hereafter RBs) and black widows ($M_c \sim 0.02 M_\odot$, hereafter BWs), respectively. In addition, it is common that eclipses of the radio emission commonly occur in observations of spider pulsars, which can be explained as the radio emission from the MSP being absorbed and/or scattered by the plasma produced at the collision between the relativistic pulsar wind and material from

the companion (Fruchter and Goss, 1992; Thompson et al., 1994; Stappers et al., 2001; Polzin et al., 2018; Zhao et al., 2020b). On the other hand, the companion stars of MSPs may also be compact objects, and particularly white dwarfs (WDs) are the most common companions among these MSP binaries (e.g. Lorimer, 2008).

MSPs are generally faint X-ray sources, with typical luminosities of $L_X \lesssim 10^{31} \text{ erg s}^{-1}$. The X-rays from MSPs commonly are observed with blackbody-like spectra (e.g. Zavlin et al., 2002; Bogdanov et al., 2006), indicating a thermal emission origin likely produced from the hotspots at the NS magnetic poles, heated by the returning particles accelerated in the pulsar magnetosphere (Harding and Muslimov, 2002). A few MSPs are relatively X-ray-bright with $L_X \gtrsim 10^{32} \text{ erg s}^{-1}$, up to $\sim 10^{33} \text{ erg s}^{-1}$, and their X-ray emission usually shows non-thermal properties (e.g. power-law spectra). For instance, the most luminous X-ray MSP in GCs found to date is PSR B1821–24 in M28, with $L_X = 1.4 \times 10^{33} \text{ erg s}^{-1}$ (0.3–8 keV, Saito et al., 1997; Becker et al., 2003; Bogdanov et al., 2011b). Moreover, the X-ray pulsations from this MSP were clearly observed in two narrow pulses (Saito et al., 1997; Rutledge et al., 2004), implying the highly beamed non-thermal emission originated from the pulsar magnetosphere. The other type of non-thermal X-ray emission from MSPs, i.e. non-pulsed non-thermal emission, is typically detected from spider pulsars and believed to be produced by relativistic intra-binary shocks as a result of collisions between pulsar wind and matter outflow from the companion (e.g. Arons and Tavani, 1993; Wadiasingh et al., 2018; Kandel et al., 2019).

X-ray studies of GC MSPs have been presented for a few GCs, especially pulsar-rich clusters such as 47 Tuc (Bogdanov et al., 2006), NGC 6397 (Bogdanov et al., 2010), M28 (Bogdanov et al., 2011b), NGC 6752 (Forestell et al., 2014), and recently on Terzan 5 (Bogdanov et al., 2021), M62 (Oh et al., 2020) and M13 (Zhao et al., 2021), as well as for several individual MSPs in globular clusters (e.g. Bassa et al., 2004; Amato et al., 2019). These studies provide opportunities to statistically investigate the X-ray properties of GC MSPs. However, different groups may apply different energy bands for spectral fitting and analysis, making it difficult to study those GC MSPs together directly.

Possenti et al. (2002) used a sample of 39 pulsars, including both MSPs and normal pulsars in GCs and the Galactic field, to re-examine the correlation between X-ray and spin-down luminosities, where they converted all the fluxes to 2–10 keV. Recently, Lee et al. (2018) focused on X-ray MSPs in the Galactic field and conducted a survey of their X-ray properties. They simply applied a pure power-law model for all of the sampled MSPs and normalized the energy band to 2–10 keV as well. However, the derived X-ray luminosities of MSPs in these works may have large uncertainties, mainly due to the difficulties of measuring distances to the field MSPs (e.g. Igoshev et al., 2016). By contrast, the distance to a GC can be measured much more accurately than to a field MSP, and hence the uncertainty of distance to MSPs in a GC may be largely reduced (now <5%, e.g. Baumgardt and Vasiliev, 2021).

In this chapter, we present an X-ray survey for all the radio-detected MSPs in Galactic GCs which have *Chandra X-ray observatory* data, and which lack the confusion of bright LMXBs. We also report the X-ray spectral analyses of two newly found MSPs in the cluster Omega Centauri, using archival *Chandra* observations, and statistically study the X-ray properties of GC MSPs, with particular attention to the implications for X-ray studies of the population of MSPs in the Galactic Center. This chapter is organized as follows. In Section 2, we described the criteria of data collection, reduction and normalization. In Section 3, we present the results of X-ray spectral fitting for the two new MSPs and newly detected X-ray sources in three GCs. Also we present the X-ray census of GC MSPs and further analyses of their X-ray properties. We discuss our results and the implications in Section 4, and we draw conclusions in Section 5.

3.2 Data Collection and Reduction

Table 3.1: Parameters for the GCs in this work.

GC Name	Distance ^a (kpc)	N_{H}^b (cm^{-2})	N_{MSP}^c	Encounter Rate ^d Γ_{SE}	Lim. L_X^e (erg s^{-1})	Reference of Lim. L_X
47 Tuc (NGC 104)	4.5	3.48×10^{20}	27	1000 ⁺¹⁵⁴ ₋₁₃₄	3×10^{29}	(1)
NGC 1851	12.1	1.74×10^{20}	13	1530 ⁺¹⁹⁸ ₋₁₈₆	*	
M53 (NGC 5024)	17.9	1.74×10^{20}	3	35.4 ^{+12.4} _{-9.6}	3×10^{31}	(2)
ω Cen (NGC 5139)	5.2	1.05×10^{21}	5	90.4 ^{+26.3} _{-20.4}	1×10^{30}	(3)
M3 (NGC 5272)	10.2	8.71×10^{19}	5	194.0 ^{+33.1} _{-18.0}	2×10^{31}	(4)
M5 (NGC 5904)	7.5	2.61×10^{20}	7	164.0 ^{+38.6} _{-0.4}	5×10^{30}	(5)
NGC 5986	10.4	2.44×10^{21}	1	61.9 ^{+15.9} _{-10.4}	**	
M4 (NGC 6121)	2.2	3.05×10^{21}	1	26.90 ^{+11.60} _{-9.56}	3×10^{29}	(5)
M13 (NGC 6205)	7.4	1.74×10^{20}	6	68.9 ^{+18.1} _{-14.6}	5×10^{30}	(5)
M12 (NGC 6218)	4.8	1.66×10^{21}	1	13.00 ^{+5.44} _{-4.03}	6×10^{30}	(5)
M10 (NGC 6254)	4.4	2.44×10^{21}	1	31.40 ^{+4.34} _{-4.08}	5×10^{30}	(5)
M62 (NGC 6266)	6.8	4.09×10^{21}	7	1670 ⁺⁷⁰⁹ ₋₅₆₉	3×10^{30}	(5)
M92 (NGC 6341)	8.3	1.74×10^{20}	1	270.0 ^{+30.1} _{-29.0}	6×10^{30}	(5)
NGC 6342	8.5	4.01×10^{21}	1	44.8 ^{+14.4} _{-12.5}	5×10^{31}	(2)
Terzan 1	6.7	1.73×10^{22}	6	0.292 ^{+0.274} _{-0.170}	2×10^{31}	(5)
M14 (NGC 6402)	9.3	5.23×10^{21}	5	124.0 ^{+31.8} _{-30.2}	6×10^{31}	(5)
NGC 6397	2.3	1.57×10^{21}	2	84.1 ^{+18.3} _{-18.3}	1×10^{29}	(5)
Terzan 5	6.9	1.99×10^{22}	38	6800 ⁺¹⁰⁴⁰ ₋₃₀₂₀	1×10^{30}	(5)
NGC 6440	8.5	9.32×10^{21}	7	1400 ⁺⁶²⁸ ₋₄₇₇	4×10^{31}	(6)
NGC 6441	11.6	4.09×10^{21}	5	2300 ⁺⁹⁷⁴ ₋₆₃₅	*	
NGC 6517	10.6	9.41×10^{21}	8	338.0 ^{+152.0} _{-97.5}	3×10^{31}	(2)

Continued on next page

Table 3.1 – *Continued from previous page*

GC Name	Distance ^a (kpc)	N_{H}^b (cm^{-2})	N_{MSP}^c	Encounter Rate ^d Γ_{SE}	Lim. L_X^e (erg s^{-1})	Reference of Lim. L_X
NGC 6522	7.7	4.18×10^{21}	4	$363.0_{-98.5}^{+113.0}$	5×10^{30}	(5)
NGC 6539	7.8	8.89×10^{21}	1	$42.1_{-15.3}^{+28.6}$	5×10^{31}	(5)
NGC 6544	3.0	6.62×10^{21}	2	$111.0_{-36.5}^{+67.8}$	6×10^{30}	(5)
NGC 6624	7.9	2.44×10^{21}	8	1150_{-178}^{+113}	*	
M28 (NGC 6626)	5.5	3.48×10^{21}	13	$648.0_{-91.1}^{+83.8}$	8×10^{29}	(5)
NGC 6652	10.0	7.84×10^{20}	2	700_{-189}^{+292}	2×10^{31}	(7)
M22 (NGC 6656)	3.2	2.96×10^{21}	2	$77.5_{-25.9}^{+31.9}$	8×10^{29}	(5)
NGC 6712	6.9	3.92×10^{21}	1	$30.80_{-6.64}^{+5.63}$	*	
NGC 6749	7.9	1.31×10^{22}	1	$51.5_{-20.9}^{+40.7}$	**	
NGC 6752	4.0	3.48×10^{20}	9	401_{-126}^{+182}	3×10^{29}	(8)
NGC 6760	7.4	6.71×10^{21}	2	$56.9_{-19.4}^{+26.6}$	1×10^{31}	(5)
M71 (NGC 6838)	4.0	2.18×10^{21}	2	$1.470_{-0.138}^{+0.146}$	2×10^{30}	(9)
M15 (NGC 7078)	10.4	8.71×10^{20}	6	4510_{-986}^{+1360}	*	
M2 (NGC 7089)	11.5	5.23×10^{20}	5	$518.0_{-71.4}^{+77.6}$	6×10^{31}	(5)
M30 (NGC 7099)	8.1	2.61×10^{20}	2	$324.0_{-81.2}^{+124.0}$	2×10^{30}	(5)

Table 3.1: *Notes:* ^a Distance to GCs collected from Harris (1996, 2010 edition); ^b Hydrogen column number density towards GCs calculated based on correlation between N_{H} and optical extinction, A_V (Bahramian et al., 2015); ^c Number of discovered MSPs; ^d Stellar encounter rate Γ_{SE} estimated by Bahramian et al. (2013), with 1- σ errors; ^e The limiting unabsorbed X-ray luminosity estimated in the band 0.3–8 keV. Reference: (1) Cheng et al. (2019); (2) this work; (3) Henleywillis et al. (2018); (4) Zhao et al. (2019); (5) Bahramian et al. (2020); (6) Pooley et al. (2002); (7) Stacey et al. (2012); (8) Forestell et al. (2014); (9) Elsner et al. (2008). * Severely contaminated by bright X-ray sources (see Verbunt and Lewin, 2006). ** No CXO observations.

Based on the catalogue of pulsars in globular clusters (230 pulsars in 36 GCs to date)¹, we first produced a list of MSPs in GCs by defining their spinning periods of $P \lesssim 25$ ms. The boundary of rotational periods between normal pulsars and MSPs is not solid and may vary depending on the research of interests. Here we chose ~ 25 ms as the upper limit. This initial filtering gave 210 MSPs in total, and each GC in the catalogue harbours at least one MSP. Table 3.1 lists all the 36 GCs studied in this work, as well as other parameters.

To obtain the X-ray luminosities of these MSPs, we looked into *Chandra X-ray Observatory* (CXO) observations. Except NGC 5986 and NGC 6749, which have no CXO observation yet, all GCs have been observed at least once with a total exposure time >10 ks. However, five GCs (NGC 1851, NGC 6441, NGC 6624, NGC 6712, and M15) are not feasible for the X-ray analysis of MSPs or other faint X-ray sources, given that one or more bright ($L_X > 10^{36}$ erg/s) XRBs are present, producing a high X-ray background throughout the cluster core (see Verbunt and Lewin, 2006, for a review of GC X-ray sources). Hence there remain 29 GCs where we can determine or constrain the X-ray luminosities of known MSPs. Several GCs and the MSPs therein have been observed and studied in X-rays thoroughly, such as 47 Tuc, M28, etc. (see Introduction), while other GCs have had deep surveys of X-ray sources before MSPs were detected therein (e.g. Henleywillis et al., 2018). Also, Bahramian et al. (2020) provided a comprehensive catalogue of faint X-ray sources in 38 GCs, which may contain information about MSPs. Three GCs (M53, NGC 6342, and NGC 6517), however, do not have published X-ray surveys yet, though archival CXO data is available on them. Therefore, we collected and extracted X-ray information (e.g. fluxes and luminosities) of GC MSPs based on previous studies of them. To normalize the X-ray energy range, we use unabsorbed X-ray luminosities in the 0.3–8 keV band as the normalization, and all the X-ray MSPs and sources studied in other energy bands will be converted into the 0.3–8 keV band via a *Chandra* proposal planning tool,

¹<http://www.naic.edu/~pfreire/GCpsr.html>

PIMMS². The choice of energy band 0.3–8 keV emphasizes the X-ray emission from MSPs, including both thermal and non-thermal X-rays.

3.2.1 GC MSPs with X-ray analysis

A few GCs contain a large number of MSPs, like 38 MSPs found in Terzan 5 and 27 MSPs found in 47 Tuc, and hence they are of great interest to study the X-ray properties of GC MSPs. Given the deep X-ray observations by CXO as well as radio timing observations of these MSPs, their X-ray spectra may be well extracted and modeled, and therefore we can simply obtain their X-ray luminosities and other properties from corresponding studies. For instance, there are 20 MSPs in 47 Tuc that have spectral analysis with well fitted models and unabsorbed luminosities (see Bogdanov et al., 2006; Bhattacharya et al., 2017). Similarly, most MSPs in M13, Terzan 5, M28, and NGC 6752 also have well determined X-ray luminosities (Bogdanov et al., 2011b; Forestell et al., 2014; Linares et al., 2014; Bogdanov et al., 2021; Zhao et al., 2021).

While new MSPs are continuously being discovered in GCs (e.g. Pan et al., 2021b; Ridolfi et al., 2021), most do not yet have precise timing positions. Alternatively, we can constrain the X-ray luminosities for MSPs without precise timing positions by setting upper limits using the known cluster X-ray sources. Given the detailed multiwavelength analyses of several GCs (e.g. Pooley et al., 2002; Edmonds et al., 2003; Heinke et al., 2005), most X-ray sources with $L_X \gtrsim 3 \times 10^{32} \text{ erg s}^{-1}$ have been identified as CVs, LMXBs, etc, and only faint X-ray sources ($L_X \lesssim 10^{32} \text{ erg s}^{-1}$) often remain unidentified. Since MSPs are typically faint X-ray emitters, we can then define the X-ray luminosity upper limit of those MSPs without X-ray identifications in one GC as the luminosity of the brightest unidentified X-ray source in that GC. Hence we simply use one upper limit of X-ray luminosity for each cluster for all the MSPs without known positions in that cluster. While for those MSPs with published timing positions but not studied yet in X-rays, we briefly look into their X-ray luminosities and place upper limits for them (see below). It is a conservative definition but fair enough to give us a sense of the X-ray brightness of those

²<https://asc.harvard.edu/toolkit/pimms.jsp>

MSPs.

We note that X-ray studies of GC sources generally assume a single power-law spectrum with a fixed photon index Γ for all the detected faint sources (e.g. Cackett et al., 2006; Henleywillis et al., 2018), and consequently the fitted parameters might not reflect their intrinsic X-ray properties.

3.2.2 GC X-ray analysis in this work

We briefly analyze CXO observations of three GCs (M53, NGC 6342, and NGC 6517) that have not been studied yet to constrain the X-ray luminosities of the sources therein. Also, we analyze X-ray spectra of two MSPs in the globular cluster Omega Centauri (aka NGC 5139, hereafter ω Cen). In addition, we extract X-ray fluxes for those MSPs with timing positions but not yet published in X-rays to calculate their upper limits of X-ray luminosities (e.g., four MSPs in M62). The data reduction and analysis were performed using CIAO³ (version 4.13, CALDB 4.9.4, Fruscione et al., 2006). All the *Chandra* observation data were first reprocessed using the `chandra_repro` script to create new level 2 event files that apply the latest calibration updates and bad pixel files. Plus, we filtered the data to the energy band 0.3–8 keV to keep consistency. No background flares were detected in the CXO observations.

M53, NGC 6342, and NGC 6517

Each of M53, NGC 6342, and NGC 6517 has been observed once by CXO in the VFAINT mode, with exposure times ranging from 15 ks to 25 ks (see Table 3.2). We formally detected X-ray sources in each GC by using `wavdetect`, a Mexican-Hat Wavelet source detection script⁴. We set the wavelet scales of 1.0, 1.4, 2.0, and 4.0, and the significance threshold of 10^{-6} (false positives per pixel). The detected X-ray sources are shown in Figure 3.1 (green contours). To generate the X-ray luminosities of those sources, we first obtained their count rates by running `dmextract` in DS9. With additional known observation information (e.g. *Chandra* cycles, detectors), we converted count rates

³Chandra Interactive Analysis of Observations, available at <https://cxc.cfa.harvard.edu/ciao/>.

⁴<https://cxc.cfa.harvard.edu/ciao/threads/wavdetect/>

Table 3.2: *Chandra* Observations of M53, NGC 6342, and NGC 6517

GC Name	Instrument	Date of Observation	Observation ID	Exposure Time (ks)
M53	ACIS-S	2006 Nov 13	6560	24.5
NGC 6342	ACIS-S	2009 Jul 10	9957	15.8
NGC 6517	ACIS-S	2009 Feb 04	9597	23.6

into unabsorbed X-ray fluxes and luminosities via PIMMS, assuming a power-law spectrum with a photon index of 1.7 for those sources, and distances from Harris (1996, 2010 revision).

ω Cen

The X-ray data of ω Cen used in this work consist of four CXO observations, with a total exposure time of 290.1 ks (see Table 3.3). All of the four observations were imaged using the ACIS-I imaging array and configured in VFaint mode. We created a co-added X-ray image of ω Cen in 0.3–8 keV band by merging four level 2 event files using `merge_obs` (Figure 3.2).

Since ω Cen has had a deep and comprehensive X-ray study recently by Henleywillis et al. (2018) (see also Cool et al. 2013), we only focus on the MSPs in ω Cen discovered since their work. There are five MSPs found to date in ω Cen (Dai et al., 2020), and only two of them (J1326–4728A and J1326–4728B) have precise timing positions. To analyse the X-ray spectra and obtain luminosities of these two MSPs, we first extracted X-ray emission from the circular regions with a 1-arcsec radius centred on the radio timing positions (green circles in Figure 3.2) by using `specextract`. We performed the extraction process for each observation separately, and then combined the spectra for each MSP correspondingly using `combine_spectra`. The background was taken from source-free annular areas around the MSPs.

Other MSPs with timing positions

There is a group of MSPs that have radio timing positions but have not been studied yet in X-rays. In this work, we briefly investigate their X-ray properties to further constrain the X-ray luminosity distribution of GC MSPs. For

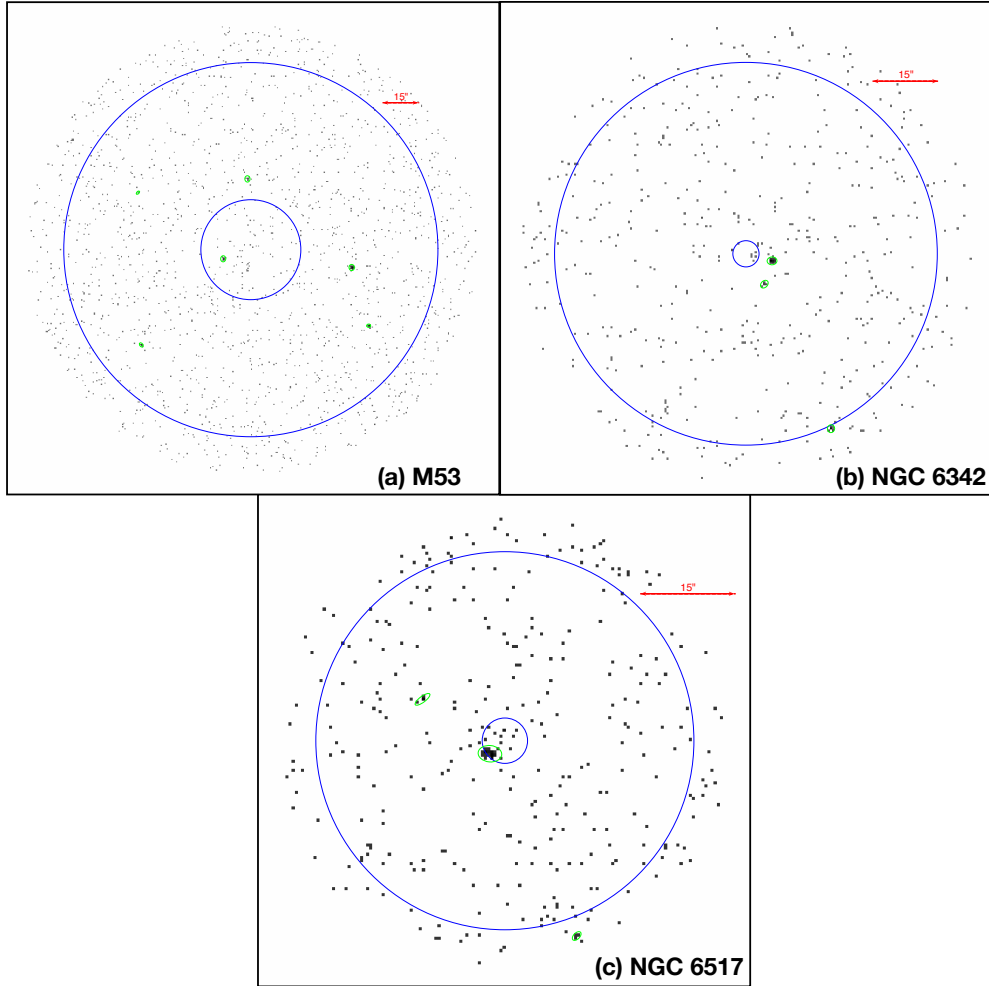


Figure 3.1: *Chandra* X-ray images in the band 0.3–8 keV of M53, or NGC 5024 (a); NGC 6342 (b); and NGC 6517 (c), respectively. The smaller blue circle in each panel shows the core region of the corresponding GC, while the larger blue circle shows the half-light radius (Harris, 1996, 2010 edition). Green contours indicate X-ray sources detected by *wavdetect* (see text for details). For each cluster, the GC region searched was defined as 1.2 times the half-light radius. North is up, and east is to the left.

Table 3.3: *Chandra* Observations of ω Cen

Instrument	Date of Observation	Observation ID	Exposure Time (ks)
ACIS-I	2000 Jan 24	653	25.0
ACIS-I	2000 Jan 25	1519	43.6
ACIS-I	2012 Apr 17	13726	173.7
ACIS-I	2012 Apr 16	13727	48.5

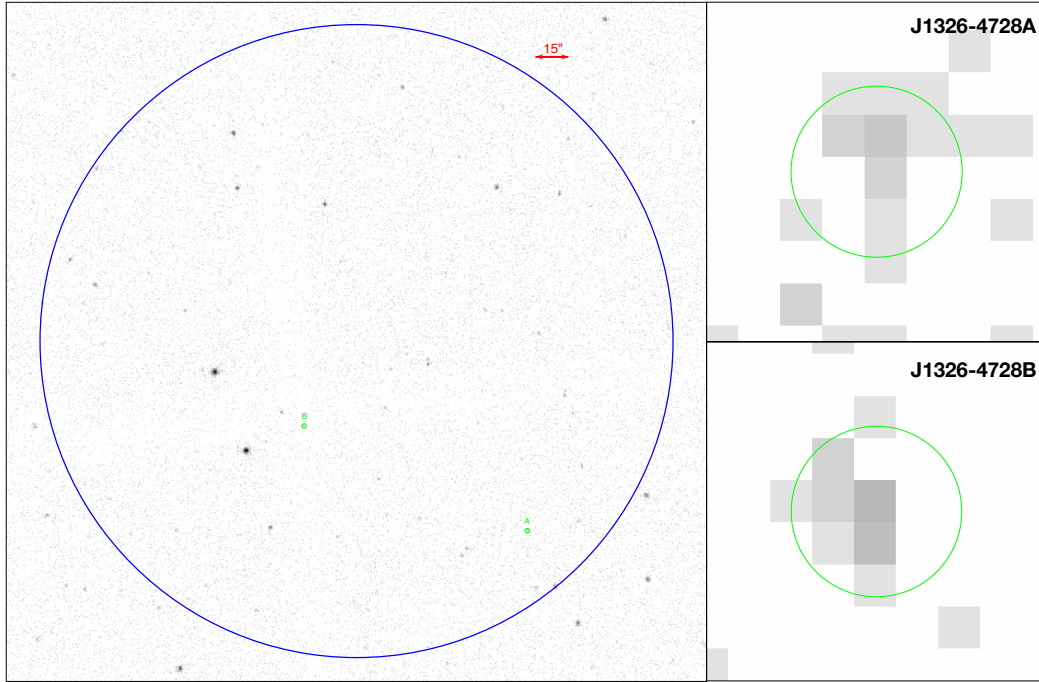


Figure 3.2: Merged *Chandra* X-ray image of ω Cen in the band of 0.3–8 keV. *Left*: The blue circle shows the core region of ω Cen centred at R.A. = 13:26:47.24, Dec. = $-47:28:46.5$ (Harris, 1996, 2010 edition). Two MSPs (J1326–4728A and J1326–4728B) with timing positions are marked using green circles with 1-arcsec radii. North is up, and east is to the left. Bright X-ray sources visible in this image contain CVs (see Cool et al., 2013; Henleywillis et al., 2018). *Right*: zoomed-in X-ray images of J1326–4728A (upper panel) and J1326–4728B (lower panel), respectively, in $4'' \times 4''$ boxes. X-ray emission from these two MSPs are seen clearly.

these MSPs, we apply CXO observations of their corresponding GCs and extract their X-ray fluxes within a circle with 1-arcsec radius and centred at their timing positions. We use `srcflux` in DS9 to calculate the unabsorbed X-ray fluxes in the band 0.3–8 keV, by assuming a single power-law model with a photon index of 1.7 and fixed values of N_{H} to corresponding GCs (see Table 3.1). If a GC has multiple archival CXO observations, we apply the one with longest exposure time. We note that, since two transient LMXBs have been discovered in the cluster NGC 6440 by *Chandra* (see e.g., in’t Zand et al., 2001; Heinke et al., 2010), we need to choose the observation (Obs ID: 947) that was not influenced by the two transients to obtain reasonable X-ray upper limits for the MSPs therein. In addition, if no X-ray counts are detected in the circular region for a MSP, we place the limiting X-ray luminosity of the corresponding GC (see Table 3.1) as its upper limit.

3.3 Analysis and Results

3.3.1 X-ray spectral fits of 2 MSPs in ω Cen

We used SHERPA, CIAO’s modeling and fitting tool, to perform the spectral fits. We assumed a fixed hydrogen column density (N_{H}) of $1.05 \times 10^{21} \text{ cm}^{-2}$ towards ω Cen, and applied the `xstbabs` model (Wilms et al., 2000) to calculate X-ray absorption by the interstellar medium. The N_{H} was estimated based on the known interstellar reddening $E(B - V)$ (Harris, 1996, 2010 edition), and the correlation between N_{H} and the optical extinction A_V (Bahramian et al., 2015), while we adopted $A_V/E(B - V) = 3.1$ (Cardelli et al., 1989). We applied the WSTAT statistic (Cash, 1979) in SHERPA for estimating the uncertainties of fitting parameters and testing the goodness-of-fit.⁵ Also we binned the spectrum of J1326–4728A to contain at least one count per bin, while the data of J1326–4728B were binned with two counts each bin.

We considered three spectral models for the X-ray emission from MSPs: blackbody (BB); power-law (PL); and neutron star hydrogen atmosphere (NSAT-MOS; Heinke et al., 2006a) models. We first used the `xsbbody` model to fit

⁵See also <https://heasarc.gsfc.nasa.gov/xanadu/xspec/manual/node312.html>.

BB spectra, and the normalization (with little affect on fitting) was fixed to reduce a free parameter and increase the degrees of freedom. For the NSATMOS spectra, we applied the `xnsatmos` model, and the NS mass and radius were fixed to $1.4 M_{\odot}$ and 10 km, respectively. Plus, the distance was frozen to 5.2 kpc, our assumed distance to ω Cen (Harris, 1996, 2010 revision). The normalization of the `xnsatmos` model, physically indicating the fraction of the NS surface emitting, has little influence on other fitting parameters, and therefore we fixed it as well to reduce an unrelated free parameter. We applied `xscflux` model to fit the unabsorbed X-ray fluxes in the band of 0.3–8 keV for BB and NSATMOS spectra (`xscflux` is a convolution model in XSPEC that is usually used for a robust calculation of unabsorbed flux of other model components). As a result, the free parameters were temperature and flux for both BB and NSATMOS models. The PL spectra were fitted using `xspegpwrlw` model, with free parameters of photon index Γ and normalization, given that the normalization is in fact the X-ray flux from the source. We applied Q-values to indicate the fitting goodness, which is a measure of probability that the simulated spectra would have a larger reduced statistic value than the observed one, if the assumed model is true and the best-fit parameters are the true parameters. We consider Q-values larger than 0.05 as acceptable. The spectral fits of all the three models for J1326–4728 A and B are listed in Table 3.4.

The spectrum of J1326–4728A is well fitted by either a BB model or an NSATMOS model, with effective temperatures of $(2.3 \pm 1.2) \times 10^6$ K and $(1.3 \pm 0.6) \times 10^6$ K, respectively. Also, the fitted unabsorbed fluxes of these two models are consistent with each other. A PL spectral model for J1326–4728A is a slightly worse fit, as the best-fit Q-value is 0.06. More importantly, the fitted photon index is 3.5 ± 1.1 , which is highly unlikely for non-thermal emission from MSPs (typically $\Gamma \sim 1 - 2$ for MSPs, e.g. Bogdanov et al., 2006, 2011b). The fitted high photon index implies a soft spectrum typically seen from blackbody-like thermal emission of MSPs (e.g. Zhao et al., 2021). Furthermore, J1326–4728A is an isolated MSP (Dai et al., 2020) and faint in X-rays ($L_X \sim 2 \times 10^{30}$ erg s $^{-1}$ in 0.3–8 keV band), consistent with a thermal

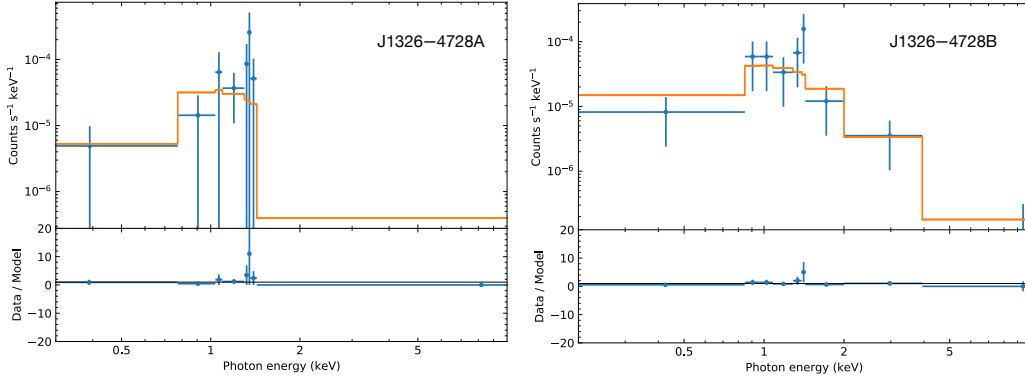


Figure 3.3: X-ray spectra and best fits of two MSPs in ω Cen, J1326–4728A (*left*, fit with an absorbed blackbody) and J1326–4728B (*right*, fit with an absorbed power-law), respectively, in energy range of 0.3–8 keV. The data of J1326–4728A are binned with 1 count/bin, while the data of J1326–4728B are binned with 2 count/bin. Both spectra are fitted via the WSTAT statistic.

model.

J1326–4728B is an eclipsing black widow pulsar, with a companion star of mass $0.016 M_{\odot}$ (Dai et al., 2020). Its X-ray spectrum can be well described by a pure PL model, with the fitted photon index $\Gamma = 2.6 \pm 0.5$ and unabsorbed luminosity $L_X = (1.1 \pm 0.3) \times 10^{31} \text{ erg s}^{-1}$. It is also likely that the X-ray spectrum is dominated by either a BB or a NSATMOS model, with fitted effective temperatures of $(3.5 \pm 1.2) \times 10^6 \text{ K}$ and $(2.5 \pm 0.6) \times 10^6 \text{ K}$, respectively, with similar fit quality ‘goodness’. Although we cannot rule out any spectral models based on Q-values, we empirically prefer a PL model for the spectrum of J1326–4728B, given that most observed eclipsing spider pulsars emit a bulk of non-thermal X-rays, like J0023–7203 J and W in 47 Tuc (Bogdanov et al., 2006). We also tested combined spectral models, i.e. BB+PL and NSATMOS+PL, but these models did not provide better fits, and hence we only show the fitting results of one-component models here. Figure 3.3 shows the X-ray spectra and the preferred fits of J1326–4728A (left panel) and J1326–4728B (right panel).

J1326–4728A			
Spectral Model	BB	PL	NSATMOS
$kT_{\text{BB}}/\Gamma/\log T_{\text{eff}}^a$	0.2 ± 0.1	3.5 ± 1.1	6.1 ± 0.2
Reduced Stat.	1.57	2.05	1.67
Q-value	0.15	0.06	0.12
$F_X(0.3\text{--}8 \text{ keV})^b$	0.6 ± 0.3	1.4 ± 0.9	0.7 ± 0.3
J1326–4728B			
Spectral Model	BB	PL	NSATMOS
$kT_{\text{BB}}/\Gamma/\log T_{\text{eff}}^a$	0.3 ± 0.1	2.6 ± 0.5	6.4 ± 0.1
Reduced Stat.	0.79	1.03	0.76
Q-value	0.60	0.41	0.62
$F_X(0.3\text{--}8 \text{ keV})^b$	1.8 ± 0.3	3.3 ± 0.9	1.9 ± 0.5

Table 3.4: Spectral fits for J1326–4728 A and B.

Notes: N_{H} was fixed for all the fits at the value to ω Cen of $1.05 \times 10^{21} \text{ cm}^{-2}$.

^a kT_{BB} : blackbody temperature in units of keV; Γ : photon index; T_{eff} : effective temperature in units of Kelvin.

^b Unabsorbed flux in units of $10^{-15} \text{ erg cm}^{-2} \text{ s}^{-1}$.

3.3.2 X-ray sources in M53, NGC 6342, and NGC 6517

After the procedure of source detection discussed in Section 3.2.2, we found six X-ray sources in M53 and three X-ray sources in each of NGC 6342 and NGC 6517. Basic X-ray information of these detected sources are listed in Table 3.5 (see also Figure 3.1).

M53 (or NGC 5024) is the most distant GC studied in this work, at a distance of 17.9 kpc. The interstellar reddening towards M53, however, is relatively low, and hence several X-ray sources therein can be relatively readily detected. One source is located in the core region, while our other detected sources are within the half-light radius. The unabsorbed X-ray luminosities (0.3–8 keV) of the six sources are in the range of $3.3 \times 10^{31} \text{ erg s}^{-1}$ to $7.6 \times 10^{32} \text{ erg s}^{-1}$, providing an estimated limiting luminosity of $3 \times 10^{31} \text{ erg s}^{-1}$.

The source detections of NGC 6342 and NGC 6517 were largely affected by the high ISM absorption and limited exposure time. Particularly, the N_{H} towards NGC 6517 is $\sim 10^{22} \text{ cm}^{-2}$, among the highest N_{H} in this work. The three detected X-ray sources in NGC 6342 have luminosities ranging from $5.1 \times 10^{31} \text{ erg s}^{-1}$ to $3.8 \times 10^{32} \text{ erg s}^{-1}$, while the X-ray luminosities of the three sources found in NGC 6517 vary from $2.7 \times 10^{31} \text{ erg s}^{-1}$ to $2.4 \times 10^{32} \text{ erg s}^{-1}$.

s^{-1} (see Table 3.5). Hence, the estimated limiting X-ray luminosities of NGC 6342 and NGC 6517 are $5 \times 10^{31} \text{ erg s}^{-1}$ and $3 \times 10^{31} \text{ erg s}^{-1}$, respectively.

For the purpose of this study, we are only interested in the upper and lower limits of the luminosities of X-ray sources in these three GCs. Further studies, like optical/radio identifications of X-ray sources therein, may be available with deeper observations and analysis in the future.

Table 3.5: Basic X-ray properties of catalogue sources in M53, NGC 6342, and NGC 6517.

GC	Source		Position (J2000)		Counts ^a (0.3–8 keV)	$F_X(0.3\text{--}8\text{ keV})^b$ ($\times 10^{-15}\text{ erg cm}^{-2}\text{ s}^{-1}$)
	ID	α (hh:mm:ss)	δ ($^{\circ}$: $'$: $''$)			
M53	1	13:12:58.4792	+18:09:25.378	13.9 \pm 3.7	4.1 \pm 1.1	
M53	2	13:12:51.7781	+18:09:33.452	34.9 \pm 5.9	10.2 \pm 1.7	
M53	3	13:12:52.2771	+18:09:57.910	67.7 \pm 8.2	19.8 \pm 2.4	
M53	4	13:12:56.0651	+18:10:01.569	19.7 \pm 4.5	5.8 \pm 1.3	
M53	5	13:12:58.5790	+18:10:29.349	2.9 \pm 1.7	0.9 \pm 0.5	
M53	6	13:12:55.3503	+18:10:35.137	13.7 \pm 3.7	4.0 \pm 1.1	
NGC 6342	1	17:21:08.7022	−19:35:54.729	20.9 \pm 4.6	15.6 \pm 3.4	
NGC 6342	2	17:21:09.7821	−19:35:21.656	7.9 \pm 2.8	5.9 \pm 2.1	
NGC 6342	3	17:21:09.6572	−19:35:16.323	58.9 \pm 7.7	43.9 \pm 5.7	
NGC 6517	1	18:01:50.6799	−8:57:33.665	25.1 \pm 5.1	17.8 \pm 3.6	
NGC 6517	2	18:01:51.4020	−8:57:25.036	4.8 \pm 2.2	3.4 \pm 1.6	
NGC 6517	3	18:01:49.7506	−8:58:02.592	2.8 \pm 1.7	2.0 \pm 1.2	

^a Estimated net counts obtained by `dmextract`; errors are set to 1- σ .

^b Unabsorbed fluxes assuming a PL model with a photon index $\Gamma = 1.7$; errors are set to 1- σ .

3.3.3 X-ray luminosity function of GC MSPs

After data collection and analysis, we finally obtain an X-ray catalogue of 175 GC MSPs (64 MSPs with determined X-ray luminosities shown in Table 3.6, and 111 MSPs with upper limits of X-ray luminosities listed in Table A.1). MSPs in NGC 1851, NGC 6441, NGC 6624, NGC 6712, and M15 are not included in this catalogue, since we could not obtain reasonable X-ray luminosity constraints for them due to the severe contamination of very bright X-ray sources in these globular clusters. Also, X-ray luminosities for MSPs in NGC 5986 and NGC 6749 are unavailable because of the lack of sensitive (*Chandra*) X-ray observations.

Using this catalogue, we are able to empirically investigate the X-ray luminosity function of GC MSPs. Figure 3.4 shows the differential X-ray luminosity distributions for two groups, MSPs with determined X-ray luminosities (blue histogram) and all MSPs in our catalogue including those with upper limits (red dashed histogram), respectively. We found that most detected GC MSPs have X-ray luminosities ranging from $\sim 10^{30}$ to $\sim 3 \times 10^{31}$ erg s^{-1} in the band 0.3–8 keV. And the X-ray luminosity distribution of measured GC MSPs is plausibly a power-law-like pattern, roughly described by $d \log(N_{\text{MSP}})/d \log(L_X) \sim -0.5$ (though this distribution is likely strongly affected by our not correcting for censorship of the data—that is, by the upper limits). On the other hand, the upper limits of X-ray luminosities are distributed more evenly between 10^{30} and 10^{33} erg s^{-1} (likely reflecting the varied X-ray exposures of GCs, principally). At the bright end, we see the well-known X-ray-bright MSP, B1821–24A ($L_X \sim 1.4 \times 10^{33}$ erg s^{-1}) in M28, alone.

It is noticeable that all the detected eclipsing spider pulsars are among the brighter GC MSP population, with X-ray luminosities of 7×10^{30} – 3×10^{32} erg s^{-1} , implying that non-thermal X-ray emission produced by intra-binary shocks dominates over thermal emission from the NS surface. More intriguingly, the X-ray luminosities of eclipsing BWs are between $L_X(0.3\text{--}8 \text{ keV})=7 \times 10^{30}$ and 1.3×10^{31} erg s^{-1} (except one at 3×10^{31}), while the

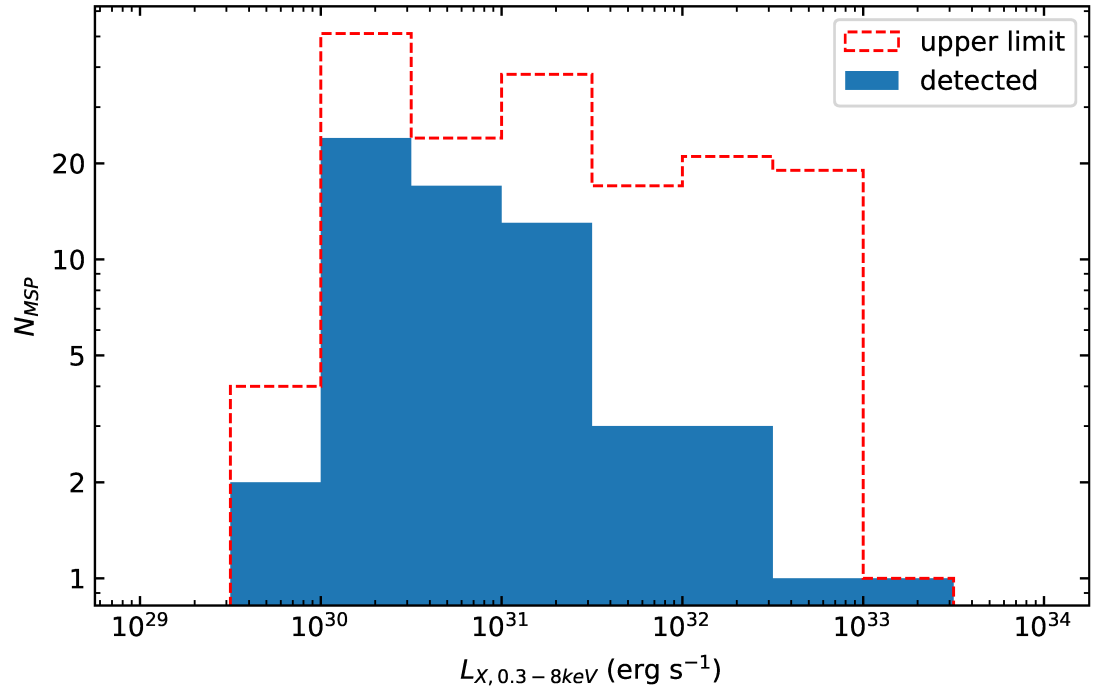


Figure 3.4: The differential X-ray luminosity distributions of GC MSPs catalogued in this work. The blue histogram shows the distribution of MSPs with determined X-ray luminosities, whereas the red dashed histogram shows the upper limits of the X-ray luminosity distribution.

detected non-eclipsing BWs are almost an order of magnitude fainter (1.5×10^{30} and 3×10^{30} erg s⁻¹) than the eclipsing BWs. This observed difference could suggest the population of non-eclipsing black widows are basically the same as the eclipsing black widows except for inclination (as suggested by Freire 2005, noting the lower mass functions of the non-eclipsing systems). In this case, the difference in L_X is also due to inclination (following the models of the inter-binary shocks that indicate the synchrotron X-rays may be beamed in the plane of the binary to some extent). Alternatively, the population of non-eclipsing black widows are actually different from the eclipsing black widows. These systems may have similar inclinations, but lower-mass companions, that do not produce as strong winds (see e.g. Bailes et al. 2011; Kaplan et al. 2018).

However, we need to note the observational biases that may significantly impact the X-ray luminosity distributions of GC MSPs. Given that few GCs have limiting X-ray luminosities lower than $\sim 10^{30}$ erg s⁻¹ (see Table 3.1), many very faint X-ray MSPs ($L_X < 10^{30}$ erg s⁻¹) are not detectable. For instance, most MSPs in Terzan 5 remain undetectable in X-rays due to the high absorption towards this GC, even though it has been observed extensively by CXO (see e.g. Bogdanov et al., 2021). Furthermore, the upper limits of X-ray luminosities for some MSPs may be quite conservative. Particularly, we simply placed one upper limit for all the MSPs without timing solutions in each GC, defined as the X-ray luminosity of the most luminous unidentified X-ray source in that GC. Therefore, we note that the upper limit of X-ray luminosity distribution does not necessarily reflect the estimated number of MSPs in each luminosity range, as they could be orders of magnitude dimmer than the placed upper limits.

Table 3.6: Determined X-ray luminosities of GC MSPs

Pulsar Name	GC Name	Period (ms)	Type ^a	Spectral Model	$L_X(0.3-8 \text{ keV})^b$ ($\times 10^{30} \text{ erg s}^{-1}$)	Ref. of L_X
J0023-7204C	47 Tuc	5.76	I	BB	$1.7^{+0.3}_{-0.6}$	1
J0024-7204D	47 Tuc	5.36	I	BB	$3.3^{+0.4}_{-0.8}$	1
J0024-7205E	47 Tuc	3.54	B	BB	$5.0^{+0.6}_{-0.9}$	1
J0024-7204F	47 Tuc	2.62	I	BB	$2.3^{+1.0}_{-0.4}$	2
J0024-7204H	47 Tuc	3.21	B	BB	$3.2^{+0.3}_{-0.8}$	1
J0023-7203J	47 Tuc	2.10	eBW	BB+PL	$11.6^{+2.3}_{-3.7}$	1
J0024-7204L	47 Tuc	4.35	I	BB	$8.6^{+0.8}_{-1.0}$	1
J0023-7205M	47 Tuc	3.68	I	BB	$2.4^{+0.3}_{-0.7}$	1
J0024-7204N	47 Tuc	3.05	I	BB	$2.4^{+0.4}_{-0.7}$	1
J0024-7204O	47 Tuc	2.64	eBW	BB+PL	$10.8^{+3.5}_{-2.1}$	1
J0024-7204Q	47 Tuc	4.03	B	BB	$2.4^{+0.3}_{-0.7}$	1
J0024-7204R	47 Tuc	3.48	eBW	BB	$7.0^{+0.4}_{-1.4}$	1
J0024-7204S	47 Tuc	2.83	B	BB	$4.2^{+0.7}_{-0.7}$	2
J0024-7204T	47 Tuc	7.59	B	BB	$1.5^{+0.3}_{-0.6}$	1
J0024-7203U	47 Tuc	4.34	B	BB	$3.2^{+0.3}_{-0.8}$	1
J0024-7204W	47 Tuc	2.35	eRB	BB+PL	$26.4^{+1.0}_{-6.3}$	1
J0024-7201X	47 Tuc	4.77	B	BB	$2.2^{+0.6}_{-0.6}$	3
J0024-7204Y	47 Tuc	2.20	B	BB	$2.5^{+0.2}_{-0.7}$	1
J0024-7205Z	47 Tuc	4.55	I	BB	$3.5^{+0.5}_{-0.5}$	2
J0024-7205aa	47 Tuc	3.69	I	BB	$0.9^{+0.4}_{-0.3}$	2
J0024-7204ab	47 Tuc	3.70	I	BB	$2.0^{+0.4}_{-0.5}$	2

Continued on next page

Table 3.6 – *Continued from previous page*

Pulsar Name	GC Name	Period (ms)	Type ^a	Spectral Model	$L_X(0.3-8 \text{ keV})^b$ ($\times 10^{30} \text{ erg s}^{-1}$)	Ref. of L_X
J1326–4728A	ω Cen	4.11	I	BB	$1.9^{+1.0}_{-1.0}$	4
J1326–4728B	ω Cen	4.79	eBW	PL	$10.7^{+3.0}_{-3.0}$	4
B1620–26	M4	11.08	O	BB	$3.0^{+0.7}_{-0.7}$	5
J1641+3627B	M13	3.53	B	PL	$9.2^{+4.6}_{-4.6}$	6
J1641+3627C	M13	3.72	I	BB	$3.9^{+1.3}_{-0.7}$	6
J1641+3627D	M13	3.12	B	BB	$5.9^{+1.3}_{-0.7}$	6
J1641+3627E	M13	2.49	eBW	PL	$12.5^{+4.6}_{-4.6}$	6
J1641+3627F	M13	3.00	B	BB	$7.9^{+1.3}_{-0.7}$	6
J1701–3006B	M62	3.59	eRB	PL	$101.0^{+25.9}_{-21.0}$	7
J1701–3006C	M62	7.61	B	PL	$59.0^{+12.0}_{-12.0}$	7
J1740–5340A	NGC 6397	3.65	eRB	PL	$22.2^{+2.6}_{-2.5}$	7
J1740–5340B	NGC 6397	5.79	eRB	PL	$67.0^{+0.5}_{-0.1}$	8, 9
J1748–2446A	Terzan 5	11.56	eRB	PL	$89.9^{+27.2}_{-27.2}$	10
J1748–2446E	Terzan 5	2.20	B	PL	$3.1^{+1.3}_{-1.1}$	10
J1748–2446F	Terzan 5	5.54	I	PL	$9.0^{+3.0}_{-2.7}$	10
J1748–2446H	Terzan 5	4.93	I	PL	$7.2^{+2.8}_{-2.5}$	10
J1748–2446K	Terzan 5	2.97	I	PL	$2.2^{+1.1}_{-0.8}$	10
J1748–2446L	Terzan 5	2.24	I	PL	$14.1^{+3.2}_{-3.1}$	10
J1748–2446N	Terzan 5	8.67	B	PL	$2.5^{+0.9}_{-0.8}$	10
J1748–2446O	Terzan 5	1.68	eBW	PL	$29.0^{+2.8}_{-2.8}$	10
J1748–2446P	Terzan 5	1.73	eRB	PL	$335.6^{+21.4}_{-18.4}$	10
J1748–2446Q	Terzan 5	2.81	B	PL	$1.1^{+0.7}_{-0.5}$	10
J1748–2446V	Terzan 5	2.07	B	PL	$16.5^{+2.7}_{-2.5}$	10

Continued on next page

Table 3.6 – *Continued from previous page*

Pulsar Name	GC Name	Period (ms)	Type ^a	Spectral Model	$L_X(0.3-8 \text{ keV})^b$ ($\times 10^{30} \text{ erg s}^{-1}$)	Ref. of L_X
J1748–2446X	Terzan 5	3.00	B	PL	$5.1^{+2.1}_{-2.0}$	10
J1748–2446Z	Terzan 5	2.46	B	PL	$11.6^{+2.1}_{-1.9}$	10
J1748–2446ad	Terzan 5	1.40	eRB	PL	$139.1^{+16.6}_{-12.5}$	10
B1821–24A	M28	3.05	I	PL	$1375.7^{+47.1}_{-32.6}$	11
J1824–2452C	M28	4.16	B	PL	$2.0^{+0.6}_{-0.5}$	11
J1824–2452E	M28	5.42	I	PL	$2.3^{+0.7}_{-0.6}$	11
J1824–2452F	M28	2.45	I	PL	$1.4^{+0.4}_{-0.3}$	11
J1824–2452H	M28	4.63	eRB	PL	$17.4^{+3.3}_{-13.0}$	11
J1824–2452I	M28	3.93	eRB	PL	$220.0^{+40.0}_{-40.0}$	12
J1824–2452J	M28	4.04	BW	PL	$1.5^{+0.2}_{-0.2}$	11
J1824–2452K	M28	4.46	B	PL	$6.2^{+0.9}_{-0.9}$	11
J1836–2354A	M22	3.35	BW	PL	$3.0^{+1.6}_{-1.0}$	13
J1911–5958A	NGC 6752	3.27	B	BB	$2.9^{+1.3}_{-1.0}$	14
J1910–5959B	NGC 6752	8.36	I	BB	$1.3^{+0.6}_{-0.4}$	14
J1911–6000C	NGC 6752	5.28	I	BB	$3.2^{+0.8}_{-0.6}$	14
J1910–5959D	NGC 6752	9.04	I	BB	$3.8^{+0.8}_{-0.6}$	14
J1910–5959E	NGC 6752	4.57	I	BB	$1.0^{+1.0}_{-0.4}$	14
J1910–5959F	NGC 6752	8.49	I	PL	$4.0^{+1.0}_{-0.7}$	15
J1953+1846A	M71	4.89	eBW	PL	$12.0^{+1.9}_{-1.9}$	16
J2140–2310A	M30	11.02	eBW	PL	$10.9^{+4.2}_{-3.6}$	17

Table 3.6: *Notes:* periods and types of MSPs were obtained from Paulo Freire’s GC Pulsar Catalog (see <http://www.naic.edu/~pfreire/GCpsr.html>).

^a Types of MSP systems; I: isolated; B: binary; BW: black widow; RB: redback; O: others (triple system); e: eclipsing.

^b Unabsorbed X-ray luminosities at the distances to corresponding GCs.

References: 1) Bogdanov et al. (2006); 2) Bhattacharya et al. (2017); 3) Ridolfi et al. (2016); 4) this work; 5) Pavlov et al. (2007); 6) Zhao et al. (2021); 7) Oh et al. (2020); 8) Bogdanov et al. (2010); 9) Pichardo Marcano et al. (2021); 10) Bogdanov et al. (2021); 11) Bogdanov et al. (2011b); 12) Linares et al. (2014); 13) Amato et al. (2019); 14) Forestell et al. (2014); 15) Cohn et al. (2021, submitted); 16) Elsner et al. (2008); 17) Zhao et al. (2020a).

3.3.4 Number of MSPs versus stellar encounter rate

We re-examined the correlation between the number of MSPs and stellar encounter rate (Γ_{SE}) for GCs in this work (see Table 3.1). It is well established that the number of X-ray binaries in a GC has a strong correlation with the GC stellar encounter rate (see e.g. Pooley et al., 2003; Heinke et al., 2003; Bahramian et al., 2013). One would naturally assume a correlation between the number of MSPs and Γ_{SE} in a GC, since MSPs are offspring of LMXBs. However, the difficulty to establish such a correlation is determining the total number of radio MSPs harboured in a GC. Bagchi et al. (2011) used sophisticated Monte Carlo simulations with various radio luminosity functions and models to calculate the population of radio MSPs in 10 GCs. They claimed that they did not find strong evidence that the number of MSPs correlates with Γ_{SE} under either model. However, Bahramian et al. (2013) produced a more sophisticated calculation of Γ_{SE} for these GCs and adopted the estimates of MSP populations from Bagchi et al. (2011, model 1), finding a significant correlation between the number of MSPs and Γ_{SE} in a GC via their statistical tests.

Here, we assume both the Γ_{SE} values from Bahramian et al. (2013) and the calculations of MSP population for 10 GCs (we also adopt the results of model 1 here; column 2 in Table 3.7) from Bagchi et al. (2011) are correct, and fit a power-law function through the data points, as standard for the correlation between the number of XRBs and Γ_{SE} . We note that due to the lack of data points, Markov Chain Monte Carlo (MCMC) method could not provide robust results, and hence we applied orthogonal distance regression method for fitting. The best-fit curve is $\log(N_{\text{MSP}}) = 0.44 \log(\Gamma_{\text{SE}}) + 0.49$, with 1-sigma errors on the slope and intercept of ± 0.07 and ± 0.21 , respectively (red solid line in Figure 3.5). Based on this correlation (assuming it is true) and the fitted function, we can then roughly estimate the total number of MSPs for each GC for a given Γ_{SE} (column 3 in Table 3.7). We calculate approximately 1460 MSPs in total in the 36 GCs in our study, which we consider as a conservative upper estimate. We consider this as a conservative upper estimate, because

Bagchi et al. (2011) also produce two other estimates with smaller predicted numbers: roughly half those of Model 1; and because Heinke et al. (2005) place an upper limit on the MSP population of 47 Tuc of <60 at 95% confidence, compared to Model 1’s 71 ± 19 . Alternative estimates from gamma-rays Abdo et al. (2010) and diffuse radio flux McConnell et al. (2004) also are well below Bagchi et al.’s Model 1 numbers — 33 ± 15 and $\lesssim 30$, respectively.

We also plotted the number of currently known radio MSPs versus Γ_{SE} for the GCs in this work (blue dots in Figure 3.5; see also Table 3.1). Furthermore, we made an aggressive estimate of the lower bound on the total population of GC MSPs. Unlike the conservative upper estimate, we consider two GCs, 47 Tuc and M13, as “well-determined” GCs, for which the currently found MSPs in these two GCs are all (or nearly all) the MSPs therein. The choice of 47 Tuc is based on comprehensive and extensive studies of this cluster. Particularly, Heinke et al. (2005) suggested a total number of ~ 25 MSPs in 47 Tuc by comparing X-ray colors, luminosities, variability, etc., of detected MSPs to those of unidentified sources using deep CXO observations. (See also the compatible estimates using gamma-rays and diffuse radio flux, mentioned above.) To date, 27 MSPs have been found in 47 Tuc (four without timing positions), and we consider this is indeed close to the total number of MSPs therein. M13 was recently observed by Wang et al. (2020) using the Five-hundred-metre Aperture Spherical radio Telescope (FAST). A new MSP (J1641+3627F) was discovered in their observations, making a total of 6 MSPs found in this cluster. Since the sensitivity of their radio observations reached down to a flux density of $0.4 \mu\text{Jy}$ to a candidate with the ratio of signal to noise of 7 (Wang et al., 2020), corresponding to a pseudo radio luminosity of $\sim 0.02 \text{ mJy kpc}^2$ at 1.4 GHz, below which no MSPs in GCs have been detected (most GC MSPs have radio specific luminosities of $\gtrsim 1 \text{ mJy kpc}^2$ at 1.4 GHz), we can confidently assume all or nearly all the MSPs in M13 have been found. We therefore fitted a power-law model across these two data points, finding a correlation of $\log(N_{\text{MSP}}) = 0.56 \log(\Gamma_{\text{SE}}) - 0.26$ (blue dashed line in Figure 3.5). We normalized the MSP populations in other GCs to this model, and thus obtained a rough lower bound (henceforth an “aggressive” estimate)

to the MSP population for them (see column 4 in Table 3.7).

It is noticeable that there is one cluster, Terzan 1 (leftmost blue dot in Figure 3.5), that falls significantly outside both aggressive and conservative model predictions. Since Terzan 1 is a so-called ‘core-collapsed’ cluster and its structural parameters are poorly measured, the calculation of Γ_{SE} depending on core values, such as core density and core radius, is generally not considered reliable (see Cackett et al., 2006; Bahramian et al., 2013). An alternative explanation of the discrepancy between the number of MSPs (and also of XRBs) and Γ_{SE} in Terzan 1 is that most stars in Terzan 1 have been stripped due to Galactic tides, leaving a core unusually rich in binaries (de Marchi et al., 1999). This is particularly plausible for Terzan 1, considering that it is located very close to the Galactic centre (Cackett et al., 2006).

Table 3.7: Estimates of MSP population in GCs

GC Name	N_{calc}^a	N_{cons}^b	N_{aggr}^c	N_{unid}^d	Ref.
47 Tuc (NGC 104)	71 ± 19	~ 65	27^e	0	1
NGC 1851	—	~ 78	~ 34	—	
M53 (NGC 5024)	—	~ 15	~ 4	5	2
ω Cen (NGC 5139)	—	~ 23	~ 7	7	3
M3 (NGC 5272)	24 ± 12	~ 32	~ 11	2	4
M5 (NGC 5904)	24 ± 11	~ 29	~ 10	1	5
NGC 5986	—	~ 19	~ 6	—	
M4 (NGC 6121)	—	~ 13	~ 4	0	6
M13 (NGC 6205)	25 ± 11	~ 20	6^e	3	5,7
M12 (NGC 6218)	—	~ 10	~ 2	0	8
M10 (NGC 6254)	—	~ 14	~ 4	0	5
M62 (NGC 6266)	—	~ 82	~ 36	4	9
M92 (NGC 6341)	—	~ 37	~ 13	5	10
NGC 6342	—	~ 17	~ 5	2	2
Terzan 1	—	~ 2	~ 0	0	11
M14 (NGC 6402)	—	~ 26	~ 8	4	5
NGC 6397	—	~ 22	~ 7	0	12
Terzan 5	167 ± 33	~ 151	~ 79	26	13
NGC 6440	88 ± 39	~ 75	~ 33	4	14
NGC 6441	—	~ 94	~ 43	—	
NGC 6517	46 ± 23	~ 40	~ 15	1	2
NGC 6522	—	~ 42	~ 15	1	5
NGC 6539	—	~ 16	~ 5	4	5

Continued on next page

Table 3.7 – *Continued from previous page*

GC Name	N_{calc}^a	N_{cons}^b	N_{aggr}^c	N_{unid}^d	Ref.
NGC 6544	–	~ 25	~ 8	1	5
NGC 6624	–	~ 69	~ 29	–	
M28 (NGC 6626)	120 ± 40	~ 54	~ 21	7	5
NGC 6652	–	~ 56	~ 22	3	15
M22 (NGC 6656)	–	~ 21	~ 6	1	5
NGC 6712	–	~ 14	~ 4	–	
NGC 6749	–	~ 18	~ 5	–	
NGC 6752	44 ± 20	~ 43	~ 16	0	16
NGC 6760	–	~ 18	~ 5	0	5
M71 (NGC 6838)	–	~ 4	~ 1	0	17,18
M15 (NGC 7078)	79 ± 30	~ 126	~ 63	–	
M2 (NGC 7089)	–	~ 49	~ 19	6	5
M30 (NGC 7099)	–	~ 40	~ 14	0	19

Table 3.7: *Notes:* ^a Calculations of MSP population for 10 GCs by Bagchi et al. (2011); ^b Conservative estimates of GC MSP population; ^c Aggressive estimates of GC MSP population; ^d Unidentified X-ray sources with $L_X > 10^{32}$ erg s⁻¹ (0.3–8 keV); ^e Selected as normalization. Reference of N_{unid} : 1)Heinke et al. (2005); 2)this work; 3)Henleywillis et al. (2018); 4)Zhao et al. (2019); 5)Bahramian et al. (2020); 6)Bassa et al. (2004); 7)Servillat et al. (2011); 8)Lu et al. (2009); 9)Oh et al. (2020); 10)Lu et al. (2011); 11)Cackett et al. (2006); 12)Bogdanov et al. (2010); 13)Heinke et al. (2006b); 14)Pooley et al. (2002); 15)Stacey et al. (2012); 16)Forestell et al. (2014); 17)Elsner et al. (2008); 18)Huang et al. (2010); 19)Zhao et al. (2020a).

3.4 Discussion

The radio MSPs in ω Cen were not discovered until a more advanced receiver, an ultra-wide-bandwidth low-frequency receiver (Hobbs et al., 2020), was installed and used on the Parkes radio telescope. Before that, however, some studies in other bands had hinted at the existence of MSPs in ω Cen. For example, Abdo et al. (2010) suggested a total of 19 ± 9 MSPs harboured in ω Cen based on gamma-ray detection of the cluster by the *Fermi* Large Area Telescope (LAT). A deep X-ray survey of ω Cen by Henleywillis et al. (2018) also implied the presence of MSPs, given that tens of unidentified sources have similar X-ray colours with the MSPs detected in 47 Tuc. Intriguingly, the X-ray counterpart to one of the MSPs in ω Cen (J1326–4728B; analyzed in

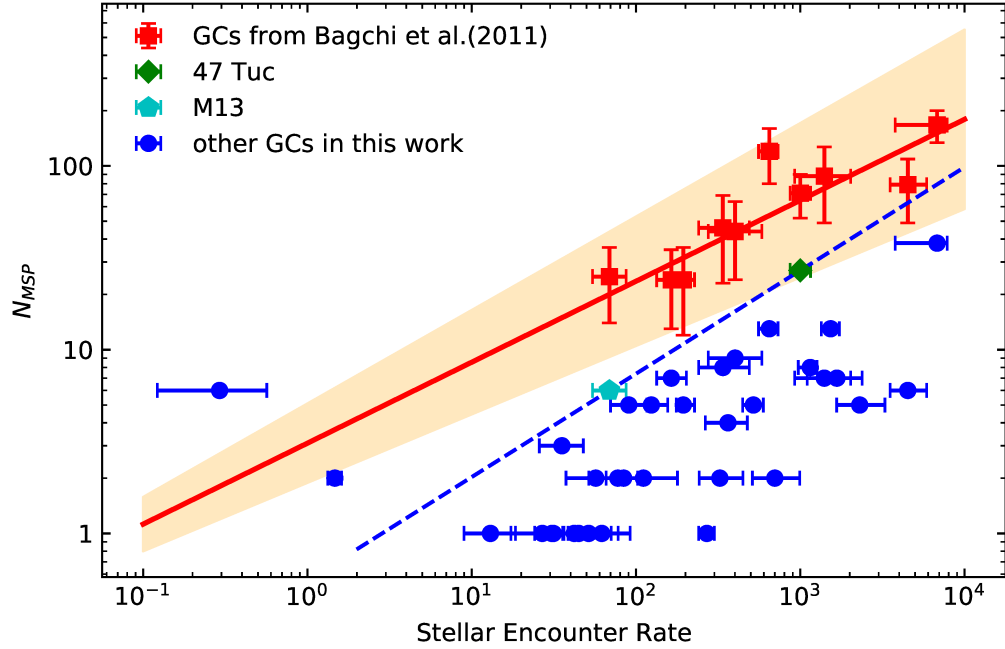


Figure 3.5: The number of MSPs in a globular cluster versus the stellar encounter rate. The blue dots show the numbers of currently known radio MSPs in GCs, while the red squares show the estimated MSP population for 10 GCs calculated by Bagchi et al. (2011, model 1). The red solid line shows the best-fit power-law model using the data points from Bagchi et al. (2011), and the yellow shade represents the 1-sigma interval. The blue dashed line shows the power-law model fitted to the data points of 47 Tuc and M13 (see text for details). All the stellar encounter rates of GCs and their corresponding errors were extracted from Bahramian et al. (2013).

this work) has been detected in previous X-ray studies (Haggard et al., 2009; Henleywillis et al., 2018, source ID 13d in their tables).

However, it is possible to nominate unidentified sources detected in other bands (e.g. X-rays and gamma-rays) as radio MSP candidates based on their observational properties. In fact, a large number of radio MSPs have recently been discovered by targeting LAT unassociated sources (see e.g. Ray et al., 2012). Moreover, dedicated analysis with X-ray, gamma-ray and optical observations also can lead to discoveries of new MSPs. For instance, Bogdanov et al. (2010) suggested an X-ray source in the cluster NGC 6397 (source ID U18 in their work) as a strong MSP candidate, given its similar X-ray and optical properties to those of the known MSP, PSR J1740–5340, in the cluster. Later, Zhao et al. (2020b) found the radio counterpart to U18 using the Australia Telescope Compact Array, while Pichardo Marcano et al. (2021) reported the optical modulation of the companion star to U18, and both of their studies provided strong evidence that U18 is a “hidden” redback MSP. The radio pulsations from this source have been detected recently by the Parkes radio telescope (Lei Zhang et al. 2021, in prep.), verifying it as a redback MSP (PSR J1740–5340B). The reason of previous non-detection of radio pulsations can be interpreted as scattering of the radio pulsations by wind from the companion (Zhao et al., 2020b).

Considering the fact that there might be a group of hidden MSPs observed in X-rays but without radio confirmation, like PSR J1326–4728B and J1740–5340B, it is also interesting to investigate the faint unidentified X-ray sources, especially those with $L_X > 10^{32}$ erg s⁻¹, where the non-thermal X-ray emission dominates. We count all the unidentified X-ray sources with $L_X > 10^{32}$ erg s⁻¹ (0.3–8 keV) in our studied GCs in Table 3.7 (column 5). We found a total of 87 unidentified X-ray sources with $L_X > 10^{32}$ erg s⁻¹ in 29 GCs, while we did not find any unidentified sources with $L_X > 10^{33}$ erg s⁻¹ in those GCs. However, we note a special case, the X-ray source B in NGC 6652 (see Heinke et al., 2001; Stacey et al., 2012), which is suggested as a transitional MSP (tMSP) in a recent work by Paduano et al. (2021). It is considered to be in an accretion-powered state currently, with an average

X-ray luminosity of $\sim 1.8 \times 10^{34}$ erg s $^{-1}$. However, since we cannot completely confirm the nature of this source until its rotation-powered MSP state is detected, we just treat it as an unidentified source with $L_X > 10^{33}$ erg s $^{-1}$ in this work. Terzan 5 contains a large number of unidentified X-ray sources, which we attribute to its high stellar encounter rate (the highest among known GCs, Bahramian et al. 2013), and the large interstellar extinction towards the cluster (Massari et al., 2012), which makes identification of optical counterparts extremely difficult (cf. Testa et al., 2012; Ferraro et al., 2015); a general search for optical/infrared counterparts of Terzan 5 X-ray sources has not yet been conducted. Another two interesting GCs are M14 and M2, where the MSPs therein were discovered recently by FAST (Pan et al., 2021b). All the detected MSPs in these two clusters are found in binary systems, while one BW and two eclipsing RB MSPs were found in M14. Since it is common that eclipsing RBs have X-ray luminosities of $L_X \gtrsim 10^{32}$ erg s $^{-1}$ (see Table 3.6), the X-ray counterparts to the two newly found RBs might be included in those unidentified sources. However, due to the lack of deep X-ray observations and radio timing solutions of these MSPs, investigation of their X-ray properties is not yet possible.

Our results allow an estimate of the X-ray detectable MSP population in the Galactic centre. An excess of gamma-rays, peaking at ~ 2 GeV, has been found towards the Galactic centre (also known as the Galactic Centre Excess, or GCE, see e.g., Hooper and Goodenough, 2011; Gordon and Macías, 2013; Ajello et al., 2016; Daylan et al., 2016), the origin of which remains unclear. Some studies suggested that the excess is generated from dark matter annihilation (e.g. Hooper and Goodenough, 2011; Daylan et al., 2016; Ackermann et al., 2017; Di Mauro, 2021), whereas other groups claimed that a population of unresolved MSPs in the Galactic bulge produces the observed gamma-ray excess (e.g., Abazajian and Kaplinghat, 2012; Brandt and Kocsis, 2015; Gonthier et al., 2018; Macias et al., 2018). If a large number of MSPs are present in the Galactic centre, one can also expect they are emitting X-rays. While *Fermi* LAT has a relatively poor angular resolution of (~ 1

degree),⁶ *Chandra*’s high angular resolution of 0.5 arcsec⁷ allows the possible detection of X-ray counterparts to MSPs as point sources in the Galactic centre. However, the large interstellar extinction towards the Galactic centre absorbs nearly all X-ray emission below 2 keV, rendering faint MSPs producing only soft blackbody-like emission (the majority of MSPs) undetectable. Only a few X-ray-bright MSPs with substantial magnetospheric (such as PSR B1821–24A in M28) or shock-powered (redbacks) X-ray emission might be detected around the Galactic centre by *Chandra*, or even XMM-Newton (with its larger point-spread function of $\sim 10''$).

Using our X-ray census of GC MSPs and our estimates of the total population of MSPs in those GCs, we are able to estimate the population of easily detectable X-ray MSPs ($L_X > 10^{33}$ erg s⁻¹ in the band 0.3–8 keV) in the Galactic bulge. We first adopt the prediction by Gonthier et al. (2018), who suggested a total of $\sim 11,000$ MSPs in the Galactic bulge are needed to produce the GCE. The number of MSPs required to explain the GCE has been estimated at 10,000–20,000 (Yuan and Zhang, 2014), 2,000–14,000 (Cholis et al., 2015b), $\sim 40,000$ (Ploeg et al., 2017), or $\sim 10,000$ (Gonthier et al., 2018), and consequently our estimation may also vary from other predictions of the number of MSPs. To calculate a lower limit of detectable X-ray MSPs in the Galactic center, we assume PSR B1821–24A is the only MSP with an X-ray luminosity more than 10^{33} erg s⁻¹ among 1500 MSPs (the conservative estimate in Table 3.7), and the MSP population in the Galactic bulge keeps the same proportion. Allowing for small-number statistics (Gehrels, 1986) gives an estimate of >1 MSP above 10^{33} erg/s for 8,700 MSPs (1σ), and thus predicts of order 1 X-ray detectable MSP in the Galactic bulge. On the other hand, if we assume the upper limit of the number of MSPs with $L_X > 10^{33}$ erg s⁻¹ (2; considering NGC 6652B) and take the “aggressive” lower estimate of 590 MSPs in these GCs, then we obtain an upper limit (1σ) of easily detectable MSPs of 1 MSP above 10^{33} erg/s for 126 MSPs, and thus predict of order 86 such easily detectable MSPs in the Galactic Centre. Performing the same

⁶<https://fermi.gsfc.nasa.gov/science/instruments/table1-1.html>

⁷<https://asc.harvard.edu/proposer/POG/>

Table 3.8: Estimates of the number of X-ray MSPs in the bulge

L_X^a (erg s $^{-1}$)	N_{det}^b	N_{upp}^c	N_{est}^d
$> 10^{32}$	5	41	21-908
$> 3 \times 10^{32}$	2	20	5-480
$> 10^{33}$	1	2	1.2-86

^aUnabsorbed luminosities in 0.3–8 keV

^bNumber of detected MSPs in GCs

^cUpper limit of the number of MSPs in GCs

^dEstimated number of MSPs in the bulge

calculation for $L_X > 10^{32}$ erg/s (still very achievable with *Chandra* in the Galactic Centre) gives a predicted range of 20 to 910 X-ray detectable MSPs in the Galactic Centre. These predictions are consistent with those of (e.g. Berteaud et al., 2020), which used an alternative method of inferring X-ray luminosity functions from gamma-ray luminosity functions. Careful study of X-ray sources in the Galactic Bulge may be able to identify plausible MSP candidates, or rule out such an MSP candidate population, which would favour a dark matter interpretation for the GCE.

3.5 Conclusions

In this work, we compiled X-ray luminosities of MSPs in GCs, including new X-ray analysis. We analysed the X-ray spectra of two MSPs (PSR J1326–4728A and J1326–4728B) in the cluster ω Cen. The unabsorbed X-ray luminosities in the band 0.3–8 keV of these two MSPs are $\sim 2 \times 10^{30}$ erg s $^{-1}$ and $\sim 1 \times 10^{31}$ erg s $^{-1}$, respectively. The X-ray spectrum of PSR J1326–4728A is well described by either a BB or a NSATOMS model, indicating thermal X-ray emission from the neutron star surface. The spectrum of PSR J1326–4728B is well-fit by a PL model, with a photon index of 2.6 ± 0.5 . Its spectrum reflects the bulk of non-thermal X-ray emission from the MSP, which is commonly observed from eclipsing spider pulsars and likely produced by intra-binary shocks. We also catalogued the X-ray sources in the clusters M53, NGC 6342, and NGC 6517. We found a total of 12 X-ray sources in these three GCs, with X-ray luminosities ranging from $\sim 3 \times 10^{31}$ erg s $^{-1}$ to $\sim 8 \times 10^{32}$ erg s $^{-1}$.

We presented a comprehensive census of X-ray MSPs in 29 Galactic GCs. We reported the X-ray luminosities or upper limits for 175 GC MSPs in our catalogue, and normalized the energy band to 0.3–8 keV. We determined X-ray luminosities for 64 GC MSPs and constrained the luminosities for others, except MSPs in 2 GCs that have no *Chandra* observations, and in 5 GCs that are severely contaminated by bright X-ray sources. We investigated the empirical MSP X-ray luminosity function using our catalogue, finding that most detected GC X-ray MSPs have luminosities between $\sim 1 \times 10^{30}$ erg s $^{-1}$ and $\sim 3 \times 10^{31}$ erg s $^{-1}$. The X-ray luminosities for eclipsing spider MSPs are generally higher than other types of MSPs, with $L_X \gtrsim 10^{31}$ erg s $^{-1}$.

We re-examined the correlation between the number of MSPs and stellar encounter rate in a GC. Using the data from Bagchi et al. (2011) and Bahramian et al. (2013), we found a relation of $\log(N_{\text{MSP}}) = 0.44 \log(\Gamma_{\text{SE}}) + 0.49$. We also fitted a curve by setting 47 Tuc and M13 as normalization, turning out a relation of $\log(N_{\text{MSP}}) = 0.56 \log(\Gamma_{\text{SE}}) - 0.26$. Furthermore, we estimated the total number of MSPs in each of the GCs in this work using both fitting relations, and suggested a conservative upper estimate of a total of around 1500 MSPs and an aggressive lower estimate of 590 MSPs, respectively, in those 36 GCs.

We empirically estimated the population of detectable MSPs in the Galactic bulge, assuming the gamma-ray excess is produced by a large number of unresolved MSPs. Based on our census of GC X-ray MSPs, we suggested of order 1-90 MSPs with $L_X > 10^{33}$ erg s $^{-1}$ in the Galactic centre, and of order 20-900 MSPs with $L_X > 10^{32}$ erg s $^{-1}$ there. As these sources are likely detected in existing archival *Chandra* and XMM-Newton observations, dedicated searches may uncover the proposed Galactic Bulge MSP population.

Chapter 4

Conclusions and Prospects

In this thesis we explored a variety of topics related to X-ray MSPs in GCs, ranging from X-ray spectral analysis of individual MSPs to investigation of the whole MSP population in GCs, and prediction of their total numbers.

In Chapter 2, we analyzed 55 ks of *Chandra* X-ray observations of the cluster M13. By using the newly reported radio timing positions of the six known MSPs in M13 (see Wang et al., 2020), we found confident X-ray counterparts to five of the six MSPs at X-ray luminosities of $L_X \sim 3 \times 10^{30} - 10^{31}$ erg s⁻¹ in the band 0.3–8 keV, including the newly discovered MSP, namely PSR J1641+3627F (M13F). We plausibly detected the X-ray counterparts to PSR J1641+3627A (M13A), for which we placed an upper limit in X-rays of 1.3×10^{30} erg s⁻¹. We argued that the unusual X-ray-faint properties of M13A is possibly due to an unfavorable inclination of its spinning axis, with one or both hotspots on the far side from Earth.

We performed X-ray spectral analysis for all the six MSPs and found their X-ray spectra are well fitted by either a pure BB or a pure PL model. The spectra of two isolated MSPs, M13A and M13C, are well described by a single BB model, as commonly seen from isolated MSPs in other GCs, indicating thermal X-ray radiation which is likely originated from the NS surface. M13E is an eclipsing black widow pulsar and its spectrum is well fitted by a pure PL model, implying a bulk of non-thermal X-rays from this system that are most likely produced by intra-binary shock. We also found the X-ray emission from M13B is principally non-thermal. Given its X-ray properties and its

companion mass of $\sim 0.2 M_{\odot}$, we argue that M13B is a redback pulsar.

Furthermore, we looked into the optical counterparts to the four MSP binaries in M13 by incorporating observations from *HST* and found optical counterparts to M13D and M13F. Based on the position of the counterpart to M13F on CMDs, its companion is mostly likely a white dwarf. The counterpart to M13D is faint and only detected in V band, and hence its position on CMDs has a large uncertainty. However, we argue that the companion star of M13D is also a white dwarf, considering the BB-like spectrum of M13D as well as a companion mass of $\sim 0.2 M_{\odot}$. As far as we know, this is the first work to predict the nature of a MSP companion by using its X-ray properties. Our work also enlarges the population of known X-ray and optical counterparts to MSPs in GCs.

In Chapter 3, we first analyzed the *Chandra* observations of the cluster Omega Cen, and analyzed the X-ray spectra of two of the five newly discovered MSPs (PSR J1326–4728A and J1326–4728B) in this GC. The unabsorbed X-ray luminosities of these two MSPs are $\sim 2 \times 10^{30}$ erg s $^{-1}$ and $\sim 1 \times 10^{31}$ erg s $^{-1}$ (0.3–8 keV), respectively. We found that PSR J1326–4728A’s X-rays appear to be dominated by thermal X-ray emission, given its X-ray spectrum is well fitted by either a BB or a NSATMOS model, and that a power-law fit is excessively steep. The X-ray spectrum of PSR J1326–4728B is well described by a single PL model with a best-fit photon index of 2.6 ± 0.5 , indicating substantial non-thermal emission from this ‘black widow’ system.

We briefly catalogued the X-ray sources in the clusters M53, NGC 6342, and NGC 6517 and found 12 X-ray sources in these three clusters, with unabsorbed luminosities between $\sim 3 \times 10^{31}$ erg s $^{-1}$ to $\sim 8 \times 10^{32}$ erg s $^{-1}$ in the band 0.3–8 keV.

We then presented a comprehensive X-ray census of MSPs in 29 Galactic GCs. We reported X-ray luminosities for 64 GC MSPs and constrained X-ray luminosities for others, except MSPs in GCs that have no CXO observations or are contaminated severely by luminous X-ray sources. We studied the empirical X-ray luminosity function of GC MSPs using our catalogue. We found that most detected X-ray MSPs in GCs have unabsorbed luminosities

ranging from $\sim 1 \times 10^{30}$ erg s $^{-1}$ to $\sim 3 \times 10^{31}$ erg s $^{-1}$, while eclipsing spider MSPs are generally X-ray-brighter than other types of MSPs with $L_X \gtrsim 10^{31}$ erg s $^{-1}$.

We estimated the total number of MSPs in those 36 GCs by considering the correlation between the number of MSPs and stellar encounter rate in GCs. With our best-fit curves and relations, we suggested a conservative estimate of a total of ~ 1500 MSPs and an aggressive estimate of 587 MSPs, respectively, in the 36 GCs. Finally we empirically estimated the number of detectable MSPs in the Galactic bulge, assuming the GCE is generated by a large population of unresolved MSPs. We suggested between 1 and 90 MSPs with $L_X > 10^{33}$ erg s $^{-1}$ and around 20–900 MSPs with $L_X > 10^{32}$ erg s $^{-1}$, respectively, in the bulge, based on our catalogue of GC X-ray MSPs.

To sum up, our work increases the sample of X-ray and optical counterparts of MSPs and provides a comprehensive census of X-ray MSPs in GCs. Based on our catalog, one can empirically study the properties of GC MSPs and compare them with newly discovered MSPs. For example, we are investigating the potential correlation between X-ray and radio luminosities of GC MSPs using our cataloged sample, which may help us understand the radiation origin and mechanism of MSPs. Also, we will continue to study newly found GC MSPs in X-rays incorporating radio and optical observations to enrich the MSP population in GCs. More importantly, my future work in the Ph.D. program will be focusing on finding and identifying MSPs and MSP candidates in the Galactic center and/or constraining the number of MSPs therein. Hopefully, my future work will at least partly provide evidence for the origin of the puzzling GCE, which may be produced by thousands of MSPs, or else by annihilating dark matter particles.

References

- K. N. Abazajian and M. Kaplinghat. Detection of a gamma-ray source in the Galactic Center consistent with extended emission from dark matter annihilation and concentrated astrophysical emission. *Phys. Rev. D*, 86(8):083511, Oct. 2012. doi: 10.1103/PhysRevD.86.083511.
- R. Abbott, T. D. Abbott, S. Abraham, F. Acernese, K. Ackley, A. Adams, C. Adams, R. X. Adhikari, V. B. Adya, C. Affeldt, and et al. Observation of Gravitational Waves from Two Neutron Star-Black Hole Coalescences. *ApJ*, 915(1):L5, July 2021. doi: 10.3847/2041-8213/ac082e.
- A. A. Abdo, M. Ackermann, M. Ajello, L. Baldini, J. Ballet, G. Barbiellini, D. Bastieri, R. Bellazzini, R. D. Blandford, and Fermi LAT Collaboration. A population of gamma-ray emitting globular clusters seen with the Fermi Large Area Telescope. *A&A*, 524:A75, Dec. 2010. doi: 10.1051/0004-6361/201014458.
- M. Ackermann, M. Ajello, A. Albert, W. B. Atwood, L. Baldini, J. Ballet, G. Barbiellini, D. Bastieri, R. Bellazzini, E. Bissaldi, R. D. Blandford, and Fermi LAT Collaboration. The Fermi Galactic Center GeV Excess and Implications for Dark Matter. *ApJ*, 840(1):43, May 2017. doi: 10.3847/1538-4357/aa6cab.
- M. Ajello, A. Albert, W. B. Atwood, G. Barbiellini, D. Bastieri, K. Bechtol, R. Bellazzini, E. Bissaldi, R. D. Blandford, E. D. Bloom, R. Bonino, E. Bottacini, T. J. Brandt, J. Bregeon, P. Bruel, R. Buehler, S. Buson, G. A. Caliandro, R. A. Cameron, R. Caputo, M. Caragiulo, P. A. Caraveo, C. Cecchi, A. Chekhtman, J. Chiang, G. Chiaro, S. Ciprini, J. Cohen-Tanugi,

- L. R. Cominsky, J. Conrad, S. Cutini, F. D’Ammando, A. de Angelis, F. de Palma, R. Desiante, L. Di Venere, P. S. Drell, C. Favuzzi, E. C. Ferrara, P. Fusco, F. Gargano, D. Gasparri, N. Giglietto, P. Giommi, F. Giordano, M. Giroletti, T. Glanzman, G. Godfrey, G. A. Gomez-Vargas, I. A. Grenier, S. Guiriec, M. Gustafsson, A. K. Harding, J. W. Hewitt, A. B. Hill, D. Horan, T. Jogler, G. Jóhannesson, A. S. Johnson, T. Kamae, C. Karwin, J. Knödlseider, M. Kuss, S. Larsson, L. Latronico, J. Li, L. Li, F. Longo, F. Loparco, M. N. Lovellette, P. Lubrano, J. Magill, S. Maldera, D. Malyshev, A. Manfreda, M. Mayer, M. N. Mazziotta, P. F. Michelson, W. Mitthumsiri, T. Mizuno, A. A. Moiseev, M. E. Monzani, A. Morselli, I. V. Moskalenko, S. Murgia, E. Nuss, M. Ohno, T. Ohsugi, N. Omodei, E. Orlando, J. F. Ormes, D. Paneque, M. Pesce-Rollins, F. Piron, G. Pivato, T. A. Porter, S. Rainò, R. Rando, M. Razzano, A. Reimer, O. Reimer, S. Ritz, M. Sánchez-Conde, P. M. Saz Parkinson, C. Sgrò, E. J. Siskind, D. A. Smith, F. Spada, G. Spandre, P. Spinelli, D. J. Suson, H. Tajima, H. Takahashi, J. B. Thayer, D. F. Torres, G. Tosti, E. Troja, Y. Uchiyama, G. Vianello, B. L. Winer, K. S. Wood, G. Zaharijas, and S. Zimmer. Fermi-LAT Observations of High-Energy Gamma-Ray Emission toward the Galactic Center. *ApJ*, 819(1):44, Mar. 2016. doi: 10.3847/0004-637X/819/1/44.
- H. Al Noori, M. S. E. Roberts, R. A. Torres, M. A. McLaughlin, P. A. Gentile, J. W. T. Hessels, P. S. Ray, M. Kerr, and R. P. Breton. X-Ray and Optical Studies of the Redback System PSR J2129-0429. *ApJ*, 861(2):89, July 2018. doi: 10.3847/1538-4357/aac828.
- M. A. Alpar, A. F. Cheng, M. A. Ruderman, and J. Shaham. A new class of radio pulsars. *Nature*, 300(5894):728–730, Dec. 1982. doi: 10.1038/300728a0.
- R. Amato, A. D’A1, M. Del Santo, D. de Martino, A. Marino, T. Di Salvo, R. Iaria, and T. Mineo. Search for multiwavelength emission from the binary millisecond pulsar PSR J1836-2354A in the globular cluster M22. *MNRAS*, 486(3):3992–4000, July 2019. doi: 10.1093/mnras/stz1100.

- B. C. Andersen and S. M. Ransom. A Fourier Domain “Jerk” Search for Binary Pulsars. *ApJ*, 863(1):L13, Aug. 2018. doi: 10.3847/2041-8213/aad59f.
- S. B. Anderson. *A Study of Recycled Pulsars in Globular Clusters*. PhD thesis, California Institute of Technology, Pasadena., Jan. 1993.
- S. B. Anderson, A. Wolszczan, S. R. Kulkarni, and T. A. Prince. Observations of Two Millisecond Pulsars in the Globular Cluster NGC 5904. *ApJ*, 482(2):870–873, June 1997. doi: 10.1086/304162.
- J. Arons and M. Tavani. High-Energy Emission from the Eclipsing Millisecond Pulsar PSR 1957+20. *ApJ*, 403:249, Jan. 1993. doi: 10.1086/172198.
- K. M. Ashman and S. E. Zepf. *Properties of globular clusters*, page 5–30. Cambridge Astrophysics. Cambridge University Press, 1998. doi: 10.1017/CBO9780511564604.003.
- D. C. Backer, S. R. Kulkarni, C. Heiles, M. M. Davis, and W. M. Goss. A millisecond pulsar. *Nature*, 300(5893):615–618, Dec. 1982. doi: 10.1038/300615a0.
- M. Bagchi, D. R. Lorimer, and J. Chennamangalam. Luminosities of recycled radio pulsars in globular clusters. *MNRAS*, 418(1):477–489, Nov. 2011. doi: 10.1111/j.1365-2966.2011.19498.x.
- A. Bahramian, C. O. Heinke, G. R. Sivakoff, and J. C. Gladstone. Stellar Encounter Rate in Galactic Globular Clusters. *ApJ*, 766(2):136, Apr. 2013. doi: 10.1088/0004-637X/766/2/136.
- A. Bahramian, C. O. Heinke, N. Degenaar, L. Chomiuk, R. Wijnands, J. Strader, W. C. G. Ho, and D. Pooley. Limits on thermal variations in a dozen quiescent neutron stars over a decade. *MNRAS*, 452(4):3475–3488, Oct. 2015. doi: 10.1093/mnras/stv1585.
- A. Bahramian, J. Strader, L. Chomiuk, C. O. Heinke, J. C. A. Miller-Jones, N. Degenaar, A. J. Tetarenko, V. Tudor, E. Tremou, L. Shishkovsky, R. Wijnands, T. J. Maccarone, G. R. Sivakoff, and S. Ransom. The MAVERIC

- Survey: A Transitional Millisecond Pulsar Candidate in Terzan 5. *ApJ*, 864 (1):28, Sept. 2018. doi: 10.3847/1538-4357/aad68b.
- A. Bahramian, J. Strader, J. C. A. Miller-Jones, L. Chomiuk, C. O. Heinke, T. J. Maccarone, D. Pooley, L. Shishkovsky, V. Tudor, Y. Zhao, K. L. Li, G. R. Sivakoff, E. Tremou, and J. Buchner. The MAVERIC Survey: Chandra/ACIS Catalog of Faint X-Ray Sources in 38 Galactic Globular Clusters. *ApJ*, 901(1):57, Sept. 2020. doi: 10.3847/1538-4357/aba51d.
- M. Bailes, S. D. Bates, V. Bhalerao, N. D. R. Bhat, M. Burgay, S. Burke-Spolaor, N. D’Amico, S. Johnston, M. J. Keith, M. Kramer, S. R. Kulkarni, L. Levin, A. G. Lyne, S. Milia, A. Possenti, L. Spitler, B. Stappers, and W. van Straten. Transformation of a Star into a Planet in a Millisecond Pulsar Binary. *Science*, 333(6050):1717, Sept. 2011. doi: 10.1126/science.1208890.
- H. Barker and N. E. Q. Paust. Isochrone Fitting of Hubble Photometry in UV-VIS-IR Bands. *PASP*, 130(985):034204, Mar. 2018. doi: 10.1088/1538-3873/aaa597.
- C. Bassa, D. Pooley, L. Homer, F. Verbunt, B. M. Gaensler, W. H. G. Lewin, S. F. Anderson, B. Margon, V. M. Kaspi, and M. van der Klis. X-Ray Sources and Their Optical Counterparts in the Globular Cluster M4. *ApJ*, 609(2):755–765, July 2004. doi: 10.1086/421259.
- C. G. Bassa, F. Verbunt, M. H. van Kerkwijk, and L. Homer. Optical identification of the companion to PSR J1911-5958A, the pulsar binary in the outskirts of NGC 6752. *A&A*, 409:L31–L34, Oct. 2003. doi: 10.1051/0004-6361:20031339.
- C. G. Bassa, A. Patruno, J. W. T. Hessels, E. F. Keane, B. Monard, E. K. Mahony, S. Bogdanov, S. Corbel, P. G. Edwards, A. M. Archibald, G. H. Janssen, B. W. Stappers, and S. Tendulkar. A state change in the low-mass X-ray binary XSS J12270-4859. *MNRAS*, 441(2):1825–1830, June 2014. doi: 10.1093/mnras/stu708.

- H. Baumgardt and E. Vasiliev. Accurate distances to Galactic globular clusters through a combination of Gaia EDR3, HST, and literature data. *MNRAS*, 505(4):5957–5977, Aug. 2021. doi: 10.1093/mnras/stab1474.
- W. Becker and J. Trümper. Detection of pulsed X-rays from the binary millisecond pulsar J0437 - 4715. *Nature*, 365(6446):528–530, Oct. 1993. doi: 10.1038/365528a0.
- W. Becker and J. Trümper. The X-ray emission properties of millisecond pulsars. *A&A*, 341:803–817, Jan. 1999.
- W. Becker, D. A. Swartz, G. G. Pavlov, R. F. Elsner, J. Grindlay, R. Mignani, A. F. Tennant, D. Backer, L. Pulone, V. Testa, and M. C. Weisskopf. Chandra X-Ray Observatory Observations of the Globular Cluster M28 and Its Millisecond Pulsar PSR B1821-24. *ApJ*, 594(2):798–811, Sept. 2003. doi: 10.1086/376967.
- S. Begin. *A search for fast pulsars in globular clusters*. PhD thesis, University of British Columbia, 2006. URL <https://open.library.ubc.ca/collections/ubctheses/24/items/1.0066153>.
- K. Belczynski, T. Bulik, I. Mandel, B. S. Sathyaprakash, A. A. Zdziarski, and J. Mikołajewska. Cyg X-3: A Galactic Double Black Hole or Black-hole-Neutron-star Progenitor. *ApJ*, 764(1):96, Feb. 2013. doi: 10.1088/0004-637X/764/1/96.
- J. Berteaud, F. Calore, M. Clavel, P. D. Serpico, G. Dubus, and P.-O. Petrucci. The Galactic bulge millisecond pulsars shining in X rays: A gamma-ray perspective. *arXiv e-prints*, art. arXiv:2012.03580, Dec. 2020.
- G. Bertone, D. Hooper, and J. Silk. Particle dark matter: evidence, candidates and constraints. *Phys. Rep.*, 405(5-6):279–390, Jan. 2005. doi: 10.1016/j.physrep.2004.08.031.
- D. Bhattacharya and E. P. J. van den Heuvel. Formation and evolution of

- binary and millisecond radio pulsars. *Phys. Rep.*, 203(1-2):1–124, Jan. 1991. doi: 10.1016/0370-1573(91)90064-S.
- S. Bhattacharya, C. O. Heinke, A. I. Chugunov, P. C. C. Freire, A. r. Ridolfi, and S. Bogdanov. Chandra studies of the globular cluster 47 Tucanae: A deeper X-ray source catalogue, five new X-ray counterparts to millisecond radio pulsars, and new constraints to r-mode instability window. *MNRAS*, 472(3):3706–3721, Dec. 2017. doi: 10.1093/mnras/stx2241.
- S. Bogdanov. X-rays from Radio Millisecond Pulsars. In P. Weltevrede, B. B. P. Perera, L. L. Preston, and S. Sanidas, editors, *Pulsar Astrophysics the Next Fifty Years*, volume 337 of *IAU Symposium*, pages 116–119, Aug. 2018. doi: 10.1017/S1743921317011553.
- S. Bogdanov and J. E. Grindlay. Deep XMM-Newton Spectroscopic and Timing Observations of the Isolated Radio Millisecond Pulsar PSR J0030+0451. *ApJ*, 703(2):1557–1564, Oct. 2009. doi: 10.1088/0004-637X/703/2/1557.
- S. Bogdanov, J. E. Grindlay, and M. van den Berg. An X-Ray Variable Millisecond Pulsar in the Globular Cluster 47 Tucanae: Closing the Link to Low-Mass X-Ray Binaries. *ApJ*, 630(2):1029–1036, Sept. 2005. doi: 10.1086/432249.
- S. Bogdanov, J. E. Grindlay, C. O. Heinke, F. Camilo, P. C. C. Freire, and W. Becker. Chandra X-Ray Observations of 19 Millisecond Pulsars in the Globular Cluster 47 Tucanae. *ApJ*, 646(2):1104–1115, Aug. 2006. doi: 10.1086/505133.
- S. Bogdanov, M. van den Berg, C. O. Heinke, H. N. Cohn, P. M. Lugger, and J. E. Grindlay. A Chandra X-ray Observatory Study of PSR J1740-5340 and Candidate Millisecond Pulsars in the Globular Cluster NGC 6397. *ApJ*, 709(1):241–250, Jan. 2010. doi: 10.1088/0004-637X/709/1/241.
- S. Bogdanov, A. M. Archibald, J. W. T. Hessels, V. M. Kaspi, D. Lorimer, M. A. McLaughlin, S. M. Ransom, and I. H. Stairs. A Chandra X-Ray

- Observation of the Binary Millisecond Pulsar PSR J1023+0038. *ApJ*, 742(2):97, Dec. 2011a. doi: 10.1088/0004-637X/742/2/97.
- S. Bogdanov, M. van den Berg, M. Servillat, C. O. Heinke, J. E. Grindlay, I. H. Stairs, S. M. Ransom, P. C. C. Freire, S. Bégin, and W. Becker. Chandra X-ray Observations of 12 Millisecond Pulsars in the Globular Cluster M28. *ApJ*, 730(2):81, Apr. 2011b. doi: 10.1088/0004-637X/730/2/81.
- S. Bogdanov, S. Guillot, P. S. Ray, M. T. Wolff, D. Chakrabarty, W. C. G. Ho, M. Kerr, F. K. Lamb, A. Lommen, R. M. Ludlam, R. Milburn, S. Montano, M. C. Miller, M. Bauböck, F. Özel, D. Psaltis, R. A. Remillard, T. E. Riley, J. F. Steiner, T. E. Strohmayer, A. L. Watts, K. S. Wood, J. Zeldes, T. Enoto, T. Okajima, J. W. Kellogg, C. Baker, C. B. Markwardt, Z. Arzoumanian, and K. C. Gendreau. Constraining the Neutron Star Mass-Radius Relation and Dense Matter Equation of State with NICER. I. The Millisecond Pulsar X-Ray Data Set. *ApJ*, 887(1):L25, Dec. 2019a. doi: 10.3847/2041-8213/ab53eb.
- S. Bogdanov, F. K. Lamb, S. Mahmoodifar, M. C. Miller, S. M. Morsink, T. E. Riley, T. E. Strohmayer, A. K. Tung, A. L. Watts, A. J. Dittmann, D. Chakrabarty, S. Guillot, Z. Arzoumanian, and K. C. Gendreau. Constraining the Neutron Star Mass-Radius Relation and Dense Matter Equation of State with NICER. II. Emission from Hot Spots on a Rapidly Rotating Neutron Star. *ApJ*, 887(1):L26, Dec. 2019b. doi: 10.3847/2041-8213/ab5968.
- S. Bogdanov, A. Bahramian, C. O. Heinke, P. C. C. Freire, J. W. T. Hessels, S. M. Ransom, and I. H. Stairs. A Deep Chandra X-Ray Observatory Study of the Millisecond Pulsar Population in the Globular Cluster Terzan 5. *ApJ*, 912(2):124, May 2021. doi: 10.3847/1538-4357/abee78.
- T. D. Brandt and B. Kocsis. Disrupted Globular Clusters Can Explain the Galactic Center Gamma-Ray Excess. *ApJ*, 812(1):15, Oct. 2015. doi: 10.1088/0004-637X/812/1/15.

- M. Burgay, N. D’Amico, A. Possenti, R. N. Manchester, A. G. Lyne, B. C. Joshi, M. A. McLaughlin, M. Kramer, J. M. Sarkissian, F. Camilo, V. Kalogera, C. Kim, and D. R. Lorimer. An increased estimate of the merger rate of double neutron stars from observations of a highly relativistic system. *Nature*, 426(6966):531–533, Dec. 2003. doi: 10.1038/nature02124.
- E. M. Cackett, R. Wijnands, C. O. Heinke, D. Pooley, W. H. G. Lewin, J. E. Grindlay, P. D. Edmonds, P. G. Jonker, and J. M. Miller. A Chandra X-ray observation of the globular cluster Terzan 1. *MNRAS*, 369(1):407–415, June 2006. doi: 10.1111/j.1365-2966.2006.10315.x.
- M. Cadelano, S. M. Ransom, P. C. C. Freire, F. R. Ferraro, J. W. T. Hessels, B. Lanzoni, C. Pallanca, and I. H. Stairs. Discovery of Three New Millisecond Pulsars in Terzan 5. *ApJ*, 855(2):125, Mar. 2018. doi: 10.3847/1538-4357/aaac2a.
- M. Cadelano, F. R. Ferraro, A. G. Istrate, C. Pallanca, B. Lanzoni, and P. C. C. Freire. An Extremely Low-mass He White Dwarf Orbiting the Millisecond Pulsar J1342+2822B in the Globular Cluster M3. *ApJ*, 875(1):25, Apr. 2019. doi: 10.3847/1538-4357/ab0e6b.
- M. Cadelano, J. Chen, C. Pallanca, A. G. Istrate, F. R. Ferraro, B. Lanzoni, P. C. C. Freire, and M. Salaris. PSR J1641+3627F: a low-mass He White Dwarf orbiting a possible high-mass neutron star in the Globular Cluster M13. *ApJ*, *in press (arXiv:2010.09740)*, 2020.
- F. Calore, I. Cholis, and C. Weniger. Background model systematics for the Fermi GeV excess. *J. Cosmology Astropart. Phys.*, 2015(3):038, Mar. 2015. doi: 10.1088/1475-7516/2015/03/038.
- A. D. Cameron, D. J. Champion, M. Kramer, M. Bailes, E. D. Barr, C. G. Bassa, S. Bhandari, N. D. R. Bhat, M. Burgay, S. Burke-Spolaor, R. P. Eatough, C. M. L. Flynn, P. C. C. Freire, A. Jameson, S. Johnston, R. Karuppusamy, M. J. Keith, L. Levin, D. R. Lorimer, A. G. Lyne, M. A. McLaughlin, C. Ng, E. Petroff, A. Possenti, A. Ridolfi, B. W.

- Stappers, W. van Straten, T. M. Tauris, C. Tiburzi, and N. Wex. The High Time Resolution Universe Pulsar Survey - XIII. PSR J1757-1854, the most accelerated binary pulsar. *MNRAS*, 475(1):L57–L61, Mar. 2018. doi: 10.1093/mnras/sly003.
- F. Camilo and F. A. Rasio. Pulsars in Globular Clusters. In F. A. Rasio and I. H. Stairs, editors, *Binary Radio Pulsars*, volume 328 of *Astronomical Society of the Pacific Conference Series*, page 147, July 2005.
- F. Camilo, D. R. Lorimer, P. Freire, A. G. Lyne, and R. N. Manchester. Observations of 20 Millisecond Pulsars in 47 Tucanae at 20 Centimeters. *ApJ*, 535(2):975–990, June 2000. doi: 10.1086/308859.
- J. A. Cardelli, G. C. Clayton, and J. S. Mathis. The Relationship between Infrared, Optical, and Ultraviolet Extinction. *ApJ*, 345:245, Oct. 1989. doi: 10.1086/167900.
- E. Carlson and S. Profumo. Cosmic ray protons in the inner Galaxy and the Galactic Center gamma-ray excess. *Phys. Rev. D*, 90(2):023015, July 2014. doi: 10.1103/PhysRevD.90.023015.
- W. Cash. Parameter estimation in astronomy through application of the likelihood ratio. *ApJ*, 228:939–947, Mar. 1979. doi: 10.1086/156922.
- Z. Cheng, Z. Li, X. Li, X. Xu, and T. Fang. Exploring the Mass Segregation Effect of X-Ray Sources in Globular Clusters: The Case of 47 Tucanae. *ApJ*, 876(1):59, May 2019. doi: 10.3847/1538-4357/ab1593.
- D. O. Chernyshov, A. E. Egorov, V. A. Dogiel, and A. V. Ivlev. On a possible origin of the gamma-ray excess around the Galactic Center. *arXiv e-prints*, art. arXiv:2108.04104, Aug. 2021.
- I. Cholis, C. Evoli, F. Calore, T. Linden, C. Weniger, and D. Hooper. The Galactic Center GeV excess from a series of leptonic cosmic-ray outbursts. *J. Cosmology Astropart. Phys.*, 2015(12):005, Dec. 2015a. doi: 10.1088/1475-7516/2015/12/005.

- I. Cholis, D. Hooper, and T. Linden. Challenges in explaining the Galactic Center gamma-ray excess with millisecond pulsars. *J. Cosmology Astropart. Phys.*, 2015(6):043, June 2015b. doi: 10.1088/1475-7516/2015/06/043.
- G. W. Clark. X-ray binaries in globular clusters. *ApJ*, 199:L143–L145, Aug. 1975. doi: 10.1086/181869.
- A. M. Cool, D. Haggard, T. Arias, M. Brochmann, J. Dorfman, A. Gafford, V. White, and J. Anderson. HST/ACS Imaging of Omega Centauri: Optical Counterparts of Chandra X-Ray Sources. *ApJ*, 763(2):126, Feb. 2013. doi: 10.1088/0004-637X/763/2/126.
- S. Dai, S. Johnston, M. Kerr, F. Camilo, A. Cameron, L. Toomey, and H. Kumamoto. Discovery of Millisecond Pulsars in the Globular Cluster Omega Centauri. *ApJ*, 888(2):L18, Jan. 2020. doi: 10.3847/2041-8213/ab621a.
- N. D’Amico, M. Bailes, A. G. Lyne, R. N. Manchester, S. Johnston, A. S. Fruchter, and W. M. Goss. PSR B1802-0 : a globular pulsar in an eccentric binary system. *MNRAS*, 260:L7–L10, Jan. 1993. doi: 10.1093/mnras/260.1.L7.
- N. D’Amico, A. G. Lyne, R. N. Manchester, A. Possenti, and F. Camilo. Discovery of Short-Period Binary Millisecond Pulsars in Four Globular Clusters. *ApJ*, 548(2):L171–L174, Feb. 2001. doi: 10.1086/319096.
- T. Daylan, D. P. Finkbeiner, D. Hooper, T. Linden, S. K. N. Portillo, N. L. Rodd, and T. R. Slatyer. The characterization of the gamma-ray signal from the central Milky Way: A case for annihilating dark matter. *Physics of the Dark Universe*, 12:1–23, June 2016. doi: 10.1016/j.dark.2015.12.005.
- G. de Marchi, B. Leibundgut, F. Paresce, and L. Pulone. A deep optical luminosity function of NGC 6712 with the VLT: Evidence for severe tidal disruption. *A&A*, 343:L9–L14, Mar. 1999.
- M. E. DeCesar, S. M. Ransom, D. L. Kaplan, P. S. Ray, and A. M. Geller. A

- Highly Eccentric 3.9 Millisecond Binary Pulsar in the Globular Cluster NGC 6652. *ApJ*, 807(2):L23, July 2015. doi: 10.1088/2041-8205/807/2/L23.
- W. T. S. Deich, J. Middleditch, S. B. Anderson, S. R. Kulkarni, T. A. Prince, and A. Wolszczan. The Binary Pulsar PSR 1908+00 in NGC 6760. *ApJ*, 410:L95, June 1993. doi: 10.1086/186888.
- D. Deras, A. Arellano Ferro, C. Lázaro, I. H. Bustos Fierro, J. H. Calderón, S. Muneer, and S. Giridhar. A new study of the variable star population in the Hercules globular cluster (M13; NGC 6205). *MNRAS*, 486(2):2791–2808, June 2019. doi: 10.1093/mnras/stz642.
- M. Di Mauro. Characteristics of the Galactic Center excess measured with 11 years of Fermi-LAT data. *Phys. Rev. D*, 103(6):063029, Mar. 2021. doi: 10.1103/PhysRevD.103.063029.
- A. E. Dolphin. WFPC2 Stellar Photometry with HSTPHOT. *PASP*, 112(776):1383–1396, Oct 2000. doi: 10.1086/316630.
- P. D. Edmonds, R. L. Gilliland, C. O. Heinke, J. E. Grindlay, and F. Camilo. Optical Detection of a Variable Millisecond Pulsar Companion in 47 Tucanae. *ApJ*, 557(1):L57–L60, Aug. 2001. doi: 10.1086/323122.
- P. D. Edmonds, R. L. Gilliland, C. O. Heinke, and J. E. Grindlay. An Extensive Census of Hubble Space Telescope Counterparts to Chandra X-Ray Sources in the Globular Cluster 47 Tucanae. I. Astrometry and Photometry. *ApJ*, 596(2):1177–1196, Oct. 2003. doi: 10.1086/378193.
- R. F. Elsner, C. O. Heinke, H. N. Cohn, P. M. Lugger, J. E. Maxwell, I. H. Stairs, S. M. Ransom, J. W. T. Hessels, W. Becker, R. H. H. Huang, P. D. Edmonds, J. E. Grindlay, S. Bogdanov, K. Ghosh, and M. C. Weisskopf. Chandra X-Ray Observatory Observations of the Globular Cluster M71. *ApJ*, 687(2):1019–1034, Nov. 2008. doi: 10.1086/591899.
- A. C. Fabian, J. E. Pringle, and M. J. Rees. Tidal capture formation of binary

- systems and X-ray sources in globular clusters. *MNRAS*, 172:15, Aug. 1975. doi: 10.1093/mnras/172.1.15P.
- R. D. Ferdman, I. H. Stairs, M. Kramer, G. H. Janssen, C. G. Bassa, B. W. Stappers, P. B. Demorest, I. Cognard, G. Desvignes, G. Theureau, M. Burgay, A. G. Lyne, R. N. Manchester, and A. Possenti. PSR J1756-2251: a pulsar with a low-mass neutron star companion. *MNRAS*, 443(3):2183–2196, Sept. 2014. doi: 10.1093/mnras/stu1223.
- F. R. Ferraro, A. Possenti, N. D’Amico, and E. Sabbi. The Bright Optical Companion to the Eclipsing Millisecond Pulsar in NGC 6397. *ApJ*, 561(1):L93–L96, Nov. 2001. doi: 10.1086/324563.
- F. R. Ferraro, C. Pallanca, B. Lanzoni, M. Cadelano, D. Massari, E. Dalessandro, and A. Mucciarelli. Probing the MSP Prenatal Stage: The Optical Identification of the X-Ray Burster EXO 1745-248 in Terzan 5. *ApJ*, 807(1):L1, July 2015. doi: 10.1088/2041-8205/807/1/L1.
- L. M. Forestell, C. O. Heinke, H. N. Cohn, P. M. Lugger, G. R. Sivakoff, S. Bogdanov, A. M. Cool, and J. Anderson. A Chandra look at the X-ray faint millisecond pulsars in the globular cluster NGC 6752. *MNRAS*, 441(1):757–768, June 2014. doi: 10.1093/mnras/stu559.
- P. E. Freeman, V. Kashyap, R. Rosner, and D. Q. Lamb. A Wavelet-Based Algorithm for the Spatial Analysis of Poisson Data. *ApJS*, 138(1):185–218, Jan. 2002. doi: 10.1086/324017.
- P. C. Freire, F. Camilo, D. R. Lorimer, A. G. Lyne, R. N. Manchester, and N. D’Amico. Timing the millisecond pulsars in 47 Tucanae. *MNRAS*, 326(3):901–915, Sept. 2001. doi: 10.1046/j.1365-8711.2001.04493.x.
- P. C. Freire, F. Camilo, M. Kramer, D. R. Lorimer, A. G. Lyne, R. N. Manchester, and N. D’Amico. Further results from the timing of the millisecond pulsars in 47 Tucanae. *MNRAS*, 340(4):1359–1374, Apr. 2003. doi: 10.1046/j.1365-8711.2003.06392.x.

- P. C. C. Freire. Eclipsing Binary Pulsars. In F. A. Rasio and I. H. Stairs, editors, *Binary Radio Pulsars*, volume 328 of *Astronomical Society of the Pacific Conference Series*, page 405, July 2005.
- P. C. C. Freire, J. W. T. Hessels, D. J. Nice, S. M. Ransom, D. R. Lorimer, and I. H. Stairs. The Millisecond Pulsars in NGC 6760. *ApJ*, 621(2):959–965, Mar. 2005. doi: 10.1086/427748.
- P. C. C. Freire, S. M. Ransom, S. Bégin, I. H. Stairs, J. W. T. Hessels, L. H. Frey, and F. Camilo. Eight New Millisecond Pulsars in NGC 6440 and NGC 6441. *ApJ*, 675(1):670–682, Mar. 2008. doi: 10.1086/526338.
- P. C. C. Freire, A. Ridolfi, M. Kramer, C. Jordan, R. N. Manchester, P. Torne, J. Sarkissian, C. O. Heinke, N. D’Amico, F. Camilo, D. R. Lorimer, and A. G. Lyne. Long-term observations of the pulsars in 47 Tucanae - II. Proper motions, accelerations and jerks. *MNRAS*, 471(1):857–876, Oct. 2017. doi: 10.1093/mnras/stx1533.
- A. S. Fruchter and W. M. Goss. The Continuum Eclipse of PSR 1957+20. *ApJ*, 384:L47, Jan. 1992. doi: 10.1086/186259.
- A. S. Fruchter, D. R. Stinebring, and J. H. Taylor. A millisecond pulsar in an eclipsing binary. *Nature*, 333(6170):237–239, May 1988. doi: 10.1038/333237a0.
- A. Fruscione, J. C. McDowell, G. E. Allen, N. S. Brickhouse, D. J. Burke, J. E. Davis, N. Durham, M. Elvis, E. C. Galle, D. E. Harris, D. P. Huenemoerder, J. C. Houck, B. Ishibashi, M. Karovska, F. Nicastro, M. S. Noble, M. A. Nowak, F. A. Primini, A. Siemiginowska, R. K. Smith, and M. Wise. CIAO: Chandra’s data analysis system. In *Society of Photo-Optical Instrumentation Engineers (SPIE) Conference Series*, volume 6270 of *Society of Photo-Optical Instrumentation Engineers (SPIE) Conference Series*, page 62701V, June 2006. doi: 10.1117/12.671760.
- N. Gehrels. Confidence Limits for Small Numbers of Events in Astrophysical Data. *ApJ*, 303:336, Apr. 1986. doi: 10.1086/164079.

- P. A. Gentile, M. S. E. Roberts, M. A. McLaughlin, F. Camilo, J. W. T. Hessels, M. Kerr, S. M. Ransom, P. S. Ray, and I. H. Stairs. X-Ray Observations of Black Widow Pulsars. *ApJ*, 783(2):69, Mar. 2014. doi: 10.1088/0004-637X/783/2/69.
- R. Giacconi, S. Murray, H. Gursky, E. Kellogg, E. Schreier, and H. Tananbaum. The Uhuru catalog of X-ray sources. *ApJ*, 178:281–308, Dec. 1972. doi: 10.1086/151790.
- R. Giacconi, S. Murray, H. Gursky, E. Kellogg, E. Schreier, T. Matilsky, D. Koch, and H. Tananbaum. The Third UHURU Catalog of X-Ray Sources. *ApJS*, 27:37, Feb. 1974. doi: 10.1086/190288.
- G. A. Gontcharov, M. Y. Khovritchev, and A. V. Mosenkov. Isochrone fitting of Galactic globular clusters - II. NGC 6205 (M13). *MNRAS*, 497(3):3674–3693, Aug. 2020. doi: 10.1093/mnras/staa1694.
- P. L. Gonthier, A. K. Harding, E. C. Ferrara, S. E. Frederick, V. E. Mohr, and Y.-M. Koh. Population Syntheses of Millisecond Pulsars from the Galactic Disk and Bulge. *ApJ*, 863(2):199, Aug. 2018. doi: 10.3847/1538-4357/aad08d.
- L. Goodenough and D. Hooper. Possible Evidence For Dark Matter Annihilation In The Inner Milky Way From The Fermi Gamma Ray Space Telescope. *arXiv e-prints*, art. arXiv:0910.2998, Oct. 2009.
- C. Gordon and O. Macías. Dark matter and pulsar model constraints from Galactic Center Fermi-LAT gamma-ray observations. *Phys. Rev. D*, 88(8):083521, Oct. 2013. doi: 10.1103/PhysRevD.88.083521.
- J. E. Grindlay, C. O. Heinke, P. D. Edmonds, S. S. Murray, and A. M. Cool. Chandra Exposes the Core-collapsed Globular Cluster NGC 6397. *ApJ*, 563(1):L53–L56, Dec. 2001. doi: 10.1086/338499.
- S. Guillot, V. M. Kaspi, R. F. Archibald, M. Bachetti, C. Flynn, F. Jankowski, M. Bailes, S. Boggs, F. E. Christensen, W. W. Craig, C. A. Hailey, F. A.

- Harrison, D. Stern, and W. W. Zhang. The NuSTAR view of the non-thermal emission from PSR J0437-4715. *MNRAS*, 463(3):2612–2622, Dec. 2016. doi: 10.1093/mnras/stw2194.
- D. Haggard, A. M. Cool, and M. B. Davies. A Chandra Study of the Galactic Globular Cluster Omega Centauri. *ApJ*, 697(1):224–236, May 2009. doi: 10.1088/0004-637X/697/1/224.
- A. K. Harding and A. G. Muslimov. Pulsar Polar Cap Heating and Surface Thermal X-Ray Emission. II. Inverse Compton Radiation Pair Fronts. *ApJ*, 568(2):862–877, Apr. 2002. doi: 10.1086/338985.
- W. E. Harris. A Catalog of Parameters for Globular Clusters in the Milky Way. *AJ*, 112:1487, Oct. 1996. doi: 10.1086/118116.
- W. E. Harris and R. Racine. Globular clusters in galaxies. *ARA&A*, 17: 241–274, Jan. 1979. doi: 10.1146/annurev.aa.17.090179.001325.
- C. He, C. Y. Ng, and V. M. Kaspi. The Correlation between Dispersion Measure and X-Ray Column Density from Radio Pulsars. *ApJ*, 768(1):64, May 2013. doi: 10.1088/0004-637X/768/1/64.
- C. O. Heinke, P. D. Edmonds, and J. E. Grindlay. Identification of the Low-Mass X-Ray Binary and Faint X-Ray Sources in NGC 6652. *ApJ*, 562(1): 363–367, Nov. 2001. doi: 10.1086/323493.
- C. O. Heinke, J. E. Grindlay, P. M. Lugger, H. N. Cohn, P. D. Edmonds, D. A. Lloyd, and A. M. Cool. Analysis of the Quiescent Low-Mass X-Ray Binary Population in Galactic Globular Clusters. *ApJ*, 598(1):501–515, Nov. 2003. doi: 10.1086/378885.
- C. O. Heinke, J. E. Grindlay, P. D. Edmonds, H. N. Cohn, P. M. Lugger, F. Camilo, S. Bogdanov, and P. C. Freire. A Deep Chandra Survey of the Globular Cluster 47 Tucanae: Catalog of Point Sources. *ApJ*, 625(2): 796–824, June 2005. doi: 10.1086/429899.

- C. O. Heinke, G. B. Rybicki, R. Narayan, and J. E. Grindlay. A Hydrogen Atmosphere Spectral Model Applied to the Neutron Star X7 in the Globular Cluster 47 Tucanae. *ApJ*, 644(2):1090–1103, June 2006a. doi: 10.1086/503701.
- C. O. Heinke, R. Wijnands, H. N. Cohn, P. M. Lugger, J. E. Grindlay, D. Pooley, and W. H. G. Lewin. Faint X-Ray Sources in the Globular Cluster Terzan 5. *ApJ*, 651(2):1098–1111, Nov. 2006b. doi: 10.1086/507884.
- C. O. Heinke, D. Altamirano, H. N. Cohn, P. M. Lugger, S. A. Budac, M. Servillat, M. Linares, T. E. Strohmayer, C. B. Markwardt, R. Wijnands, J. H. Swank, C. Knigge, C. Bailyn, and J. E. Grindlay. Discovery of a Second Transient Low-Mass X-ray Binary in the Globular Cluster Ngc 6440. *ApJ*, 714(1):894–903, May 2010. doi: 10.1088/0004-637X/714/1/894.
- S. Henleywillis, A. M. Cool, D. Haggard, C. Heinke, P. Callanan, and Y. Zhao. A Deep X-ray Survey of the globular cluster Omega Centauri. *MNRAS*, 479(2):2834–2852, Sept. 2018. doi: 10.1093/mnras/sty675.
- J. W. T. Hessels, S. M. Ransom, I. H. Stairs, P. C. C. Freire, V. M. Kaspi, and F. Camilo. A Radio Pulsar Spinning at 716 Hz. *Science*, 311(5769):1901–1904, Mar. 2006. doi: 10.1126/science.1123430.
- J. W. T. Hessels, S. M. Ransom, I. H. Stairs, V. M. Kaspi, and P. C. C. Freire. A 1.4 GHz Arecibo Survey for Pulsars in Globular Clusters. *ApJ*, 670(1):363–378, Nov. 2007. doi:10.1086/521780.
- A. Hewish, S. J. Bell, J. D. H. Pilkington, P. F. Scott, and R. A. Collins. Observation of a Rapidly Pulsating Radio Source. *Nature*, 217(5130):709–713, Feb. 1968. doi: 10.1038/217709a0.
- J. G. Hills. The formation of binaries containing black holes by the exchange of companions and the X-ray sources in globular clusters. *MNRAS*, 175:1P–4P, Apr. 1976. doi: 10.1093/mnras/175.1.1P.

G. Hobbs, A. Archibald, Z. Arzoumanian, D. Backer, M. Bailes, N. D. R. Bhat, M. Burgay, S. Burke-Spolaor, D. Champion, I. Cognard, W. Coles, J. Cordes, P. Demorest, G. Desvignes, R. D. Ferdman, L. Finn, P. Freire, M. Gonzalez, J. Hessels, A. Hotan, G. Janssen, F. Jenet, A. Jessner, C. Jordan, V. Kaspi, M. Kramer, V. Kondratiev, J. Lazio, K. Lazaridis, K. J. Lee, Y. Levin, A. Lommen, D. Lorimer, R. Lynch, A. Lyne, R. Manchester, M. McLaughlin, D. Nice, S. Osłowski, M. Pilia, A. Possenti, M. Purver, S. Ransom, J. Reynolds, S. Sanidas, J. Sarkissian, A. Sesana, R. Shannon, X. Siemens, I. Stairs, B. Stappers, D. Stinebring, G. Theureau, R. van Haasteren, W. van Straten, J. P. W. Verbiest, D. R. B. Yardley, and X. P. You. The International Pulsar Timing Array project: using pulsars as a gravitational wave detector. *Classical and Quantum Gravity*, 27(8):084013, Apr. 2010. doi: 10.1088/0264-9381/27/8/084013.

G. Hobbs, R. N. Manchester, A. Dunning, A. Jameson, P. Roberts, D. George, J. A. Green, J. Tuthill, L. Toomey, J. F. Kaczmarek, S. Mader, M. Marquarding, A. Ahmed, S. W. Amy, M. Bailes, R. Beresford, N. D. R. Bhat, D. C. J. Bock, M. Bourne, M. Bowen, M. Brothers, A. D. Cameron, E. Carretti, N. Carter, S. Castillo, R. Chekkala, W. Cheng, Y. Chung, D. A. Craig, S. Dai, J. Dawson, J. Dempsey, P. Doherty, B. Dong, P. Edwards, T. Ergesh, X. Gao, J. Han, D. Hayman, B. Indermuehle, K. Jeganathan, S. Johnston, H. Kanoniuk, M. Kesteven, M. Kramer, M. Leach, V. McIntyre, V. Moss, S. Osłowski, C. Phillips, N. Pope, B. Preisig, D. Price, K. Reeves, L. Reilly, J. Reynolds, T. Robishaw, P. Roush, T. Ruckley, E. Sadler, J. Sarkissian, S. Severs, R. Shannon, K. Smart, M. Smith, S. Smith, C. Sobey, L. Staveley-Smith, A. Tzioumis, W. van Straten, N. Wang, L. Wen, and M. Whiting. An ultra-wide bandwidth (704 to 4 032 MHz) receiver for the Parkes radio telescope. *Publ. Astron. Soc. Australia*, 37:e012, Apr. 2020. doi: 10.1017/pasa.2020.2.

J. Hong, M. van den Berg, E. M. Schlegel, J. E. Grindlay, X. Koenig, S. Laycock, and P. Zhao. X-Ray Processing of ChaMPlane Fields: Methods and

- Initial Results for Selected Anti-Galactic Center Fields. *ApJ*, 635:907–919, Dec. 2005. doi: 10.1086/496966.
- D. Hooper and L. Goodenough. Dark matter annihilation in the Galactic Center as seen by the Fermi Gamma Ray Space Telescope. *Physics Letters B*, 697(5):412–428, Mar. 2011. doi: 10.1016/j.physletb.2011.02.029.
- R. H. H. Huang, W. Becker, P. D. Edmonds, R. F. Elsner, C. O. Heinke, and B. C. Hsieh. Study of Hubble Space Telescope counterparts to Chandra X-ray sources in the globular cluster M 71. *A&A*, 513:A16, Apr. 2010. doi: 10.1051/0004-6361/200811245.
- P. J. Humphrey, W. Liu, and D. A. Buote. χ^2 and Poissonian Data: Biases Even in the High-Count Regime and How to Avoid Them. *ApJ*, 693(1): 822–829, Mar. 2009. doi: 10.1088/0004-637X/693/1/822.
- A. Igoshev, F. Verbunt, and E. Cator. Distance and luminosity probability distributions derived from parallax and flux with their measurement errors. With application to the millisecond pulsar PSR J0218+4232. *A&A*, 591: A123, June 2016. doi: 10.1051/0004-6361/201527471.
- J. J. M. in’t Zand, M. H. van Kerkwijk, D. Pooley, F. Verbunt, R. Wijnands, and W. H. G. Lewin. Identification of the Optical and Quiescent Counterparts to the Bright X-Ray Transient in NGC 6440. *ApJ*, 563(1):L41–L44, Dec. 2001. doi: 10.1086/338361.
- D. Kandel, R. W. Romani, and H. An. The Synchrotron Emission Pattern of Intrabinary Shocks. *ApJ*, 879(2):73, July 2019. doi: 10.3847/1538-4357/ab24d9.
- D. L. Kaplan, K. Stovall, M. H. van Kerkwijk, C. Fremling, and A. G. Istrate. A Dense Companion to the Short-period Millisecond Pulsar Binary PSR J0636+5128. *ApJ*, 864(1):15, Sept. 2018. doi: 10.3847/1538-4357/aad54c.
- J. I. Katz. Two kinds of stellar collapse. *Nature*, 253(5494):698–699, Feb. 1975. doi: 10.1038/253698a0.

- M. Kramer, I. H. Stairs, R. N. Manchester, M. A. McLaughlin, A. G. Lyne, R. D. Ferdman, M. Burgay, D. R. Lorimer, A. Possenti, N. D'Amico, J. M. Sarkissian, G. B. Hobbs, J. E. Reynolds, P. C. C. Freire, and F. Camilo. Tests of General Relativity from Timing the Double Pulsar. *Science*, 314 (5796):97–102, Oct. 2006. doi: 10.1126/science.1132305.
- S. R. Kulkarni, S. B. Anderson, T. A. Prince, and A. Wolszczan. Old pulsars in the low-density globular clusters MI3 and M53. *Nature*, 349(6304):47–49, Jan. 1991. doi: 10.1038/349047a0.
- J. Lee, C. Y. Hui, J. Takata, A. K. H. Kong, P. H. T. Tam, and K. S. Cheng. X-Ray Census of Millisecond Pulsars in the Galactic Field. *ApJ*, 864(1):23, Sept. 2018. doi: 10.3847/1538-4357/aad284.
- M. Linares, A. Bahramian, C. Heinke, R. Wijnands, A. Patruno, D. Altamirano, J. Homan, S. Bogdanov, and D. Pooley. The neutron star transient and millisecond pulsar in M28: from sub-luminous accretion to rotation-powered quiescence. *MNRAS*, 438(1):251–261, Feb. 2014. doi: 10.1093/mnras/stt2167.
- D. R. Lorimer. Binary and Millisecond Pulsars. *Living Reviews in Relativity*, 11(1):8, Nov. 2008. doi: 10.12942/lrr-2008-8.
- T.-N. Lu, A. K. H. Kong, C. Bassa, F. Verbunt, W. H. G. Lewin, S. F. Anderson, and D. Pooley. X-ray Sources and their Optical Counterparts in the Galactic Globular Cluster M12 (NGC 6218). *ApJ*, 705(1):175–183, Nov. 2009. doi: 10.1088/0004-637X/705/1/175.
- T.-N. Lu, A. K. H. Kong, F. Verbunt, W. H. G. Lewin, S. F. Anderson, and D. Pooley. Chandra and HST Studies of the X-Ray Sources in Galactic Globular Cluster M92. *ApJ*, 736(2):158, Aug. 2011. doi: 10.1088/0004-637X/736/2/158.
- R. S. Lynch, S. M. Ransom, P. C. C. Freire, and I. H. Stairs. Six New Recycled Globular Cluster Pulsars Discovered with the Green Bank Telescope. *ApJ*, 734(2):89, June 2011. doi: 10.1088/0004-637X/734/2/89.

- R. S. Lynch, P. C. C. Freire, S. M. Ransom, and B. A. Jacoby. The Timing of Nine Globular Cluster Pulsars. *ApJ*, 745(2):109, Feb. 2012. doi: 10.1088/0004-637X/745/2/109.
- A. Lyne and F. Graham-Smith. *11 Millisecond and binary pulsars*, page 151–169. Cambridge Astrophysics. Cambridge University Press, 4 edition, 2012a. doi: 10.1017/CBO9780511844584.012.
- A. Lyne and F. Graham-Smith. *14 Supernovae and their remnants*, page 192–206. Cambridge Astrophysics. Cambridge University Press, 4 edition, 2012b. doi: 10.1017/CBO9780511844584.015.
- A. G. Lyne, S. H. Mankelow, J. F. Bell, and R. N. Manchester. Radio pulsars in Terzan 5. *MNRAS*, 316(3):491–493, Aug. 2000. doi: 10.1046/j.1365-8711.2000.03517.x.
- A. G. Lyne, M. Burgay, M. Kramer, A. Possenti, R. N. Manchester, F. Camilo, M. A. McLaughlin, D. R. Lorimer, N. D’Amico, B. C. Joshi, J. Reynolds, and P. C. C. Freire. A Double-Pulsar System: A Rare Laboratory for Relativistic Gravity and Plasma Physics. *Science*, 303(5661):1153–1157, Feb. 2004. doi: 10.1126/science.1094645.
- O. Macias, C. Gordon, R. M. Crocker, B. Coleman, D. Paterson, S. Horiuchi, and M. Pohl. Galactic bulge preferred over dark matter for the Galactic centre gamma-ray excess. *Nature Astronomy*, 2:387–392, Mar. 2018. doi: 10.1038/s41550-018-0414-3.
- R. Main, I. S. Yang, V. Chan, D. Li, F. X. Lin, N. Mahajan, U.-L. Pen, K. Vanderlinde, and M. H. van Kerkwijk. Pulsar emission amplified and resolved by plasma lensing in an eclipsing binary. *Nature*, 557(7706):522–525, May 2018. doi: 10.1038/s41586-018-0133-z.
- R. N. Manchester, A. G. Lyne, C. Robinson, N. D’Amico, M. Bailes, and J. Lim. Discovery of ten millisecond pulsars in the globular cluster 47 Tucanae. *Nature*, 352(6332):219–221, July 1991. doi: 10.1038/352219a0.

- R. N. Manchester, G. B. Hobbs, A. Teoh, and M. Hobbs. The Australia Telescope National Facility Pulsar Catalogue. *AJ*, 129(4):1993–2006, Apr. 2005. doi: 10.1086/428488.
- D. Massari, A. Mucciarelli, E. Dalessandro, F. R. Ferraro, L. Origlia, B. Lanzoni, G. Beccari, R. M. Rich, E. Valenti, and S. M. Ransom. High-resolution Reddening Map in the Direction of the Stellar System Terzan 5. *ApJ*, 755(2):L32, Aug. 2012. doi: 10.1088/2041-8205/755/2/L32.
- D. McConnell, A. A. Deshpande, T. Connors, and J. G. Ables. The radio luminosity distribution of pulsars in 47 Tucanae. *MNRAS*, 348(4):1409–1414, Mar. 2004. doi: 10.1111/j.1365-2966.2004.07447.x.
- M. C. Miller, F. K. Lamb, A. J. Dittmann, S. Bogdanov, Z. Arzoumanian, K. C. Gendreau, S. Guillot, A. K. Harding, W. C. G. Ho, J. M. Lattimer, R. M. Ludlam, S. Mahmoodifar, S. M. Morsink, P. S. Ray, T. E. Strohmayer, K. S. Wood, T. Enoto, R. Foster, T. Okajima, G. Prigozhin, and Y. Soong. PSR J0030+0451 Mass and Radius from NICER Data and Implications for the Properties of Neutron Star Matter. *ApJ*, 887(1):L24, Dec. 2019. doi: 10.3847/2041-8213/ab50c5.
- S. Murgia. The Fermi-LAT Galactic Center Excess: Evidence of Annihilating Dark Matter? *Annual Review of Nuclear and Particle Science*, 70:455–483, Oct. 2020. doi: 10.1146/annurev-nucl-101916-123029.
- K. Oh, C. Y. Hui, K. L. Li, and A. K. H. Kong. Multi-epoch X-ray imaging of globular cluster M62 with Chandra. *MNRAS*, 498(1):292–303, Oct. 2020. doi: 10.1093/mnras/staa2462.
- A. Paduano, A. Bahramian, J. C. A. Miller-Jones, A. Kawka, J. Strader, L. Chomiuk, C. O. Heinke, T. J. Maccarone, C. T. Britt, R. M. Plotkin, A. W. Shaw, L. Shishkovsky, E. Tremou, V. Tudor, and G. R. Sivakoff. The MAVERIC Survey: Simultaneous Chandra and VLA observations of the transitional millisecond pulsar candidate NGC 6652B. *MNRAS*, 506(3):4107–4120, Sept. 2021. doi: 10.1093/mnras/stab1928.

- C. Pallanca, S. M. Ransom, F. R. Ferraro, E. Dalessandro, B. Lanzoni, J. W. T. Hessels, I. Stairs, and P. C. C. Freire. Radio Timing and Optical Photometry of the Black Widow System PSR J1518+0204C in the Globular Cluster M5. *ApJ*, 795(1):29, Nov. 2014. doi: 10.1088/0004-637X/795/1/29.
- Z. Pan, S. M. Ransom, D. R. Lorimer, W. C. Fiore, L. Qian, L. Wang, B. W. Stappers, G. Hobbs, W. Zhu, Y. Yue, P. Wang, J. Lu, K. Liu, B. Peng, L. Zhang, and D. Li. The FAST Discovery of an Eclipsing Binary Millisecond Pulsar in the Globular Cluster M92 (NGC 6341). *ApJ*, 892(1):L6, Mar. 2020. doi: 10.3847/2041-8213/ab799d.
- Z. Pan, X. Ma, L. Qian, L. Wang, Z. Yan, J. Luo, S. M. Ransom, D. R. Lorimer, and P. Jiang. Three Pulsars Discovered by FAST in the Globular Cluster NGC 6517 with a Pulsar Candidate Sifting Code Based on Dispersion Measure to Signal-to-Noise Ratio Plots. *arXiv e-prints*, art. arXiv:2103.14927, Mar. 2021a.
- Z. Pan, L. Qian, X. Ma, K. Liu, L. Wang, J. Luo, Z. Yan, S. Ransom, D. Lorimer, D. Li, and P. Jiang. FAST Globular Cluster Pulsar Survey: Twenty-four Pulsars Discovered in 15 Globular Clusters. *ApJ*, 915(2):L28, July 2021b. doi: 10.3847/2041-8213/ac0bbd.
- A. Papitto, C. Ferrigno, E. Bozzo, N. Rea, L. Pavan, L. Burderi, M. Burgay, S. Campana, T. di Salvo, M. Falanga, M. D. Filipović, P. C. C. Freire, J. W. T. Hessels, A. Possenti, S. M. Ransom, A. Riggio, P. Romano, J. M. Sarkissian, I. H. Stairs, L. Stella, D. F. Torres, M. H. Wieringa, and G. F. Wong. Swings between rotation and accretion power in a binary millisecond pulsar. *Nature*, 501(7468):517–520, Sept. 2013. doi: 10.1038/nature12470.
- G. G. Pavlov, O. Kargaltsev, G. P. Garmire, and A. Wolszczan. X-Ray Emission from the Planet Pulsar B1257+12. *ApJ*, 664(2):1072–1078, Aug. 2007. doi: 10.1086/518926.
- M. Pichardo Marcano, L. E. Rivera Sandoval, T. J. Maccarone, Y. Zhao, and C. O. Heinke. A 2-d orbital period for a redback millisecond pulsar candidate

- in the globular cluster NGC 6397. *MNRAS*, 503(1):L51–L55, May 2021. doi: 10.1093/mnrasl/slab024.
- H. Ploeg, C. Gordon, R. Crocker, and O. Macias. Consistency between the luminosity function of resolved millisecond pulsars and the galactic center excess. *J. Cosmology Astropart. Phys.*, 2017(8):015, Aug. 2017. doi: 10.1088/1475-7516/2017/08/015.
- P. Podsiadlowski. Irradiation-driven mass transfer in low-mass X-ray binaries. *Nature*, 350(6314):136–138, Mar. 1991. doi: 10.1038/350136a0.
- E. J. Polzin, R. P. Breton, A. O. Clarke, V. I. Kondratiev, B. W. Stappers, J. W. T. Hessels, C. G. Bassa, J. W. Broderick, J. M. Grießmeier, C. Sobey, S. ter Veen, J. van Leeuwen, and P. Weltevrede. The low-frequency radio eclipses of the black widow pulsar J1810+1744. *MNRAS*, 476(2):1968–1981, May 2018. doi: 10.1093/mnras/sty349.
- D. Pooley, W. H. G. Lewin, F. Verbunt, L. Homer, B. Margon, B. M. Gaensler, V. M. Kaspi, J. M. Miller, D. W. Fox, and M. van der Klis. Chandra Observation of the Globular Cluster NGC 6440 and the Nature of Cluster X-Ray Luminosity Functions. *ApJ*, 573(1):184–190, July 2002. doi: 10.1086/340498.
- D. Pooley, W. H. G. Lewin, S. F. Anderson, H. Baumgardt, A. V. Filippenko, B. M. Gaensler, L. Homer, P. Hut, V. M. Kaspi, J. Makino, B. Margon, S. McMillan, S. Portegies Zwart, M. van der Klis, and F. Verbunt. Dynamical Formation of Close Binary Systems in Globular Clusters. *ApJ*, 591(2): L131–L134, July 2003. doi: 10.1086/377074.
- A. Possenti, R. Cerutti, M. Colpi, and S. Mereghetti. Re-examining the X-ray versus spin-down luminosity correlation of rotation powered pulsars. *A&A*, 387:993–1002, June 2002. doi: 10.1051/0004-6361:20020472.
- A. Possenti, N. D’Amico, R. N. Manchester, F. Camilo, A. G. Lyne, J. Sarkissian, and A. Corongiu. Three Binary Millisecond Pulsars in NGC 6266. *ApJ*, 599(1):475–484, Dec. 2003. doi: 10.1086/379190.

- A. Possenti, N. D’Amico, A. Corongiu, D. Manchester, J. Sarkissian, F. Camilo, and A. Lyne. A Dozen New Pulsars from the Parkes Globular Cluster Search. In F. A. Rasio and I. H. Stairs, editors, *Binary Radio Pulsars*, volume 328 of *Astronomical Society of the Pacific Conference Series*, page 189, July 2005.
- B. J. Prager, S. M. Ransom, P. C. C. Freire, J. W. T. Hessels, I. H. Stairs, P. Arras, and M. Cadelano. Using Long-term Millisecond Pulsar Timing to Obtain Physical Characteristics of the Bulge Globular Cluster Terzan 5. *ApJ*, 845(2):148, Aug. 2017. doi: 10.3847/1538-4357/aa7ed7.
- L. Qian and Z. Pan. Spatial Modulation Search Applied to the Search and Confirmation of Highly Scintillated Pulsars at FAST with A Pulsar Discovered in M3. *arXiv e-prints*, art. arXiv:2107.02749, July 2021.
- S. M. Ransom, L. J. Greenhill, J. R. Herrnstein, R. N. Manchester, F. Camilo, S. S. Eikenberry, and A. G. Lyne. A Binary Millisecond Pulsar in Globular Cluster NGC 6544. *ApJ*, 546(1):L25–L28, Jan. 2001. doi: 10.1086/318062.
- S. M. Ransom, I. H. Stairs, D. C. Backer, L. J. Greenhill, C. G. Bassa, J. W. T. Hessels, and V. M. Kaspi. Green Bank Telescope Discovery of Two Binary Millisecond Pulsars in the Globular Cluster M30. *ApJ*, 604(1):328–338, Mar. 2004. doi: 10.1086/381730.
- S. M. Ransom, J. W. T. Hessels, I. H. Stairs, P. C. C. Freire, F. Camilo, V. M. Kaspi, and D. L. Kaplan. Twenty-One Millisecond Pulsars in Terzan 5 Using the Green Bank Telescope. *Science*, 307(5711):892–896, Feb. 2005. doi: 10.1126/science.1108632.
- P. S. Ray, A. A. Abdo, D. Parent, D. Bhattacharya, B. Bhattacharyya, F. Camilo, I. Cognard, G. Theureau, E. C. Ferrara, A. K. Harding, D. J. Thompson, P. C. C. Freire, L. Guillemot, Y. Gupta, J. Roy, J. W. T. Hessels, S. Johnston, M. Keith, R. Shannon, M. Kerr, P. F. Michelson, R. W. Romani, M. Kramer, M. A. McLaughlin, S. M. Ransom, M. S. E. Roberts,

- P. M. Saz Parkinson, M. Ziegler, D. A. Smith, B. W. Stappers, P. Weltevrede, and K. S. Wood. Radio Searches of Fermi LAT Sources and Blind Search Pulsars: The Fermi Pulsar Search Consortium. *arXiv e-prints*, art. arXiv:1205.3089, May 2012.
- A. Ridolfi, P. C. C. Freire, P. Torne, C. O. Heinke, M. van den Berg, C. Jordan, M. Kramer, C. G. Bassa, J. Sarkissian, N. D’Amico, D. Lorimer, F. Camilo, R. N. Manchester, and A. Lyne. Long-term observations of the pulsars in 47 Tucanae - I. A study of four elusive binary systems. *MNRAS*, 462(3): 2918–2933, Nov. 2016. doi: 10.1093/mnras/stw1850.
- A. Ridolfi, T. Gautam, P. C. C. Freire, S. M. Ransom, S. J. Buchner, A. Possenti, V. Venkatraman Krishnan, M. Bailes, M. Kramer, B. W. Stappers, F. Abbate, E. D. Barr, M. Burgay, F. Camilo, A. Corongiu, A. Jameson, P. V. Padmanabh, L. Vleeschower, D. J. Champion, W. Chen, M. Geyer, A. Karastergiou, R. Karuppusamy, A. Parthasarathy, D. J. Reardon, M. Serylak, R. M. Shannon, and R. Spiewak. Eight new millisecond pulsars from the first MeerKAT globular cluster census. *MNRAS*, 504(1): 1407–1426, June 2021. doi: 10.1093/mnras/stab790.
- T. E. Riley, A. L. Watts, S. Bogdanov, P. S. Ray, R. M. Ludlam, S. Guillot, Z. Arzoumanian, C. L. Baker, A. V. Bilous, D. Chakrabarty, K. C. Gendreau, A. K. Harding, W. C. G. Ho, J. M. Lattimer, S. M. Morsink, and T. E. Strohmayer. A NICER View of PSR J0030+0451: Millisecond Pulsar Parameter Estimation. *ApJ*, 887(1):L21, Dec. 2019. doi: 10.3847/2041-8213/ab481c.
- M. S. E. Roberts. New Black Widows and Redbacks in the Galactic Field. In M. Burgay, N. D’Amico, P. Esposito, A. Pellizzoni, and A. Possenti, editors, *American Institute of Physics Conference Series*, volume 1357 of *American Institute of Physics Conference Series*, pages 127–130, Aug. 2011. doi: 10.1063/1.3615095.
- M. S. E. Roberts, M. A. McLaughlin, P. A. Gentile, P. S. Ray, S. M. Ransom,

- and J. W. T. Hessels. X-Ray Studies of Redbacks. *arXiv e-prints*, art. arXiv:1502.07208, Feb. 2015.
- C. Robinson, A. G. Lyne, R. N. Manchester, M. Bailes, N. D’Amico, and S. Johnston. Millisecond pulsars in the globular cluster 47 Tucanae. *MNRAS*, 274(2):547–554, May 1995. doi: 10.1093/mnras/274.2.547.
- R. E. Rutledge, D. W. Fox, S. R. Kulkarni, B. A. Jacoby, I. Cognard, D. C. Backer, and S. S. Murray. Microsecond Timing of PSR B1821-24 with Chandra High Resolution Camera-S. *ApJ*, 613(1):522–531, Sept. 2004. doi: 10.1086/380299.
- Y. Saito, N. Kawai, T. Kamae, S. Shibata, T. Dotani, and S. R. Kulkarni. Detection of Magnetospheric X-Ray Pulsation from Millisecond Pulsar PSR B1821-24. *ApJ*, 477(1):L37–L40, Mar. 1997. doi: 10.1086/310512.
- E. L. Sandquist, M. Gordon, D. Levine, and M. Bolte. A Re-evaluation of the Evolved Stars in the Globular Cluster M13. *AJ*, 139(6):2374–2409, June 2010. doi: 10.1088/0004-6256/139/6/2374.
- M. Servillat, N. A. Webb, F. Lewis, C. Knigge, M. van den Berg, A. Dieball, and J. Grindlay. A Dwarf Nova in the Globular Cluster M13. *ApJ*, 733(2): 106, June 2011. doi: 10.1088/0004-637X/733/2/106.
- A. W. Shaw, C. O. Heinke, A. W. Steiner, S. Campana, H. N. Cohn, W. C. G. Ho, P. M. Lugger, and M. Servillat. The radius of the quiescent neutron star in the globular cluster M13. *MNRAS*, 476(4):4713–4718, June 2018. doi: 10.1093/mnras/sty582.
- S. Sigurdsson, H. B. Richer, B. M. Hansen, I. H. Stairs, and S. E. Thorsett. A Young White Dwarf Companion to Pulsar B1620-26: Evidence for Early Planet Formation. *Science*, 301(5630):193–196, July 2003. doi: 10.1126/science.1086326.
- M. Sirianni, M. J. Jee, N. Benítez, J. P. Blakeslee, A. R. Martel, G. Meurer, M. Clampin, G. De Marchi, H. C. Ford, R. Gilliland, G. F. Hartig, G. D.

- Illingworth, J. Mack, and W. J. McCann. The Photometric Performance and Calibration of the Hubble Space Telescope Advanced Camera for Surveys. *PASP*, 117:1049–1112, Oct. 2005. doi: 10.1086/444553.
- E. M. Splaver, D. J. Nice, I. H. Stairs, A. N. Lommen, and D. C. Backer. Masses, Parallax, and Relativistic Timing of the PSR J1713+0747 Binary System. *ApJ*, 620(1):405–415, Feb. 2005. doi: 10.1086/426804.
- V. Springel, S. D. M. White, C. S. Frenk, J. F. Navarro, A. Jenkins, M. Vogelsberger, J. Wang, A. Ludlow, and A. Helmi. Prospects for detecting supersymmetric dark matter in the Galactic halo. *Nature*, 456(7218):73–76, Nov. 2008. doi: 10.1038/nature07411.
- W. S. Stacey, C. O. Heinke, H. N. Cohn, P. M. Lugger, and A. Bahramian. An Examination of the X-Ray Sources in the Globular Cluster NGC 6652. *ApJ*, 751(1):62, May 2012. doi: 10.1088/0004-637X/751/1/62.
- I. H. Stairs. Pulsars in Binary Systems: Probing Binary Stellar Evolution and General Relativity. *Science*, 304(5670):547–552, Apr. 2004. doi: 10.1126/science.1096986.
- B. W. Stappers, M. Bailes, A. G. Lyne, F. Camilo, R. N. Manchester, J. S. Sandhu, M. Toscano, and J. F. Bell. The nature of the PSR J2051-0827 eclipses. *MNRAS*, 321(3):576–584, Mar. 2001. doi: 10.1046/j.1365-8711.2001.04074.x.
- B. W. Stappers, B. M. Gaensler, V. M. Kaspi, M. van der Klis, and W. H. G. Lewin. An X-ray nebula associated with the millisecond pulsar B1957+20. *Science*, 299:1372–1374, Jan. 2003. doi: 10.1126/science.1079841.
- K. Stovall, P. C. C. Freire, S. Chatterjee, P. B. Demorest, D. R. Lorimer, M. A. McLaughlin, N. Pol, J. van Leeuwen, R. S. Wharton, B. Allen, M. Boyce, A. Brazier, K. Caballero, F. Camilo, R. Camuccio, J. M. Cordes, F. Crawford, J. S. Deneva, R. D. Ferdman, J. W. T. Hessels, F. A. Jenet, V. M. Kaspi, B. Knispel, P. Lazarus, R. Lynch, E. Parent, C. Patel, Z. Pleunis,

- S. M. Ransom, P. Scholz, A. Seymour, X. Siemens, I. H. Stairs, J. Swiggum, and W. W. Zhu. PALFA Discovery of a Highly Relativistic Double Neutron Star Binary. *ApJ*, 854(2):L22, Feb. 2018. doi: 10.3847/2041-8213/aaad06.
- J. Strader, S. Swihart, L. Chomiuk, A. Bahramian, C. Britt, C. C. Cheung, K. Dage, J. Halpern, K.-L. Li, R. P. Mignani, J. A. Orosz, M. Peacock, R. Salinas, L. Shishkovsky, and E. Tremou. Optical Spectroscopy and Demographics of Redback Millisecond Pulsar Binaries. *ApJ*, 872(1):42, Feb. 2019. doi: 10.3847/1538-4357/aafbba.
- W. Sutantyo. The formation of globular cluster X-ray sources through neutron star - giant collisions. *A&A*, 44:227–230, Nov. 1975.
- M. Takahashi, S. Shibata, K. Torii, Y. Saito, N. Kawai, M. Hirayama, T. Dotani, S. Gunji, H. Sakurai, I. H. Stairs, and R. N. Manchester. Pulsed X-Ray Emission from the Fastest Millisecond Pulsar: PSR B1937+21 with ASCA. *ApJ*, 554(1):316–321, June 2001. doi: 10.1086/321330.
- J. H. Taylor, L. A. Fowler, and P. M. McCulloch. Measurements of general relativistic effects in the binary pulsar PSR1913 + 16. *Nature*, 277(5696): 437–440, Feb. 1979. doi: 10.1038/277437a0.
- V. Testa, T. di Salvo, F. D’Antona, M. T. Menna, P. Ventura, L. Burderi, A. Riggio, R. Iaria, A. D’Aì, A. Papitto, and N. Robba. The near-IR counterpart of IGR J17480-2446 in Terzan 5. *A&A*, 547:A28, Nov. 2012. doi: 10.1051/0004-6361/201219904.
- C. Thompson, R. D. Blandford, C. R. Evans, and E. S. Phinney. Physical Processes in Eclipsing Pulsars: Eclipse Mechanisms and Diagnostics. *ApJ*, 422:304, Feb. 1994. doi: 10.1086/173728.
- S. E. Thorsett, Z. Arzoumanian, M. M. McKinnon, and J. H. Taylor. The Masses of Two Binary Neutron Star Systems. *ApJ*, 405:L29, Mar. 1993. doi: 10.1086/186758.

- M. H. van Kerkwijk, C. G. Bassa, B. A. Jacoby, and P. G. Jonker. Optical Studies of Companions to Millisecond Pulsars. In F. A. Rasio and I. H. Stairs, editors, *Binary Radio Pulsars*, volume 328 of *Astronomical Society of the Pacific Conference Series*, page 357, July 2005.
- J. van Paradijs, J. Allington-Smith, P. Callanan, P. A. Charles, B. J. M. Hassall, G. Machin, K. O. Mason, T. Naylor, and A. P. Smale. Optical observations of the eclipsing binary radio pulsar PSR1957 + 20. *Nature*, 334(6184):684–686, Aug. 1988. doi: 10.1038/334684a0.
- F. Verbunt and P. Hut. The Globular Cluster Population of X-Ray Binaries. In D. J. Helfand and J. H. Huang, editors, *The Origin and Evolution of Neutron Stars*, volume 125, page 187, Jan. 1987.
- F. Verbunt and W. H. G. Lewin. *Globular cluster X-ray sources*, volume 39, pages 341–379. 2006.
- F. Verbunt, L. Kuiper, T. Belloni, H. M. Johnston, A. G. de Bruyn, W. Hermsen, and M. van der Klis. High-energy observations of the millisecond pulsar PSR J0218+4232. *A&A*, 311:L9–L12, July 1996.
- Z. Wadiasingh, C. Venter, A. K. Harding, M. Böttcher, and P. Kilian. Pressure Balance and Intrabinary Shock Stability in Rotation-powered-state Redback and Transitional Millisecond Pulsar Binary Systems. *ApJ*, 869(2):120, Dec. 2018. doi: 10.3847/1538-4357/aaed43.
- L. Wang, B. Peng, B. W. Stappers, K. Liu, M. J. Keith, A. G. Lyne, J. Lu, Y.-Z. Yu, F. Kou, J. Yan, P. Jiang, C. Jin, D. Li, Q. Li, L. Qian, Q. Wang, Y. Yue, H. Zhang, S. Zhang, Y. Zhu, and FAST Collaboration. Discovery and Timing of Pulsars in the Globular Cluster M13 with FAST. *ApJ*, 892(1):43, Mar. 2020. doi: 10.3847/1538-4357/ab76cc.
- J. Wilms, A. Allen, and R. McCray. On the Absorption of X-Rays in the Interstellar Medium. *ApJ*, 542(2):914–924, Oct. 2000. doi: 10.1086/317016.

- Q. Yuan and B. Zhang. Millisecond pulsar interpretation of the Galactic center gamma-ray excess. *Journal of High Energy Astrophysics*, 3:1–8, Sept. 2014. doi: 10.1016/j.jheap.2014.06.001.
- V. E. Zavlin. XMM-Newton Observations of Four Millisecond Pulsars. *ApJ*, 638(2):951–962, Feb. 2006. doi: 10.1086/449308.
- V. E. Zavlin. Studying millisecond pulsars in X-rays. *Ap&SS*, 308(1-4):297–307, Apr. 2007. doi: 10.1007/s10509-007-9297-y.
- V. E. Zavlin, G. G. Pavlov, D. Sanwal, R. N. Manchester, J. Trümper, J. P. Halpern, and W. Becker. X-Radiation from the Millisecond Pulsar J0437-4715. *ApJ*, 569(2):894–902, Apr. 2002. doi: 10.1086/339351.
- L. Zhang and K. S. Cheng. X-ray and gamma-ray emission from millisecond pulsars. *A&A*, 398:639–646, Feb. 2003. doi: 10.1051/0004-6361:20021570.
- L. Zhang, R. N. Manchester, A. D. Cameron, G. Hobbs, D. Li, S. Dai, Q. Zhi, Z. Zhu, J. Wang, L. Toomey, Y. Feng, S. Wang, and S. Zhang. Wideband Monitoring Observations of PSR J1803-3002A in the Globular Cluster NGC 6522. *ApJ*, 905(1):L8, Dec. 2020. doi: 10.3847/2041-8213/abca40.
- J. Zhao, Y. Zhao, and C. O. Heinke. Chandra and HST studies of six millisecond pulsars in the globular cluster M13. *MNRAS*, 502(2):1596–1604, Apr. 2021. doi: 10.1093/mnras/stab117.
- Y. Zhao, C. O. Heinke, H. N. Cohn, P. M. Lugger, and A. M. Cool. Identifications of faint Chandra sources in the globular cluster M3. *MNRAS*, 483(4):4560–4577, Mar. 2019. doi: 10.1093/mnras/sty3384.
- Y. Zhao, C. O. Heinke, H. N. Cohn, P. M. Lugger, S. Guillot, C. Echiburú, L. Shishkovsky, J. Strader, L. Chomiuk, A. Bahramian, J. C. A. Miller-Jones, T. J. Maccarone, E. Tremou, and G. R. Sivakoff. A deep Chandra survey for faint X-ray sources in the Galactic globular cluster M30, and searches for optical and radio counterparts. *MNRAS*, 499(3):3338–3355, Dec. 2020a. doi: 10.1093/mnras/staa2927.

Y. Zhao, C. O. Heinke, V. Tudor, A. Bahramian, J. C. A. Miller-Jones, G. R. Sivakoff, J. Strader, L. Chomiuk, L. Shishkovsky, T. J. Maccarone, M. Pichardo Marcano, and J. D. Gelfand. The MAVERIC survey: a hidden pulsar and a black hole candidate in ATCA radio imaging of the globular cluster NGC 6397. *MNRAS*, 493(4):6033–6049, Apr. 2020b. doi: 10.1093/mnras/staa631.

Appendix A

Upper limits of X-ray luminosities

We present the upper limits of X-ray luminosities for 111 GC MSPs in Table A.1. These MSPs are not eligible for performing specific X-ray spectral analysis, and hence we placed an upper limit of L_X for each of them. The criteria of determining upper limits have been discussed in Section 3.2.

Table A.1: 111 GC MSPs with upper limits of X-ray luminosities.

Pulsar Name	GC Name	Period (ms)	Type	$L_X(0.3-8 \text{ keV})$	Ref.
J0024-7204G	47 Tuc (NGC 104)	4.04	I	2.0E+31	1
J0024-7204I	47 Tuc (NGC 104)	3.48	BW	2.0E+31	1
J0024-7204P	47 Tuc (NGC 104)	3.64	BW	2.0E+31	2
J0024-7204V	47 Tuc (NGC 104)	4.81	eRB	2.0E+31	2
J0024-7204ac	47 Tuc (NGC 104)	2.74	eBW	2.0E+31	3
J0024-7204ad	47 Tuc (NGC 104)	3.74	eRB	2.0E+31	3
J1312+1810B	M53 (NGC 5024)	6.24	B	7.6E+32	4
J1312+1810C	M53 (NGC 5024)	12.53	I	7.6E+32	4
J1312+1810D	M53 (NGC 5024)	6.07	B	7.6E+32	4
J1326-4728C	ω Cen (NGC 5139)	6.87	I	3.0E+32	5
J1326-4728D	ω Cen (NGC 5139)	4.58	I	3.0E+32	5
J1326-4728E	ω Cen (NGC 5139)	4.21	I	3.0E+32	5
J1342+2822A	M3 (NGC 5272)	2.55	BW	1.3E+31	6
J1342+2822B	M3 (NGC 5272)	2.39	B	8.8E+30	6
J1342+2822C	M3 (NGC 5272)	2.17	I	1.3E+31	6
J1342+2822D	M3 (NGC 5272)	5.44	B	1.3E+31	6
J1342+2822E	M3 (NGC 5272)	5.47	B	1.3E+31	6
J1342+2822F	M3 (NGC 5272)	4.40	B	1.3E+31	6
B1516+02A	M5 (NGC 5904)	5.55	I	1.8E+30	7

Continued on next page

Table A.1 – *Continued from previous page*

Pulsar Name	GC Name	Period (ms)	Type	$L_X(0.3-8 \text{ keV})$	Ref.
B1516+02B	M5 (NGC 5904)	7.95	B	1.8E+30	7
J1518+0204C	M5 (NGC 5904)	2.48	eBW	9.5E+30	8
J1518+0204D	M5 (NGC 5904)	2.99	B	1.6E+32	9
J1518+0204E	M5 (NGC 5904)	3.18	B	1.6E+32	9
J1518+0204F	M5 (NGC 5904)	2.65	B	1.6E+32	10
J1518+0204G	M5 (NGC 5904)	2.75	B	1.6E+32	11
J1641+3627A	M13 (NGC 6205)	10.38	I	1.3E+30	12
J1647-0156A	M12 (NGC 6218)	2.36	B	1.9E+32	13
J1657-0406A	M10 (NGC 6254)	4.73	-	5.9E+31	14
J1657-0406B	M10 (NGC 6254)	7.35	B	5.9E+31	14
J1701-3006A	M62 (NGC 6266)	5.24	B	3.5E+30	15
J1701-3006D	M62 (NGC 6266)	3.42	B	6.8E+30	16
J1701-3006E	M62 (NGC 6266)	3.23	eBW	5.6E+31	16
J1701-3006F	M62 (NGC 6266)	2.29	BW	3.6E+31	16
J1701-3006G	M62 (NGC 6266)	4.61	B	1.0E+32	17
J1717+4308A	M92 (NGC 6341)	3.16	eRB	3.1E+31	18
J1721-1936B	NGC 6342	2.57	I	3.8E+32	19
J1735-3028B	Terzan 1	11.14	I	8.5E+31	20
J1735-3028C	Terzan 1	6.04	I	8.5E+31	20
J1735-3028D	Terzan 1	5.39	I	8.5E+31	20
J1735-3028E	Terzan 1	3.08	I	8.5E+31	20
J1735-3028F	Terzan 1	5.21	I	8.5E+31	20
J1735-3028G	Terzan 1	3.92	I	8.5E+31	20
J1737-0314A	M14 (NGC 6420)	1.98	BW	3.2E+31	4
J1737-0314B	M14 (NGC 6420)	8.52	B	7.2E+32	10
J1737-0314C	M14 (NGC 6420)	8.46	B	7.2E+32	10
J1737-0314D	M14 (NGC 6420)	2.89	eRB	7.2E+32	10
J1737-0314E	M14 (NGC 6420)	2.28	eRB	7.2E+32	10
J1748-2446C	Terzan 5	8.44	I	9.5E+29	21
J1748-2446D	Terzan 5	4.71	I	1.2E+30	22
J1748-2446G	Terzan 5	21.67	I	3.0E+30	22
J1748-2446I	Terzan 5	9.57	B	3.0E+30	22
J1748-2446M	Terzan 5	3.57	B	3.0E+30	22
J1748-2446R	Terzan 5	5.03	I	3.0E+30	22
J1748-2446S	Terzan 5	6.12	I	3.0E+30	22
J1748-2446T	Terzan 5	7.08	I	3.0E+30	22
J1748-2446U	Terzan 5	3.29	B	3.0E+30	22
J1748-2446W	Terzan 5	4.21	B	3.0E+30	22
J1748-2446Y	Terzan 5	2.05	B	3.0E+30	22
J1748-2446aa	Terzan 5	5.79	I	3.0E+30	23
J1748-2446ab	Terzan 5	5.12	I	3.0E+30	23
J1748-2446ac	Terzan 5	5.09	I	3.0E+30	23

Continued on next page

Table A.1 – *Continued from previous page*

Pulsar Name	GC Name	Period (ms)	Type	$L_X(0.3-8 \text{ keV})$	Ref.
J1748–2446ae	Terzan 5	3.66	B	3.0E+30	23
J1748–2446af	Terzan 5	3.30	I	3.0E+30	23
J1748–2446ag	Terzan 5	4.45	I	3.0E+30	23
J1748–2446ah	Terzan 5	4.97	I	3.0E+30	23
J1748–2446ai	Terzan 5	21.23	B	3.0E+30	23
J1748–2446aj	Terzan 5	2.96	I	3.0E+30	24
J1748–2446ak	Terzan 5	1.89	I	3.0E+30	24
J1748–2446al	Terzan 5	5.95	I	3.0E+30	24
J1748–2446am	Terzan 5	2.93	B	3.0E+30	25
J1748–2446an	Terzan 5	4.80	B	3.0E+30	26
J1748–2021B	NGC 6440	16.76	B	1.6E+32	27
J1748–2021C	NGC 6440	6.23	I	1.6E+31	27
J1748–2021D	NGC 6440	13.50	eRB	1.9E+31	27
J1748–2021E	NGC 6440	16.26	I	1.1E+31	27
J1748–2021F	NGC 6440	3.79	B	1.7E+31	27
J1748–2021G	NGC 6440	5.21	I	2.6E+32	28
J1748–2021H	NGC 6440	2.85	B	2.6E+32	28
J1801–0857A	NGC 6517	7.18	I	1.6E+31	29
J1801–0857C	NGC 6517	3.74	I	1.0E+32	29
J1801–0857D	NGC 6517	4.23	I	3.0E+31	29
J1801–0857E	NGC 6517	7.60	I	2.4E+32	30
J1801–0857F	NGC 6517	24.89	I	2.4E+32	30
J1801–0857H	NGC 6517	5.64	I	3.0E+31	30
J1801–0857I	NGC 6517	3.25	I	2.4E+32	30
J1803–3002A	NGC 6522	7.10	I	5.0E+30	31
J1803–3002B	NGC 6522	4.40	I	5.0E+32	32
J1803–3002C	NGC 6522	5.84	I	5.0E+32	32
J1803–3002D	NGC 6522	5.53	I	5.0E+32	33
B1802–07	NGC 6539	23.10	B	1.6E+31	34
J1807–2459A	NGC 6544	3.06	BW	6.3E+30	35
J1807–2459B	NGC 6544	4.19	B	6.0E+30	36
J1824–2452B	M28 (NGC 6626)	6.55	I	3.0E+30	37
J1824–2452G	M28 (NGC 6626)	5.91	BW	1.3E+31	37
J1824–2452L	M28 (NGC 6626)	4.10	BW	2.2E+32	38
J1824–2452M	M28 (NGC 6626)	9.57	B	8.2E+32	39
J1824–2452N	M28 (NGC 6626)	3.35	BW	8.2E+32	39
J1835–3259A	NGC 6652	3.89	B	2.0E+31	40
J1835–3259B	NGC 6652	1.83	B	1.1E+32	41
J1836–2354B	M22 (NGC 6656)	3.23	I	8.0E+29	42
J1910–5959G	NGC 6752	4.79	I	5.0E+31	43
J1910–5959H	NGC 6752	2.01	I	5.0E+31	43
J1910–5959I	NGC 6752	2.65	I	5.0E+31	43

Continued on next page

Table A.1 – *Continued from previous page*

Pulsar Name	GC Name	Period (ms)	Type	$L_X(0.3-8 \text{ keV})$	Ref.
J1911+0102A	NGC 6760	3.62	BW	1.0E+31	44
J1911+0102B	NGC 6760	5.38	I	1.0E+31	45
J2133–0049A	M2 (NGC 7089)	10.15	B	8.6E+32	10
J2133–0049B	M2 (NGC 7089)	6.97	B	8.6E+32	10
J2133–0049C	M2 (NGC 7089)	3.00	B	8.6E+32	10
J2133–0049D	M2 (NGC 7089)	4.22	B	8.6E+32	10
J2133–0049E	M2 (NGC 7089)	3.70	B	8.6E+32	10
J2140–2310B	M30 (NGC 7099)	13.00	B	1.1E+31	46

Table A.1: References (for X-ray limits, and pulsar properties): 1) Manchester et al. (1991); Robinson et al. (1995); Freire et al. (2001); Heinke et al. (2005); Freire et al. (2017); 2) Camilo et al. (2000); Ridolfi et al. (2016); Heinke et al. (2005); 3) Heinke et al. (2005); Ridolfi et al. (2021); 4) Pan et al. (2021b) and this work; 5) Henleywillis et al. (2018); Dai et al. (2020); 6) Hessels et al. (2007); Zhao et al. (2019); Pan et al. (2021b); Qian and Pan (2021), this work; 7) Anderson et al. (1997), this work; 8) Hessels et al. (2007); Pallanca et al. (2014), this work; 9) Hessels et al. (2007); Bahramian et al. (2020); 10) Bahramian et al. (2020); Pan et al. (2021b); 11) Bahramian et al. (2020), Pan et al. in prep; 12) Kulkarni et al. (1991); Wang et al. (2020); Zhao et al. (2021); 13) Lu et al. (2009), Pan & FAST team in prep; 14) Pan et al. (2021b); Bahramian et al. (2020); 15) D’Amico et al. (2001); Possenti et al. (2003); Lynch et al. (2012), this work; 16) Lynch et al. (2012), this work; 17) Ridolfi et al. (2021); Oh et al. (2020); 18) Lu et al. (2011); Pan et al. (2020, 2021b), this work; 19) TRAPUM in prep; 20) Cackett et al. (2006), DeCesar et al. in prep; 21) Lyne et al. (2000); Prager et al. (2017); Bogdanov et al. (2021); 22) Ransom et al. (2005); Prager et al. (2017); Bogdanov et al. (2021); 23) Prager et al. (2017); Bogdanov et al. (2021); 24) Prager et al. (2017); Cadelano et al. (2018); Bogdanov et al. (2021), 25) Andersen and Ransom (2018); Bogdanov et al. (2021); 26) Bogdanov et al. (2021); Ridolfi et al. (2021); 27) Freire et al. (2008), this work; 28) Pooley et al. (2002), TRAPUM in prep, this work; 29) Lynch et al. (2011), this work; 30) Pan et al. (2021a), this work; 31) Possenti et al. (2005); Bahramian et al. (2020); Zhang et al. (2020), this work; 32) Bahramian et al. (2020), GBT team in prep; 33) Bahramian et al. (2020); Ridolfi et al. (2021); 34) D’Amico et al. (1993); Thorsett et al. (1993), this work; 35) D’Amico et al. (2001); Ransom et al. (2001); Lynch et al. (2012), this work; 36) Lynch et al. (2012); Bahramian et al. (2020), this work; 37) Begin (2006); Bogdanov et al. (2011b); 38) Bogdanov et al. (2011b), GBT team in prep; 39) Bahramian et al. (2020), TRAPUM in prep; 40) Stacey et al. (2012); DeCesar et al. (2015); 41) Stacey et al. (2012), Gautam et al. in prep; 42) Lynch et al. (2011); Bahramian et al. (2020), this work; 43) Forestell et al. (2014), TRAPUM in prep; 44) Deich et al. (1993); Freire et al. (2005); Bahramian et al. (2020), this work; 45) Freire et al. (2005); Bahramian et al. (2020), this work; 46) Ransom et al. (2004); Zhao et al. (2020a).